Design of Tag-Recapture Experiments for Estimating Yellowfin Tuna Stock Dynamics, Mortality, and Fishery Interactions

Peter J. Bills and John R. Sibert

SOEST 97-05
JIMAR Contribution 97-313

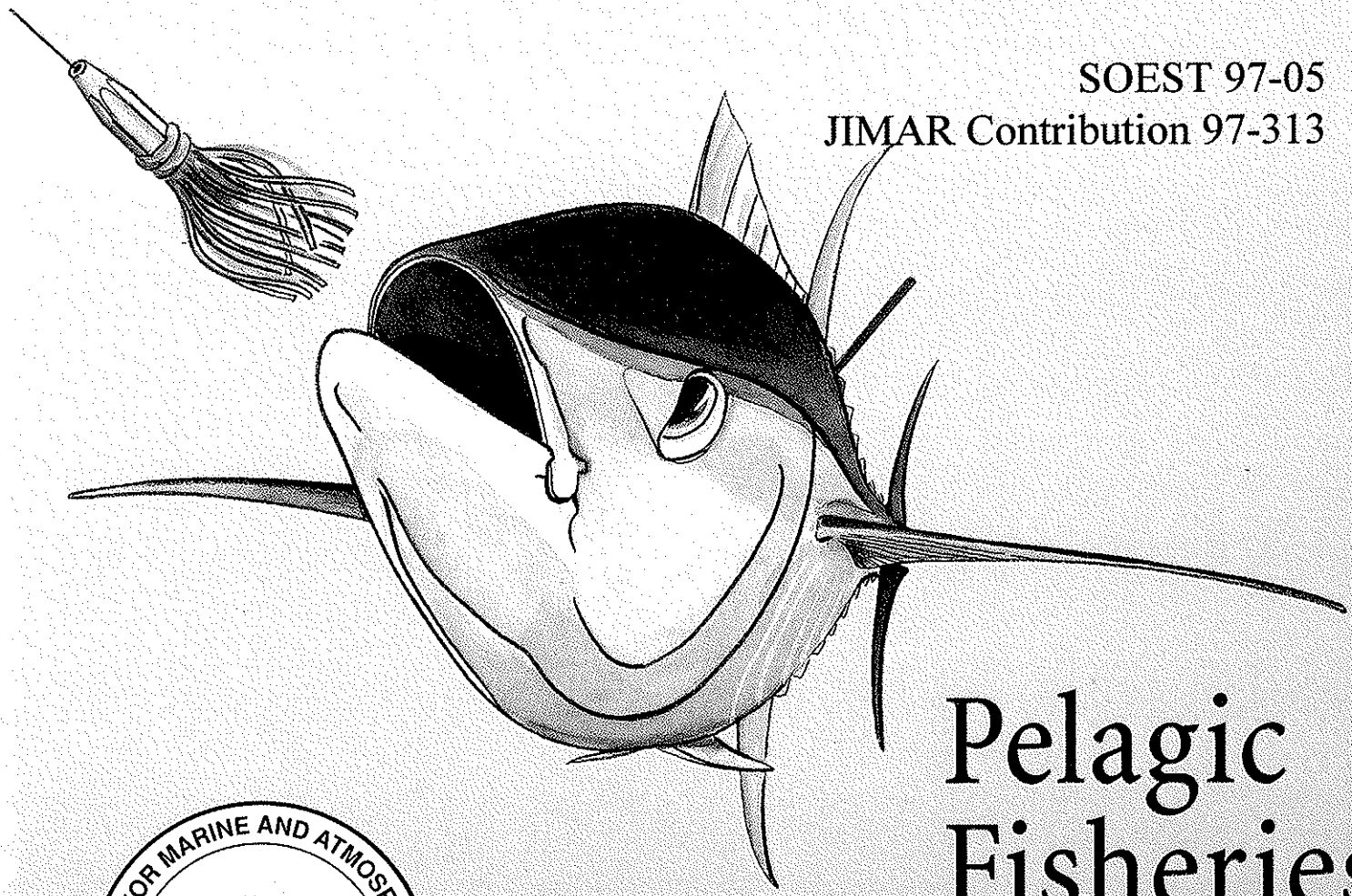

Pelagic Fisheries Research Program

JOINT INSTITUTE FOR MARINE AND ATMOSPHERIC RESEARCH ~UH-NOAA~
JIMAR

Design of Tag-Recapture Experiments for Estimating Yellowfin Tuna Stock Dynamics, Mortality, and Fishery Interactions

Peter J. Bills
and
John R. Sibert

Joint Institute of Marine and Atmospheric Research
Pelagic Fisheries Research Program
University of Hawaii
Honolulu, HI

SOEST 97-05
JIMAR Contribution 97-313

Bills, P. J., and J. R. Sibert, Design of Tag-Recapture Experiments for Estimating Yellowfin Tuna Stock Dynamics, Mortality, and Fishery Interactions, 80 pp, University of Hawaii, Joint Institute for Marine and Atmospheric Research, 1000 Pope Road, Honolulu, HI, 96822, 1997.

Contents

1 Introduction 2

2 Model of Hawaiian waters 3

3 Data analysis 3
- 3.1 Initial subdivision into 5 fleets 4
- 3.2 Annually cyclic data 5
- 3.3 Expressing troll and handline catch as numbers of fish 5
- 3.4 Initial estimates of catchability 5
- 3.5 Establishing inshore and offshore handline fleets 5
- 3.6 Ahi (yellowfin and bigeye) coded as "yellowfin" 16
- 3.7 Six fleets and final catchability estimate 18

4 Mathematical Model 21

5 Finite difference solution 23
- 5.1 Finite difference approximations 23
- 5.2 Boundary and initial conditions 26
- 5.3 Conditions for non-negative values 27
- 5.4 Regionalization and re-parameterization 29
- 5.5 Parameter estimation 30

6 Hypotheses 31
- 6.1 Release sites 31
- 6.2 Regionalization 32
- 6.3 Catch, effort, and "redistributed catch" at the release sites 33
- 6.4 Release strategy 33
- 6.5 Movement hypothesis 36
- 6.6 Natural mortality hypotheses 37

7 Results 38
- 7.1 Multiple release site strategy 38
  - 7.1.1 Simulated recaptures using $M = 0.05$, 0.10, and 0.30 46
  - 7.1.2 Results using M = 0.10 47
  - 7.1.3 Effect of altering reporting rate 48
  - 7.1.4 Effect of altering tag release numbers 48
  - 7.1.5 Modeling fleet interactions 59

8 Recommendations 60
- 8.1 Spatially variable random movement parameter 60
- 8.2 Catchabilities 60
- 8.3 Age structure 61

8.4 Tagging mortality 61
8.5 Oceanic movement included as a background movement field 61
8.6 Adopting a higher order numerical scheme 63
8.7 Improving the prediction of tag return numbers 63

9 Conclusions 63

10 Appendix 67
10.1 Non-physical diffusion from upwind differencing 67
10.2 Halt time step discretizations 68
10.3 Mathematical requirements for non-negativity 69
10.4 Predicted number of tag returns 69
10.5 Seasonal oceanographic flow patterns from a numerical model 71
10.6 Complete results of 12 tests 71

Abstract

Large scale tag release-recapture programs initiated with a view to providing information for fisheries management are both lengthy and expensive. The objective of this project is to use computer simulations to establish whether such a program might be useful in answering questions about yellowfin tuna in the Hawaiian Islands EEZ.

Computer simulations were carried out using a seasonal hypothesis for bulk behavioral movement of tagged yellowfin (tags) to determine if the mortality and movement parameters could be faithfully reproduced by the available estimation software. Two numerical schemes were compared, each under open and closed boundary conditions. Three values for monthly natural mortality were used and results for a 10%/month natural mortality rate are given in detail. The effects of adjusting reporting rates and numbers of tag releases are also examined.

Assuming that tag recapture percentages indicate catch percentages, fleet interactions can be estimated by manipulating fleet participation. These experiments, using 1991-92 effort data, suggest that the interaction between longline and nearshore fleets is only a few percent. Interaction between the three nearshore fleets is similarly either negligible or only a few percent, but this latter result may reflect our restructuring of the supplied data set for the nearshore fleets. Restructuring of the handline data set, in particular, was necessitated following input from the National Marine Fisheries Service (NMFS) concerning a group of handliners who work certain seamounts and weather buoys, and was also prompted by inexplicably high ratios noted at these locations between actual catch and an estimate of catch based on global CPUE (catch per unit effort).

Parameter values were accurately recovered in model regions encompassing the release sites. Confidence in the values depends directly on the number of recaptures made in a given region: the greater the number of recaptures, the more accurate the mean of the estimates and the smaller the accompanying standard deviation.

Based on these results and others obtained using simple one-season hypotheses for behavioral movement, we believe that reliable movement and mortality data are recoverable from a sensibly posed tag release-recapture experiment for the Hawaiian Islands EEZ. Release numbers of the order of 500 per month at each site should provide a workable compromise between parameter estimation accuracy and the field expense in conducting the experiment. This figure should be achievable using scientific personnel and a dedicated vessel; it is not likely to be achieved using the services and the boats of local fishermen.

Major findings have been posted on the World Wide Web, along with several **mpeg** movies of tuna movement under hypothetical scenarios. To access these, enter the URL

`http://www.soest.hawaii.edu/PFRP`

on a web browser. Cross-links to related projects are given.

1 Introduction

The objective of this project is to use computer simulation techniques to determine the practicability of mounting a release-and-recapture program for tagged yellowfin tuna in the Hawaiian Islands EEZ and adjacent central Pacific waters. The study was to propose an experimental design whose analysis would reveal yellowfin tuna dynamics and fleet interactions in the region.

The computer model used for the Hawaiian Islands and surrounding waters is given in Section 2. NMFS (Honolulu) supplied effort and catch data for the years 1991-92; a discussion of the data appears in Section 3. Following both a suggestion from NMFS and a comprehensive comparison of observed catch and estimated catch (based on global CPUE), the data supplied for two nearshore fleets have been reallocated to three fleets to emphasize the performance of a small but significant group of handliners.

The mathematical model used is discussed in Section 4. The movement parameters obtainable from release-recapture experiments using dart tags are those of *bulk movement* since the paths taken by individuals in the released cohorts are unknown. If such bulk movement is assumed to have both directed and random components, the well known advection-diffusion model can be used to model the movement with the advection parameter interpreted as the component of net *directed movement* and the diffusion parameter as the component of net *random movement.*

Finite difference schemes for the solution of the partial differential equation are presented in Section 5, along with boundary formulations and conditions for non-negative solutions. The accuracy of the available movement model was examined and a more accurate scheme for numerical approximation has been proposed. Its stability depends on the value of the Peclet number, a dimensionless quantity measuring the relative importance of the directed and random components of movement. An improved scheme for predicting tag recaptures has also been implemented.

The natural mortality and seasonal movement hypotheses used are given in Section 6. Data from the chosen release sites are examined, and it is argued that tagging should be performed by scientists operating from a chartered or dedicated vessel. Regionalization of the model area, carried out in order to reduce the number of estimable parameters, is discussed.

Results are given in Section 7; these include the effect on parameter estimates of altering reporting rates and tag release numbers and a discussion of fleet interactions. Recommendations for improving the movement and parameter estimation software to achieve higher accuracy and confidence in the results are given in Section 8 and conclusions are presented in Section 9.

An appendix includes a discussion of the non-physical component of random movement introduced by the use of the upwind scheme, the discretizations used by both the upwind

and centered-space schemes, and the scheme for more accurately estimating tag recaptures. Seasonal oceanographic flow patterns obtained from a numerical model are included for reference. Finally, results derived from 12 sets of simulations spanning the use of three natural mortality values, two numerical schemes, and two methods of fixing boundary conditions are given.

2 Model of Hawaiian waters

Fishing effort and catch data provided by NMFS (Honolulu) are available at a resolution of $1° \times 1°$ (latitude by longitude) for longline fleets and $\frac{1}{3}° \times \frac{1}{3}°$ for handline and troll fleets. Models at resolutions of $1° \times 1°$ and $\frac{1}{3}° \times \frac{1}{3}°$ have therefore been proposed, the first for use in this report and the second for possible future research utilizing the detailed structure of the troll and handline data. No more will be said here about the $\frac{1}{3}° \times \frac{1}{3}°$ model.

The $1° \times 1°$ model measures $30° \times 25°$ and is shown in Figure 1. At this resolution, only the island of Hawaii can be represented. The model is confined to the region 10°-35°N latitude and 145°-175°W longitude because this covers the areas of major yellowfin effort and catch for the years 1991 and 1992 (see also Curran *et al.*, 1996, Figure 12); the model region could be expanded with corresponding computational penalties.

Analysis of the swordfish longline data shows that only 2.3% of its yellowfin catch (64 of 2734 fish caught in the period 1991-92) was made outside this region; on the other hand 16.8% of effort was expended outside the region, reflecting the primary target of the swordfish fishery. Examination of the tuna longline data shows that 7.9% (414 of 5272 fish) of its yellowfin catch was taken outside the region; only 0.73% of effort corresponded to extra-regional excursions which were to lower latitudes (3°-6° N). Only 0.4% (39 of 10,308 fish) of the mixed longline yellowfin catch was taken outside the region, representing some lower and some higher latitude excursions; the effort corresponding to external catch was 2.2%. The activities of the troll and handline fleets are contained within this region, being restricted to the island chain and its vicinity.

3 Data analysis

NMFS (Honolulu) provided spatially and monthly indexed 1991-92 effort and catch data for longline, troll and handline fisheries. To preserve the confidentiality of fishing operations, data were withheld from the spatially indexed data sets where fewer than 3 records occurred in any 1° square geographic bin in one year for the longline data, and similarly in any $\frac{1}{3}°$ square in the case of the troll and handline data. The yroll and handline data were aggregated to 1° square bins.

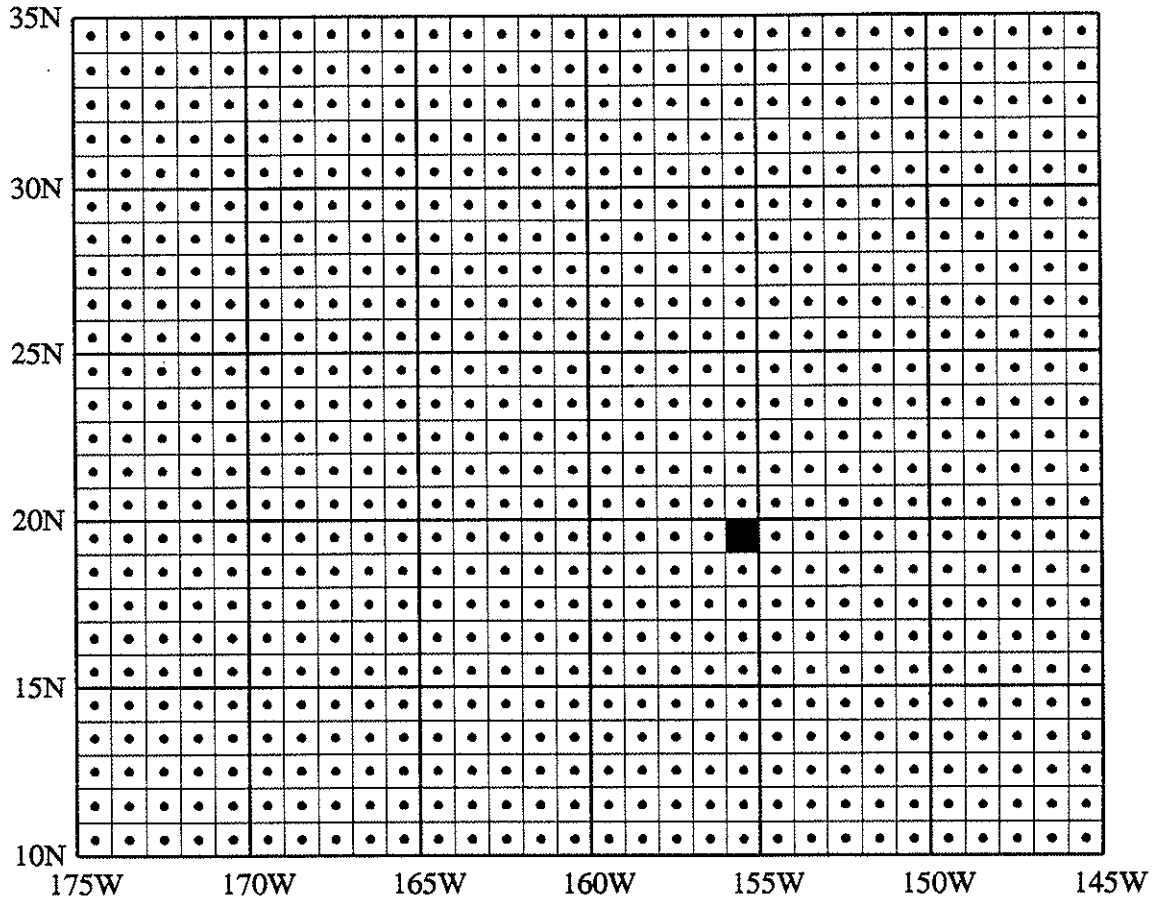

Figure 1: The 1°×1° grid used for the Hawaiian Island region (Hawaii = black square).

As stated above, the data are presented in two ways. A *spatially indexed* set is given by location, with figures in the same month for 1991 and 1992 summed; for example, effort and catch at location L during March 1991 and March 1992 for fleet f is summed and presented as a line entry in this file. A *monthly indexed* set consists of 24 line summaries of effort and catch values for all locations at which reports are available; since these entries are location independent, all available data are incorporated without breaching confidentiality. Comparison of the two data sets shows how much has had been withheld for each fleet in the case of the spatially indexed files.

3.1 Initial subdivision into 5 fleets

NMFS indexed the longline data according to target species groups (swordfishes, tunas, or mixed), so on this basis it is subdivided into 3 fleets, He *et al.* (in press). These fleets are named the swordfish longline (with fleet code SSLL), tuna longline (TTLL) and mixed

longline (MMLL) fleets. Fleet codes for the Hawaii troll and handline fisheries are HITR and HIHL, respectively.

The percentages of spatially indexed data withheld are 14% for SSLL, 18% for TTLL, 11% for MMLL and 3.9% each for HITR and HIHL.

3.2 Annually cyclic data

Computer simulations of at least two years duration were proposed using the spatially indexed data sets. Since these data are summed over 1991-92, we are obliged to average the effort and catch values as for a single hypothetical year and assume that the annual activities of the fleets were cyclic.

The assumption of annual cyclicity was checked for each fleet using the monthly indexed data set, remembering that these data include items outside the model region in the case of the longline fleets. This was done by plotting catch (in *numbers* for the longline fleets, *pounds* for the troll and handline fleets) versus effort (in *hooks* for the longliners, *trips* for the troll and handliners) for each fleet. These plots appear in Figure 2. Inspection shows that troll and handline operations were strongly cyclic for 1991 and 1992; annual longline operations with respect to yellowfin were only weakly cyclic. The troll and handline fleets accounted for approximately 75% (see next subsection) of yellowfin catch during 1991-92, so to that extent the assumption of yearly cyclicity is valid.

3.3 Expressing troll and handline catch as numbers of fish

While the longline catch data are expressed as numbers of fish caught, the troll and handline catch is given in pounds. Tuna are represented as numbers of fish in the computer simulation programs used, so the troll and handline catch data had to be converted. NMFS supplied a simple conversion table, reproduced here as Table 1. The conversion statistics are necessarily approximate; there is no yardstick to compare a yellowfin caught by a longline fleet in, say, March with a yellowfin caught by the troll or handline fleets in the same month.

Based on the conversion, Table 2 gives the numbers of yellowfin caught by the 5 fleets in the 1991-92 period, estimates for the HITR and HIHL fleets being given to the nearest integer.

3.4 Initial estimates of catchability

The catchability coefficient q_f for fleet f is related to catch C_f and effort E_f by

$$C_f = q_f E_f P \tag{1}$$

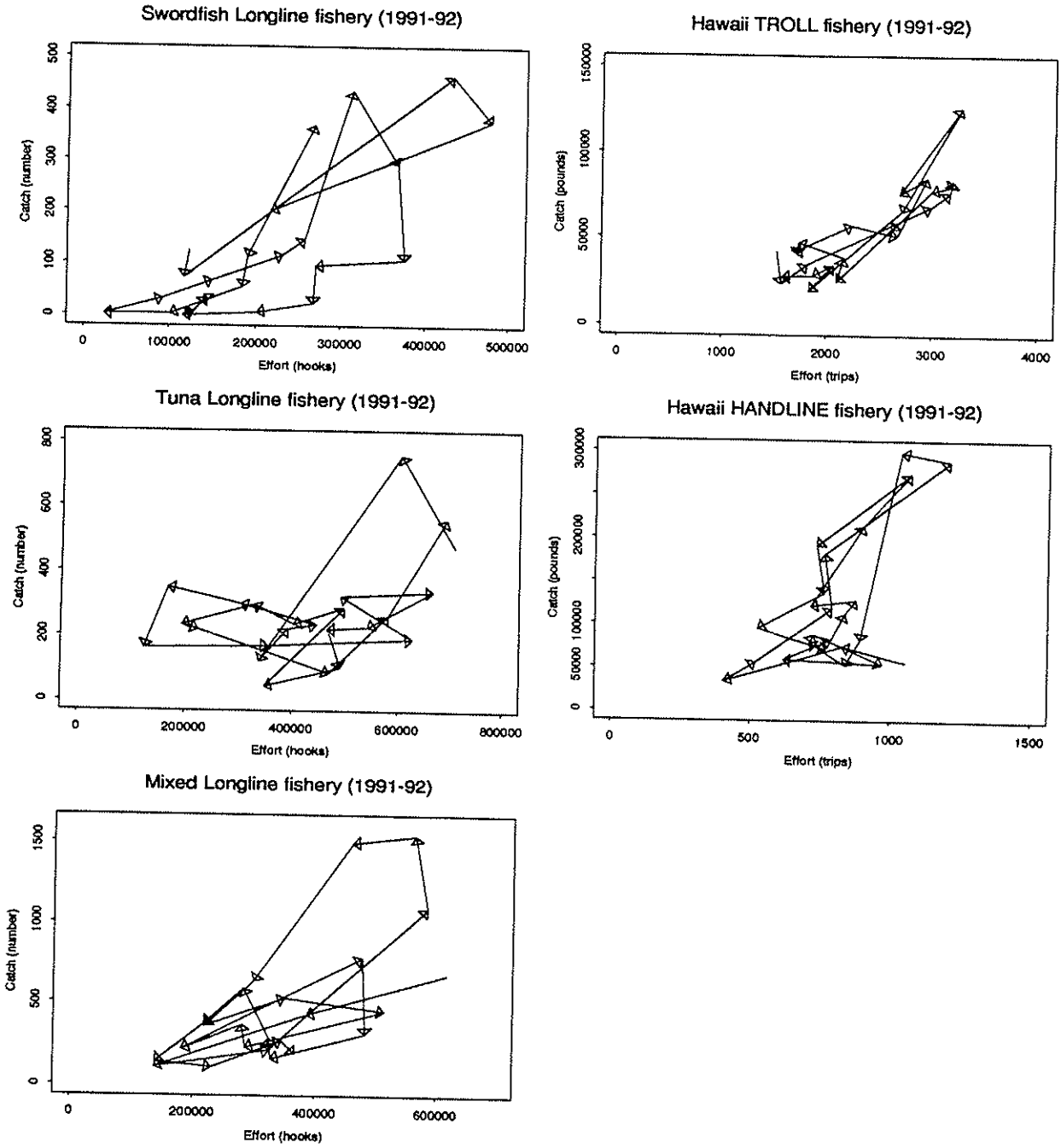

Figure 2: Catch versus effort for the longline, troll, and handline fleets. Data points for these plots come from the monthly indexed data files released by NMFS; for the longline fleets they contain some entries for effort and catch outside the model region. January 1991 effort and catch values are represented by the starting point of the first arrow; successive monthly values are represented by successive vector end points.

Table 1: Average quarterly weight (lb) for a yellowfin caught by troll and handline fleets.

Quarter	Troll	Handline
1st: Jan, Feb, Mar	22.05	26.46
2nd: Apr, May, Jun	50.71	72.75
3rd: Jul, Aug, Sep	79.37	112.44
4th: Oct, Nov, Dec	33.07	41.89

Table 2: Numbers of yellowfin (YF) caught within the model region. For HITR and HIHL fleets, integer estimates are given. Percentages do not sum to 100% due to rounding errors.

Fleet	Number YF caught 1991-92 within model region	Percentage of total
SSLL	2670	2.86%
TTLL	4858	5.20%
MMLL	10269	10.98%
HITR	29527 (est.)	31.58%
HIHL	46177 (est.)	49.39%

where P represents the population of yellowfin; q_f is taken to be a constant throughout the year. The parameters q_f are needed because the available software estimates catch from the effort distribution; the number of recaptures made by each fleet from a release of tags is estimated in the same manner. While P is unknowable, it is possible to estimate the parameters q_f from tag-recapture data (e.g. see Sibert *et al.*, 1996) but in the present case there are little data available and so estimates must be obtained by other means.

We estimate the fleet catchability constants using the catch per unit effort (CPUE) ratios as the starting point. (Section 8.2 recommends a more accurate estimate wherein the catchabilities are allowed to vary monthly.)

Table 3 reports the estimates for fleet catchability obtained. These estimates use CPUEs based only on effort and catch entries for 1° bins *within* the model region and on yields expressed in numbers for the troll and handline fisheries.

The estimates were obtained by treating the data in two blocks: (1) the longline block and (2) the troll and handline block. Within each block, fleet catchability constants are assumed to maintain a fixed relativity. Since catchability is related to gear efficiency, this block treatment is probably more accurate for the longline fleets than the troll and handline fleets.

Starting with q = CPUE for a given fleet, q was systematically reduced by coarse factors

Table 3: Initial CPUE and catchability estimates for the 5 fleets within the model region.

Fleet	CPUE during 1991-92 within model region	Divisor	q_f
SSLL	0.0007675	/800	0.000000959
TTLL	0.0005362	/800	0.000000670
MMLL	0.001511	/800	0.000001889
HITR	0.5295	/16000	0.00003310
HIHL	2.456	/16000	0.0001535

of 10 and fine factors of 2 until the monthly percentages of fish caught in each bin seemed to be at sensible levels. Further adjustments were then made by imposing the restriction that the recapture percentages predicted by simulations be within the 5-10% range. This rather subjective approach lead to the choice of divisors and catchability estimates listed in Table 3. Note that the divisors for each fleet within a given fleet block are the same.

3.5 Establishing inshore and offshore handline fleets

There are distinct differences in the way one group of handliners operates compared to the rest (Boggs, personal communication). During the period 1994-95 NMFS recorded the activities of these handliners, noting that they concentrated on certain offshore fishing grounds. The offshore bins targeted are listed in Table 4 by Hawaii's Aquatic Resource Division (HARD) index, which encodes the geographic coordinates of the southeast corner of a given 1° bin. Catches taken by the 5 fleets in the period 1991-92 are given. Clearly the sites are primarily targeted by handliners.

The proximity of the listed offshore sites to the island of Hawaii is shown in Figure 3. Site 15716 has been added because the weatherbuoy in site 15717 is close to latitude 16° N and there is a possibility of misidentification with the southern site; it will be seen below that extraordinary catches in 15716 confirm it should be added to the offshore handline domain. No catch was attributed to site 16223 in the period 1991-92, so only the other 5 sites will make up the offshore handline domain in this work.

One can use the fleet data sets to verify that certain handliners are predominantly targeting these 5 sites as follows. First note that the product CPUE $\times$ effort gives the recorded catch over the model region for a year if applied to the year's effort distribution. The spatial "catch" is distributed according to the effort field, so while the two catch totals are the same, the distribution of catch based on effort is not the actual catch distribution; however, it should be similar.

Table 4: Catch at Cross Seamount and four weather buoy sites during 1991-92. Catch is in numbers of yellowfin; for the troll and handliners, the numbers are estimated using Table 2. The HDAR code (see text) of each $1°\times1°$ bin is given in double quotes along with the geographic coordinates of its southeast corner. (Note: it will be seen in Section 3.6 that 13-45% of handline catch at Cross and the remaining sites is yellowfin, the remainder being bigeye—this is due to a reporting anachronism.)

Fleet	Cross	Weather Buoys				Percentage
	15818	15717	15217	16019	16223	of fleet
	18N 158W	17N 157W	17N 152W	19N 160W	23N 162W	catch
SSLL	–	–	–	–	–	–
TTLL	417	57	9	79	–	11.6
MMLL	417	–	–	23	3	4.3
HITR	1243	545	–	–	100	6.4
HIHL	9894	7884	1388	1257	–	44.2

Taking the bin-wise ratio of actual catch to effort-distributed catch, one expects unity wherever the effort-distributed catch is the same as the actual catch. The two distributions might be expected to vary by perhaps a factor of 10 either way; in that case reasonable bounds to the variation of the ratio values are 0.1 and 10. In order for effort-distributed catch to be credited, there must have been positive effort expended in a given bin; in isolated instances there may have been effort with no catch. For present purposes, we assign the character "..." to bins where effort is zero; islands and land masses are represented in the same way.

Maps of bin-wise ratios of annual catch to annual effort-distributed catch are given in Figures 4-8 for fleets SSLL, TTLL, MMLL, HITR and HIHL. The position of Hawaii is represented by the small boxed region in each figure. Since the ratios are given to only one decimal place, ratios less than 0.05 appear as "0.0". Figure 9 shows the ratios obtained when the data sets of all 5 fleets are combined.

Figure 9 shows several ratios greater than 10; the sites corresponding to these values coincide with Cross Seamount and the three southernmost weatherbuoy sites originally suggested by NMFS (see Table 4). This suggests that CPUE for these sites is significantly different from those listed in Table 3, but does not identify the fleet(s) responsible.

Strong evidence that handliners are responsible for the high ratios is seen in Figure 8, where each ratio greater than 10 corresponds to one of the 5 southern bins of Figure 3. Note that site 15716 has a ratio value comparable to that at site 15717, which is why it has been added to the offshore handline site list.

Figure 7 also shows several ratios greater than 10, two of which correspond to Cross and site 15717. It is possible that some trips that started out as troll excursions became handline

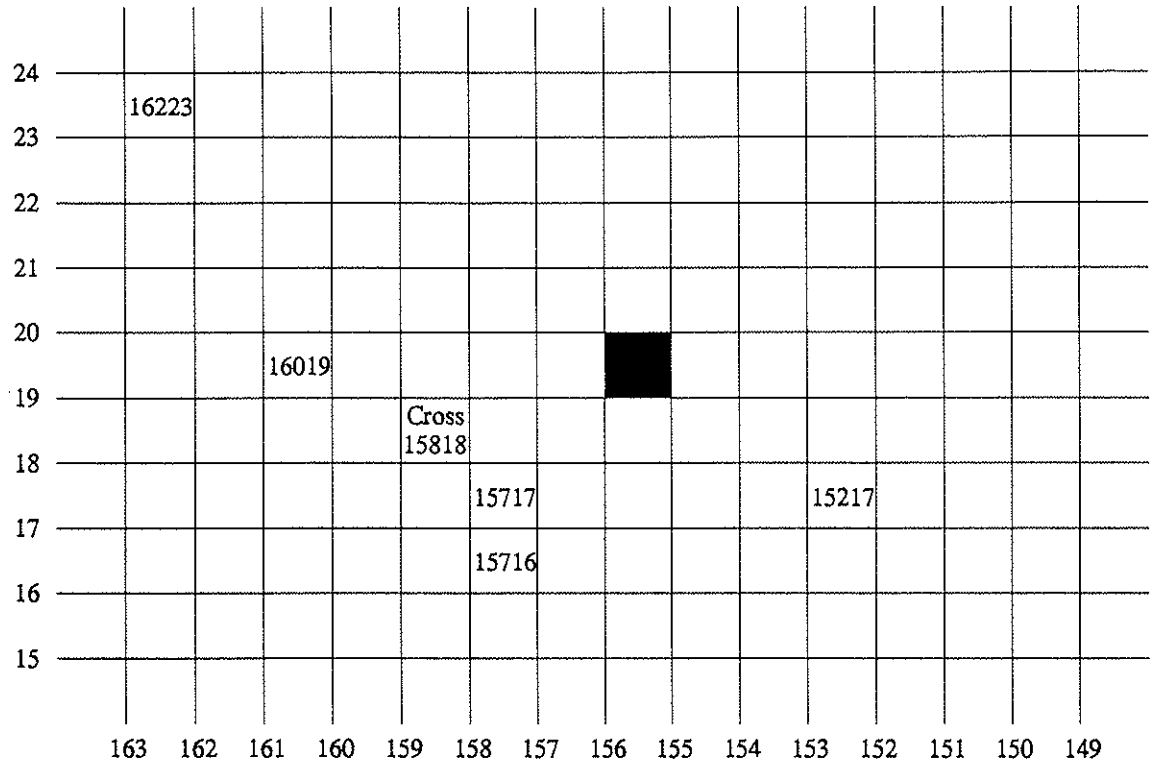

Figure 3: The proximity of offshore handline sites to Hawaii. Site 15716 has been added to the list supplied by NMFS (Honolulu). No catch was reported at site 16223 during 1991–92 so only the southernmost 5 sites will here make up the offshore handline fishing domain.

trips as gear was switched in order to take the unexpectedly high number of fish available; thus some of the HITR figures may represent miscoding. (Alternatively one may contemplate there being two fleets of trollers, one comprising boats that venture farther than others and switch gear as the occasion demands.)

The approach adopted to process these extraordinarily high ratios in both the HITR and HIHL data was to group all catches made at Cross and the four southern weather buoy sites labelled in Figure 3 into an offshore handline fleet coded HIOH and to move catches corresponding to other anomalously high ratios of the HITR data to what remains of the old handline fleet, renamed the inshore handline fleet and coded HIIH. Ratio values for the HIIH and HIOH data are given in Figures 11 and 12. The remaining troll fleet data were allocated to a reduced troll fleet coded HIRT (Hawaii reduced troll) and corresponding ratios appear in Figure 10.

Having restructured the data to exhibit consistency of CPUE value, we learned there was a species reporting problem with the offshore handline data. This is the subject of Section 3.6, to follow. (The ratios given in Figure 12 reflect the resolution of this species reporting problem.)

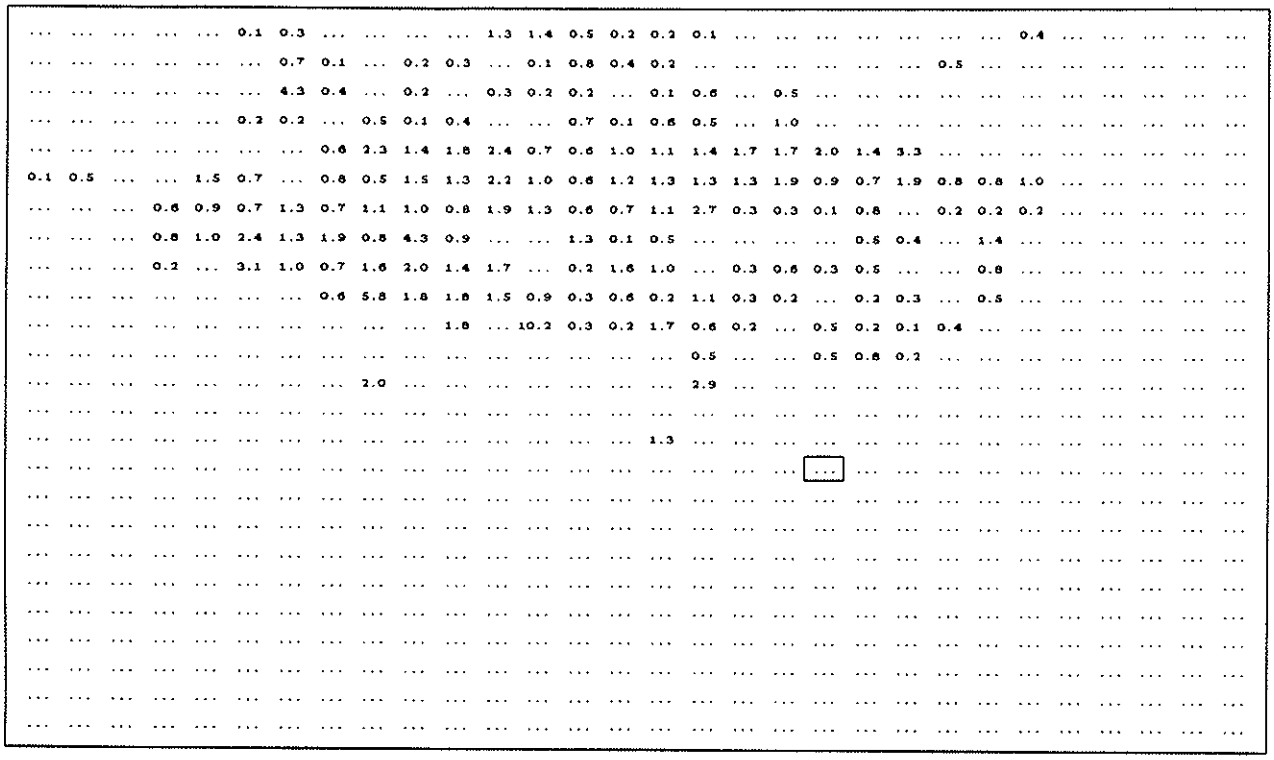

Figure 4: Annual ratios of catch to effort-distributed catch for the SSLL fleet.

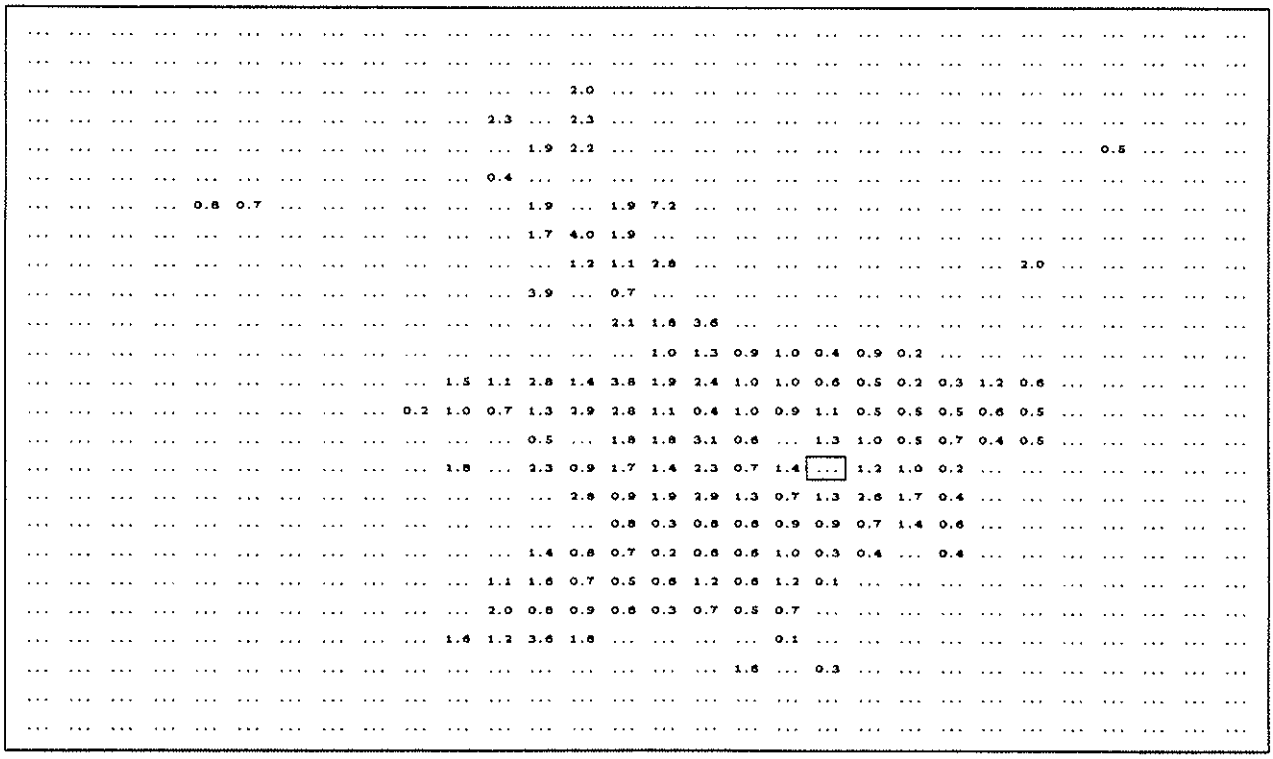

Figure 5: Annual ratios of catch to effort-distributed catch for the TTLL fleet.

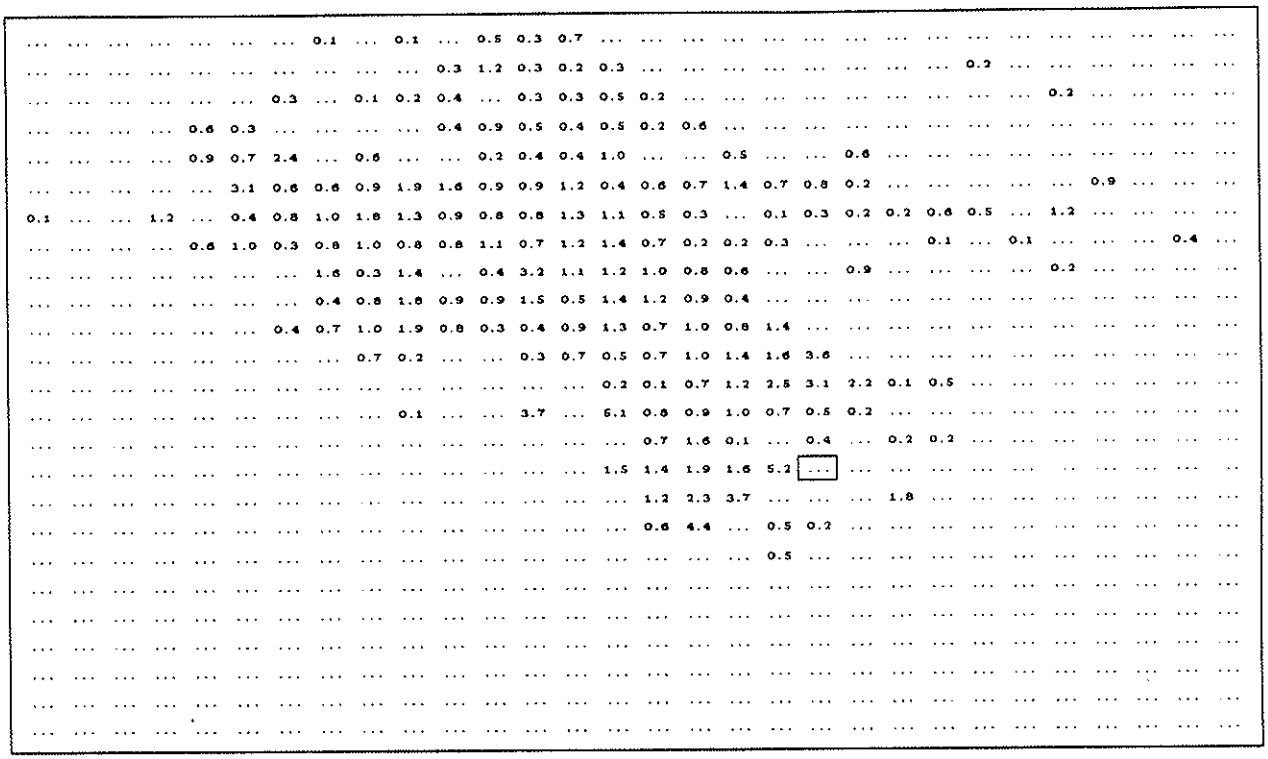

Figure 6: Annual ratios of catch to effort-distributed catch for the MMLL fleet.

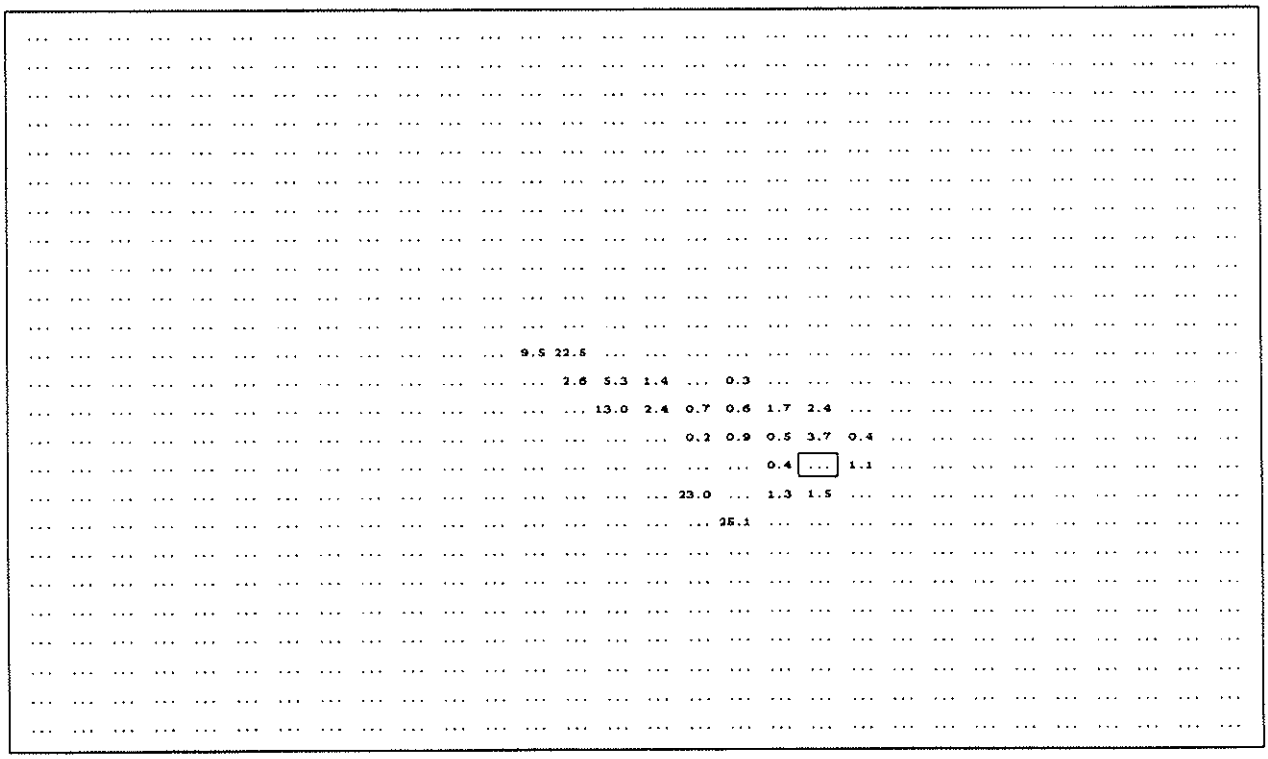

Figure 7: Annual ratios of catch to effort-distributed catch for the HITR fleet.

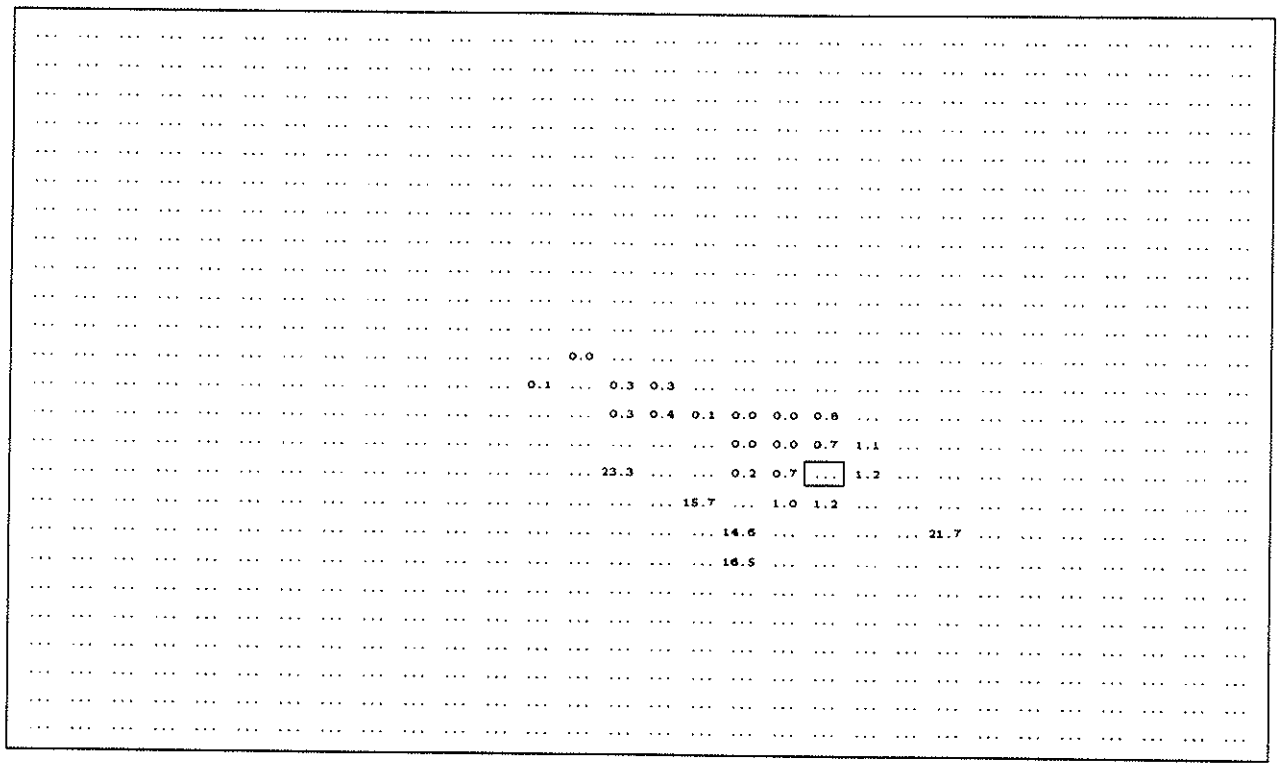

Figure 8: Annual ratios of catch to effort-distributed catch for the HIHL fleet.

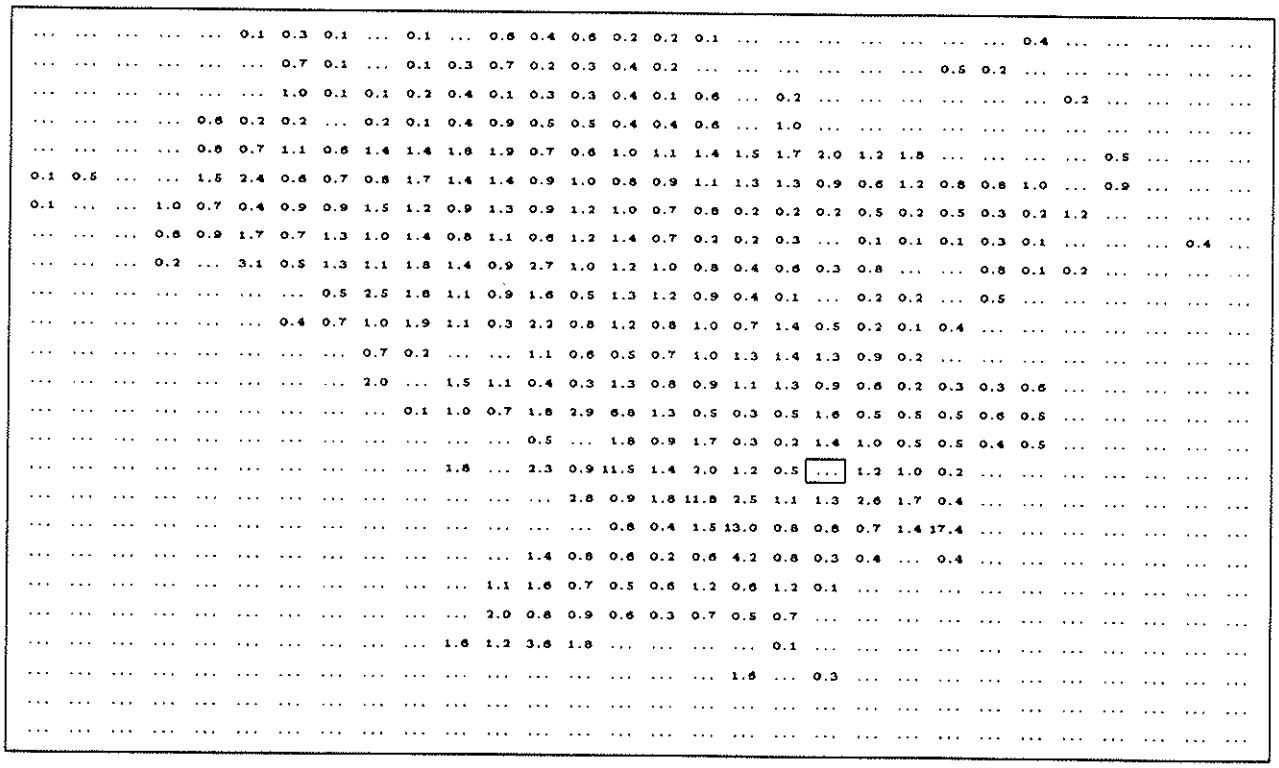

Figure 9: Annual ratios of catch to effort-distributed catch using all fleets (original data).

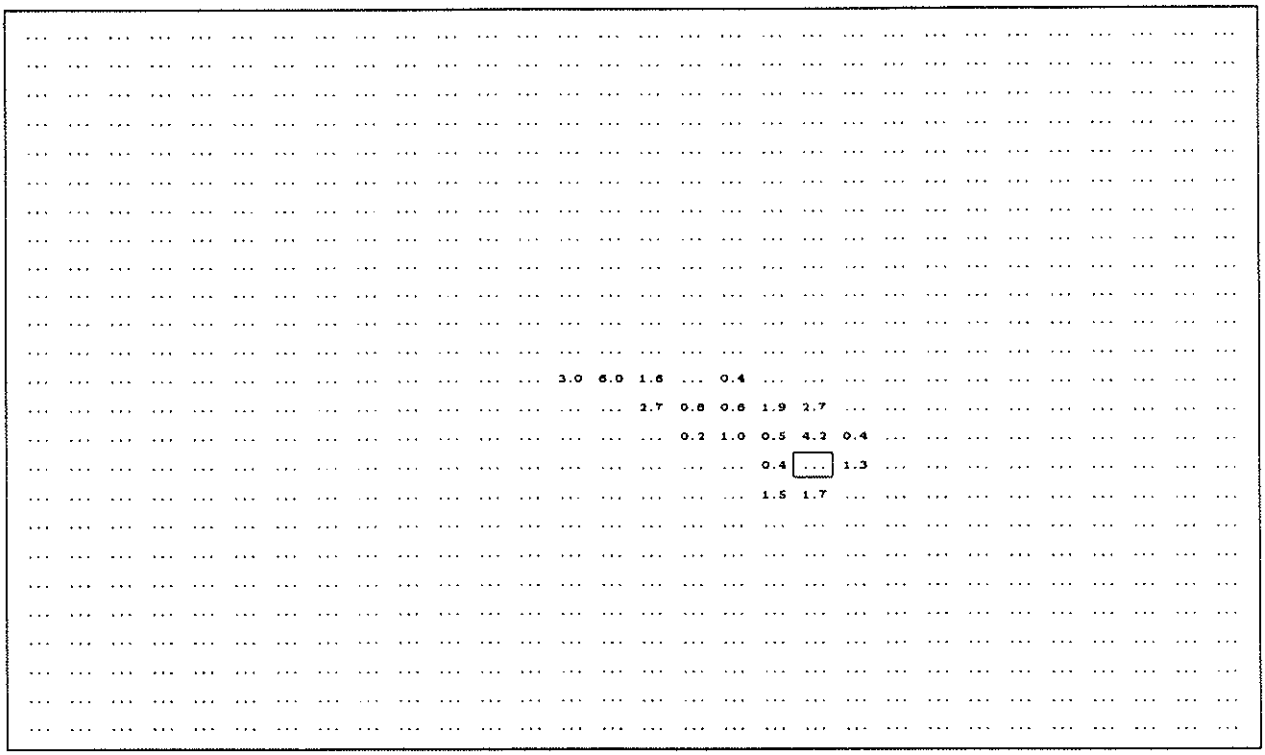

Figure 10: Annual ratios of catch to effort-distributed catch for the HIRT fleet.

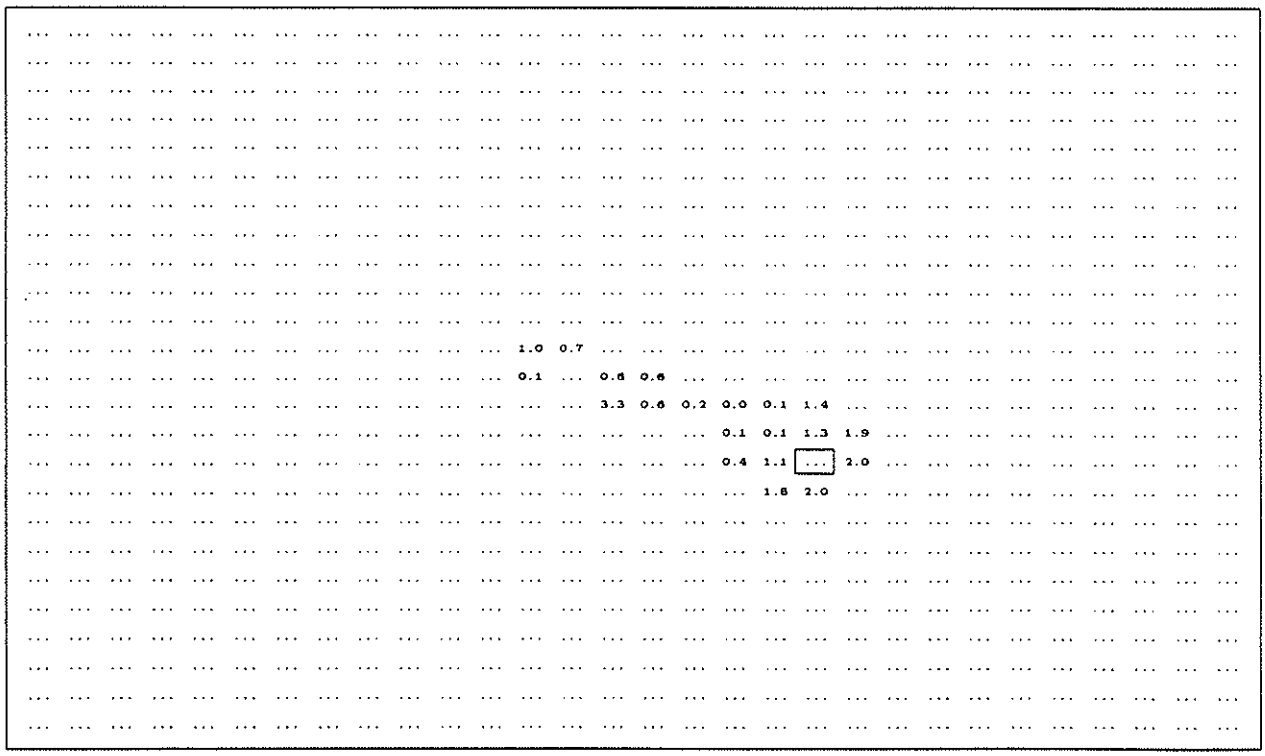

Figure 11: Annual ratios of catch to effort-distributed catch for the HIIH fleet.

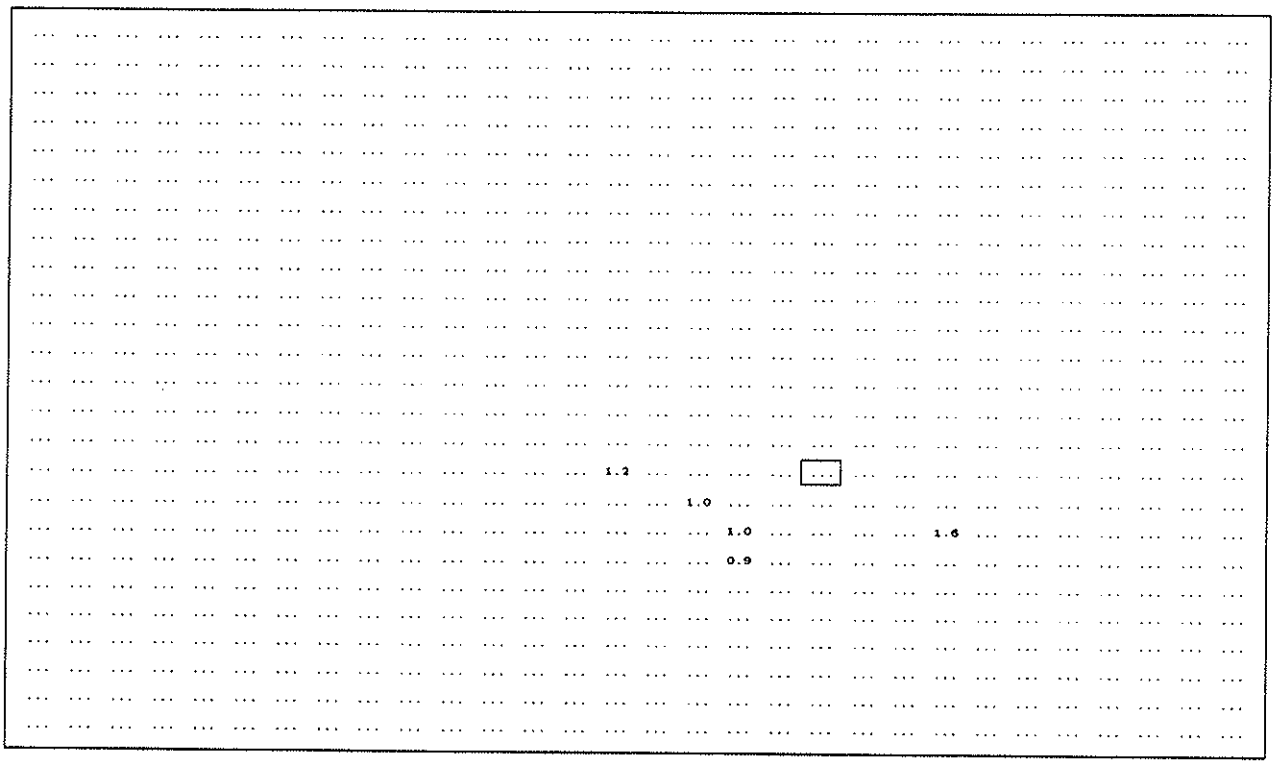

Figure 12: Annual ratios of catch to effort-distributed catch for the HIOH fleet.

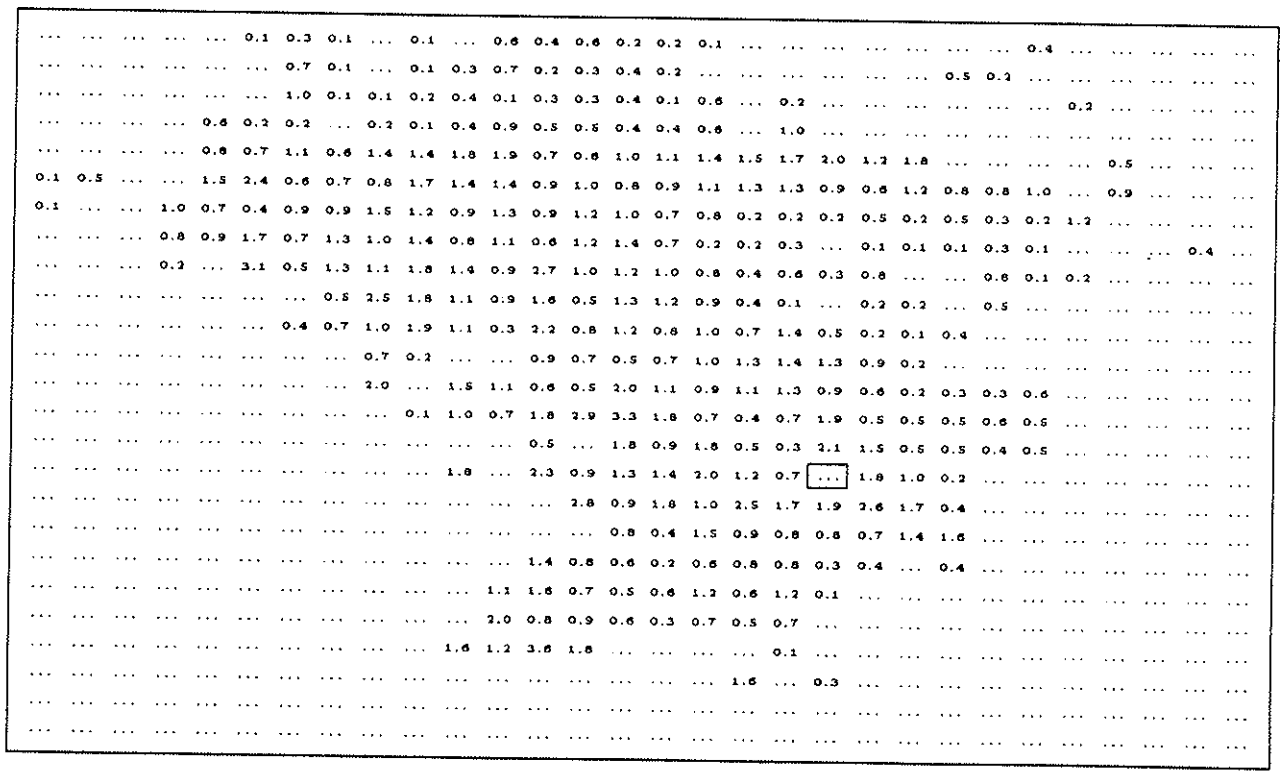

Figure 13: Annual ratios of catch to effort-distributed catch: all fleets (re-allocated data).

The ratios for the longline fleets are generally within the supposed bounds of 0.1 and 10; the only anomalous ratio is 10.2 for the SSLL data (Figure 4) at a site to the northwest of Hawaii. Since this value is close to the upper bound and involves only 25 yellowfin over the period 1991–92, no reorganization of the longline data has been carried out.

Figure 13 shows the effect on ratios when the reorganized data of the HIRT, HIIH, and HIOH fleets are combined with the longline data. Large ratios, betraying anomalous CPUEs, no longer appear. The same is observed in Figures 10-12.

3.6 Ahi (yellowfin and bigeye) coded as "yellowfin"

Offshore handliners report bigeye *and* yellowfin collectively as "ahi" and the Hawaii Aquatic Resources Division codes them as "yellowfin". Thus the offshore handline "yellowfin" component of the original data includes bigeye as well as yellowfin.

NMFS emphasizes that such species mixing is not a problem with the majority of handliners whose catch is correctly classified as yellowfin. The problem is not one of species misidentification but simply a reporting anachronism. A new reporting form is being tested.

The problem needs to be rectified for this study because, without correction, CPUE for the offshore handliners will be overstated. (A side effect of correction is that the offshore data component transferred from the HITR set to the HIOH set is adjusted even though it may not have suffered a reporting problem; this possibility will not be explored here.)

Since information on catch composition at Cross and the weather buoys for 1991 and 1992 is not available, it has to be estimated. We require

1. estimates of actual bigeye and yellowfin composition in offshore handline catch at Cross and the weather buoys,
2. estimates of total "ahi" (i.e. bigeye and yellowfin) and total bigeye catch reported to HARD for these sites, and
3. quarterly estimates of the average weight of yellowfin caught at these sites in order to estimate the numbers of yellowfin caught.

The necessary information is only available for Cross and the adjacent weather buoy. Since catch at the weather buoys is one seventh that at Cross, we suppose the species mix at all offshore handline weatherbuoy sites is the same.

Table 5 gives the percentage mix of bigeye and yellowfin caught in 28 offshore handline trips. Taking quarterly arithmetic means, Table 6 gives quarterly estimates of *observed* species mix in offshore handling catch. We assume these are valid for 1991–92.

Table 5: Percentage bigeye (% BE) observed in 28 offshore handline trips.

Year	Month	% BE	Year	Month	% BE
94	4	97.490	95	3	91.158
94	4	86.563	95	3	89.889
94	5	98.843	95	3	82.263
94	8	74.583	95	3	96.033
94	8	94.585	95	3	58.288
94	8	99.255	95	3	43.888
94	9	75.411	95	3	100.000
94	9	96.186	95	4	97.921
94	9	63.113	95	4	85.043
94	9	64.225	95	4	67.085
94	9	89.324	95	5	89.846
94	11	58.284	95	5	69.080
94	11	18.086	95	8	81.311
94	12	86.910	95	10	56.369

Table 6: Quarterly observed species mix of yellowfin and bigeye in offshore handline trips.

Quarter	Observed % YF	Observed % BE
1	19.8	80.2
2	13.5	86.5
3	18.0	82.0
4	45.1	54.9

Tables 7 and 8 show the percentages of HARD data for Cross and the adjacent weather buoy coded as "yellowfin" and bigeye. Again taking quarterly arithmetic means, this *reported* percentage of "yellowfin" catch is summrized in Table 9.

The rightmost column of Table 10 lists quarterly average weights of yellowfin caught during the 28 offshore handline trips whose species mix is given in Table 5 (data supplied by NMFS). This additional information is used to estimate the numbers of yellowfin in the HIOH data set. We assume the average weights given in Table 1 for the HITR data apply to the new HIRT data and those for HIHL apply to HIIH, and we repeat them here for completeness.

Table 7: 1991-92: HDAR coded "Yellowfin" and Bigeye at Cross and Finch weather buoy.

Year	Month	Cross		Finch weather buoy	
		"Yellowfin"	Bigeye	"Yellowfin"	Bigeye
91	1	57.43	42.57	.	.
91	2	100.00	0.00	73.36	26.64
91	3	.	.	.	.
91	4	90.60	9.40	100.00	0.00
91	5	58.63	41.37	.	.
91	6	84.87	15.13	.	.
91	7	100.00	0.00	.	.
91	8	81.63	18.37	.	.
91	9	100.00	0.00	12.33	87.67
91	10	100.00	0.00	30.02	69.98
91	11	52.98	47.02	88.18	11.82
91	12	100.00	0.00	100.00	0.00
92	1	63.53	36.47	76.08	23.92
92	2	86.19	13.81	82.71	17.29
92	3	75.95	24.05	95.01	4.99
92	4	48.57	51.43	74.38	25.62
92	5	76.47	23.53	84.86	15.14
92	6	77.47	22.53	92.14	7.86
92	7	100.00	0.00	100.00	0.00
92	8	55.05	44.95	100.00	0.00
92	9	96.14	3.86	100.00	0.00
92	10	92.50	7.50	87.80	12.20
92	11	87.50	12.50	87.33	12.67
92	12	70.33	29.67	100.00	0.00

3.7 Six fleets and final catchability estimates

Reorganization of the troll and handline data into three fleets together with the resolution of the species miscoding problem requires that Table 2 be recalculated as follows (Table 11).

These new numbers provide the CPUE values and catchability estimates given in Table 12 and will be used in the modeling simulations.

Table 8: 1993-94: HDAR coded "Yellowfin" and Bigeye at Cross and at Finch weather buoy.

Year	Month	Cross		Finch weather buoy	
		"Yellowfin"	Bigeye	"Yellowfin"	Bigeye
93	1	79.49	20.51	100.00	0.00
93	2	87.51	12.49	100.00	0.00
93	3	80.52	19.48	.	.
93	4	100.00	0.00	.	.
93	5	92.08	7.92	.	.
93	6	94.30	5.70	.	.
93	7	88.07	11.93	100.00	0.00
93	8	80.27	19.73	100.00	0.00
93	9	94.23	5.77	100.00	0.00
93	10	100.00	0.00	100.00	0.00
93	11	99.32	0.68	100.00	0.00
93	12	83.63	16.37	100.00	0.00
94	1	90.02	9.98	95.10	4.90
94	2	31.38	68.62	100.00	0.00
94	3	76.21	23.79	28.42	71.58
94	4	67.96	32.04	42.90	57.10
94	5	57.72	42.28	75.83	24.17
94	6	46.15	53.85	100.00	0.00
94	7	100.00	0.00	100.00	0.00
94	8	100.00	0.00	0.00	100.00
94	9	77.15	22.85	50.56	49.44
94	10	57.97	42.03	71.85	28.15
94	11	77.60	22.40	40.86	59.14
94	12	71.18	28.82	100.00	0.00

Table 9: Quarterly HDAR reported "yellowfin" catch at Cross and weather buoy 15717.

[Quarter	Reported % "YF" at Cross	Reported % "YF" at "15717"
1	75.3	83.4
2	74.6	81.4
3	89.4	76.3
4	82.8	83.8

Table 10: Conversion table: average quarterly weight (lb) for yellowfin caught by the HIRT, HIIH and HIOH fleets.

Quarter	Troll	Handline	
		Inshore	Offshore
	HIRT	HIIH	HIOH
1	22.05	26.46	13.28
2	50.71	72.75	31.73
3	79.37	112.44	22.22
4	33.07	41.89	27.99

Table 11: Numbers of yellowfin caught within the model region. For HIRT, HIIH and HIOH fleets, integer estimates are given. (Compare with Table 2.)

Fleet	Number YF caught 1991-92 within model region	Percentage of total
SSLL	2670	3.16
TTLL	4858	5.74
MMLL	10269	12.14
HIRT	26221 (est.)	31.00
HIIH	26376 (est.)	31.19
HIOH	14182 (est.)	16.77

Table 12: Final CPUE figures and catchability estimates for the 6 fleets in the model region.

Fleet	CPUE during 1991-92 within model region	Divisor	q_f
SSLL	0.0007675	/800	0.000000959
TTLL	0.0005362	/800	0.000000670
MMLL	0.001511	/800	0.000001889
HIRT	0.4734	/16000	0.00002958
HIIH	1.427	/16000	0.00008916
HIOH	20.80	/16000	0.001300

4 Mathematical Model

The mathematical model used in this analysis is based on that of Sibert and Fournier (1994). Let $\tilde{N}(x, y, t; c)$ be the density of tags at point (x, y) in the ocean at time t making up tag release cohort c. The aggregate density of tags from all cohorts released to time t is given by

$$N(x, y, t) = \sum_{c=1}^{C_t} \tilde{N}(x, y, t; c) .$$

N is assumed to satisfy the advection-diffusion-mortality equation

$$\frac{\partial N}{\partial t} + \frac{\partial uN}{\partial x} + \frac{\partial vN}{\partial y} = \frac{\partial}{\partial x}\left(D_x \frac{\partial N}{\partial x}\right) + \frac{\partial}{\partial y}\left(D_y \frac{\partial N}{\partial y}\right) - ZN \tag{2}$$

where the advection parameters (u, v) are interpreted as the directed components of behavioral movement and the diffusion parameters D_x, D_y as the random components of behavioral movement; D_x, D_y are positive quantities on physical and dimensional grounds. Here, however, D_x, D_y will be replaced by a single parameter $D = D(x, y, t)$, thereby halving the number of random movement parameters to be estimated; the use of two random movement parameters is recommended for future research (see Section 8.1).

Boundary and initial conditions are required to complete the specification of (2).

Either closed or open boundary conditions can be used. Closed conditions should be specified around islands and along continental coastlines. Closed conditions along external model boundaries should also be specified if the entire habitat is modelled or if there is strong reason to believe the tags do not venture outside the model region (to a significant extent) during the simulation. In this case, a reflection condition on N is used together with an impermeability condition on the normal directed component of movement. Thus

$$\begin{aligned} \frac{\partial N}{\partial x} &= 0 \quad \text{and} \quad u = 0 \quad \text{on eastern and western closed boundaries, and} \\ \frac{\partial N}{\partial y} &= 0 \quad \text{and} \quad v = 0 \quad \text{on northern and southern closed boundaries.} \end{aligned}$$

These conditions can be used to ensure that tag numbers are conserved in the numerical model when both natural and fishing mortality are zero.

Open boundary conditions should be specified along external boundaries if a subset of the known habitat is modelled and there is good reason to believe that once fish leave the model domain, they do not return. In this case, the advective flux of tags across a given boundary is assumed to be that of tags nearby; for example,

$$\left.\frac{\partial uN}{\partial x}\right|_b = \left.\frac{\partial uN}{\partial x}\right|_i$$

where b denotes a point on the external boundary and i denotes an interior point close to the boundary. The diffusive flux of tags near external boundaries is assumed to be zero; for example,

$$\frac{\partial}{\partial x}\left(D\frac{\partial N}{\partial x}\right)\bigg|_i = 0$$

where i again denotes an interior point close to the external boundary.

The initial condition used for N is

$$N(x,y,0) = \begin{cases} \sum_c \tilde{N}(x_c, y_c, 0; c) & \text{over all tag release sites,} \\ 0 & \text{at other sites,} \end{cases}$$

where $\tilde{N}(x_c, y_c, 0; c)$ is the number of tags released at point (x_c, y_c) in tag cohort c at time 0. In the case of a cohort release s at a subsequent time t_s and position (x_s, y_s), the density of tags at that point is assigned to be the sum of its present value and the cohort contribution, i.e.

$$N(x_s, y_s, t_s) \leftarrow N(x_s, y_s, t_s) + \tilde{N}(x_s, y_s, t_s; s)\,.$$

To highlight the importance of the relative strengths of the directed and random components of behavioral movement, we non-dimensionalize (2) using

$$x^* = x/L, \quad y^* = y/B \quad \text{and} \quad t^* = t/T,$$

where L and B are characteristic length scales (such as the length and breadth of the model domain) and T is a characteristic time scale (such as the duration of a model simulation or the period of supposed migration). We further substitute

$$u^* = u/U, \quad v^* = v/V \quad \text{and} \quad D^* = D/D_0$$

where (U, V) is a characteristic vector of directed movement in the x and y directions, and D_0 is a characteristic value of random movement. There is nothing to be gained by scaling N since the relative tag distribution remains the same after such a scaling. Upon substitution,

$$\frac{\partial N}{\partial t^*} + U\frac{T}{L}\frac{\partial u^* N}{\partial x^*} + V\frac{T}{B}\frac{\partial v^* N}{\partial y^*} = D_0\frac{T}{L^2}\frac{\partial}{\partial x^*}\left(D^*\frac{\partial N}{\partial x^*}\right) + D_0\frac{T}{B^2}\frac{\partial}{\partial y^*}\left(D^*\frac{\partial N}{\partial y^*}\right) - (TZ)N$$

from which global Peclet numbers may be defined in the x and y directions as the respective ratios of the coefficients of directed and random movement:

$$Pe(x) = \frac{UL}{D_0} \quad \text{and} \quad Pe(y) = \frac{VB}{D_0}\,.$$

If Pe is small the random component of movement dominates; if Pe is large the directed component dominates (Neuman, 1981). The values of the Peclet numbers are important in the numerical approximation of Equation (2) (see next section). Global Peclet numbers are useful characterizations of uniform movement; for the more usual case of non-uniform movement, Pe may vary from point to point so we define local Peclet numbers by replacing the global values U, V, L, B and D_0 with local values; for example, L and B could be replaced by the grid element dimensions Δx and Δy in a numerical model.

5 Finite difference solution

The Alternating Direction Implicit (ADI) scheme (Press et al., p. 856, 1992) is used to solve the finite difference form of (2). A regular grid of $1° \times 1°$ squares is used (Figure 1) and grid points are located at the centers of the squares. Tag density N and the movement parameters u, v, D are defined at each grid point.

The ADI approach uses two implicit sweeps of the model domain, the first in the x direction over the first half time step and the second in the y direction over the second half time step. The method is unconditionally stable, meaning that local instabilities are not amplified by the solution process. In the present application, ADI is also computationally efficient because the systems of equations solved are tridiagonal. Further details of the ADI method can be found in Sibert and Fournier (1994).

5.1 Finite difference approximations

If n denotes the entry time level and $(n+1)$ the exit level, the time derivative in (2) at position $(i\Delta x, j\Delta y)$ is differenced as

$$\left.\frac{\partial N}{\partial t}\right|_{i,j}^{n+1} \simeq \frac{N_{i,j}^{n+1} - N_{i,j}^{n}}{\Delta t}.$$

Subscripts i and j specify the spatial location of a grid point as being $(i\Delta x, j\Delta y)$; superscript n specifies time $n\Delta t$.

Two approaches for approximating the first derivatives in the directed movement terms are considered: approximation by first-order backward differencing, known as "upwind" or "upstream" differencing (Roache, 1972; Press et al., 1992; Sibert and Fournier, 1994) and approximation by second-order centered-space differencing.

Upwind differencing is robust but contributes numerical (i.e. non-physical) diffusion to the solution field (O'Brien, 1986; see also Appendix 10.1) which may confound the estimation of the actual (i.e. physical) random movement parameter values when applied to real data. In spite of this feature, upwind differencing is often used since it has the advantage of not introducing negative densities; in practice one cannot justify negative tag densities, so solutions generated by the finite difference scheme should be positive. Upwind differencing may also be used in the early stages of parameter estimation when parameter values are either guessed or inferred from observation. (Finite difference equations at the first half time step for the upwind scheme are given in Appendix 10.2. Equations for the full time step can be stated by analogy.) Upwind differencing of the directed movement terms takes the form

$$\left.\frac{\partial uN}{\partial x}\right|_{i,j}^{n} \simeq \begin{cases} \frac{u_{i,j}\,N_{i,j}^{n} - u_{i-1,j}\,N_{i-1,j}^{n}}{\Delta x}, & u_{i,j} > 0 \\ \frac{u_{i+1,j}\,N_{i+1,j}^{n} - u_{i,j}\,N_{i,j}^{n}}{\Delta x}, & u_{i,j} < 0 \end{cases}, \quad \left.\frac{\partial vN}{\partial y}\right|_{i,j}^{n} \simeq \begin{cases} \frac{v_{i,j}\,N_{i,j}^{n} - v_{i,j-1}\,N_{i,j-1}^{n}}{\Delta y}, & v_{i,j} > 0 \\ \frac{v_{i,j+1}\,N_{i,j+1}^{n} - v_{i,j}\,N_{i,j}^{n}}{\Delta y}, & v_{i,j} < 0 \end{cases}.$$

Centered-space differencing is more accurate than upwind differencing provided the dimensionless Peclet numbers (see Section 4) are not greater than two (Price *et al.*, 1966; Roache, 1972; Leonard, 1979; Neuman, 1981; Noye, 1987; Abbott and Basco, 1989); if greater than two, grid-scale oscillations are introduced to the solution field and may lead to the prediction of negative densities. (The finite difference equation at the first half time step level for the centered-space scheme is given in Appendix 10.2.) The requirement for non-oscillatory numerical solutions at position (i, j) during a given season is

$$|Pe(x)|_{i,j} = \frac{|u_{i,j}|\Delta x}{D_{i,j}} \leq 2 \quad \text{and} \quad |Pe(y)|_{i,j} = \frac{|v_{i,j}|\Delta y}{D_{i,j}} \leq 2\,. \tag{3}$$

Huyakorn and Pinder (1983) state: "In most cases involving non-uniform flow, acceptable numerical solutions with very mild oscillations are achieved even when the local Peclet number is as high as 10" (ibid, p. 206). Centered-space differencing of the directed movement terms takes the form

$$\left.\frac{\partial uN}{\partial x}\right|_{i,j}^{n} \simeq \frac{u_{i+1,j}\,N^n_{i+1,j} - u_{i-1,j}\,N^n_{i-1,j}}{2\Delta x}\,, \qquad \left.\frac{\partial vN}{\partial y}\right|_{i,j}^{n} \simeq \frac{v_{i,j+1}\,N^n_{i,j+1} - v_{i,j-1}\,N^n_{i,j-1}}{2\Delta y}\,.$$

Inspection of Table 2 from Sibert *et al.* (1996) indicates that the Huyakorn and Pinder (1983) criterion is met for most regions in a two season model of the western Pacific used to estimate skipjack movements from tag-recapture data; the parameter values are determined using upwind differencing and instead of calculating Peclet numbers, they calculate an *ichthyokinematic ratio* which takes the form of a Peclet number with u and v replaced by $r = \sqrt{u^2 + v^2}$. The criterion is not met only where the estimates for the random movement parameter are low. These low estimates are physically unrealistic and are due to the dispersive nature of the upwind method. If centered-space differencing is used, the estimates for random movement in these regions are increased and the Huyakorn and Pinder criterion is met everywhere. Table 13 reproduces the relevant part of Table 2 from Sibert *et al.* and lists the greater of the two Peclet values associated with each set of parameter estimates using upwind and centered-space differencing.

The second derivatives in the random movement terms are approximated by three-point central differences and have the form

$$\begin{aligned}
\left.\frac{\partial}{\partial x}\left(D\frac{\partial N}{\partial x}\right)\right|_{i,j}^{n} &\simeq N^n_{i-1,j}\,\frac{D_{i-1,j} + D_{i,j}}{2(\Delta x)^2} - N^n_{i,j}\,\frac{D_{i-1,j} + 2D_{i,j} + D_{i+1,j}}{2(\Delta x)^2} + N^n_{i+1,j}\,\frac{D_{i,j} + D_{i+1,j}}{2(\Delta x)^2}, \\
\left.\frac{\partial}{\partial y}\left(D\frac{\partial N}{\partial y}\right)\right|_{i,j}^{n} &\simeq N^n_{i,j-1}\,\frac{D_{i,j} + D_{i,j-1}}{2(\Delta y)^2} - N^n_{i,j,}\,\frac{D_{i,j-1} + 2D_{i,j} + D_{i,j+1}}{2(\Delta y)^2} + N^n_{i,j+1}\,\frac{D_{i,j+1} + D_{i,j}}{2(\Delta y)^2}.
\end{aligned}$$

Mortality Z is separated into two components according to

$$Z^n_{i,j} = M + \sum_f F^n_{i,j;f}$$

Table 13: Parameter estimates and corresponding Peclet numbers derived from the SSAP (Skipjack Survey and Assessment Programme, 1977-1982) skipjack data set using upwind and centered-space differencing for the directed movement terms. Peclet number is calculated using $|Pe| = 30 \max\{|u|\Delta x, |v|\Delta y\}/D$ where (u, v) (nm/dy) are the parameters for directed movement and D (nm^2/mo) is the parameter for random movement; the 30 factor is required for unit scaling (30 dy = 1 mo).

Season 1	UPWIND estimates					CENTERED-SPACE estimates			
Region	u	v	D	$\|Pe\|$		u	v	D	$\|Pe\|$
1	4.67	−0.15	7097	1.18		4.78	0.13	10273	0.84
2	0.25	−4.16	14811	0.51		2.14	−3.30	8573	0.69
3	−5.00	−0.36	84576	0.11		−4.86	−1.20	95219	0.09
4	−0.46	−0.41	15666	0.05		−1.22	−0.93	21108	0.10
5	−1.00	0.28	250	7.18		−0.91	0.56	432	3.77
6	−1.09	2.13	5431	0.71		1.66	1.65	1413	2.11
7	−0.26	−0.91	0	$\gg 1$		0.39	−0.15	966	0.72
8	−17.77	1.00	56448	0.57		−16.68	0.79	47479	0.63
9	−0.03	0.79	11658	0.12		−0.18	0.50	491	1.82
10	0.95	2.39	35	$\gg 1$		1.85	1.51	1896	1.76

Season 2	UPWIND estimates					CENTERED-SPACE estimates			
Region	u	v	D	$\|Pe\|$		u	v	D	$\|Pe\|$
1	2.27	−2.07	19207	0.21		2.21	−1.73	14967	0.27
2	4.68	0.98	3006	2.80		3.21	0.65	5287	1.09
3	6.82	10.05	148720	0.12		5.21	12.00	240989	0.09
4	−3.65	−0.72	32531	0.20		−5.10	−0.95	34336	0.27
5	−2.50	−6.47	8895	1.31		−1.98	−5.03	5035	1.80
6	6.47	1.05	8773	1.33		5.73	2.66	16138	0.64
7	1.82	0.03	8786	0.37		0.72	−0.42	9885	0.13
8	1.23	−4.12	2470	3.01		1.13	−0.40	329	6.18
9	0.29	2.85	0	$\gg 1$		−0.58	0.58	521	2.00
10	−0.49	−1.25	321	6.99		−1.15	−0.67	1035	2.01

where $F^n_{i,j;f}$ is fishing mortality due to fleet f operating in grid element (i, j) at time level n and M is mortality due to other causes or "natural" mortality. Natural mortality is assumed to be constant throughout for all time. Fishing mortality is assumed to be a simple function of observed fishing effort, viz.

$$F^n_{i,j;f} = q_f E^n_{i,j;f} \tag{4}$$

where $E^n_{i,j;f}$ is the observed fishing effort of fleet f operating in grid box (i, j) at time level n and q_f is a fleet specific proportionality constant or catchability coefficient. This formulation

for fishing mortality allows fishing effort to be specified for each fleet at the spatial and temporal resolution of the model. For a given fleet, q_f is spatially and temporally constant but may, in principle, be varied by month (see Section 8.2).

5.2 Boundary and initial conditions

Boundary and initial conditions must be specified in order to solve the finite difference equations derived for Equation (2).

The numerical implementation of closed boundary conditions for upwind and centered-space schemes differs only for the directed movement parameters. Consider the one-dimensional grid point lattice of Figure 14. In the x direction, the reflection conditions on N at each boundary have the numerical counterparts:

$$N_0 = N_1 \quad \text{and} \quad N_{I+1} = N_I \,.$$

If upwinding is used, the impermeability condition is differenced as

$$\begin{cases} u_0 = 0 & \text{and} \quad u_I = 0 \quad \text{when} \quad u < 0\,, \\ u_1 = 0 & \text{and} \quad u_{I+1} = 0 \quad \text{when} \quad u > 0 \end{cases}$$

and guarantees tag conservation in the absence of mortality. If the centered-space scheme is used, the impermeability condition at both ends is differenced as

$$u_0 = -u_1 \quad \text{and} \quad u_{I+1} = -u_I$$

and is tag conservative from one time level to the next if there is no natural or fishing mortality.

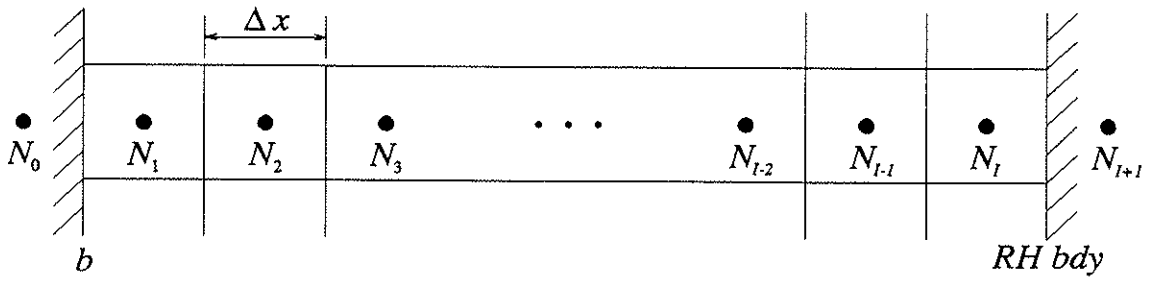

Figure 14: Grid setup showing grid point labels and closed boundaries.

Consider now the application of open boundary conditions at the left hand boundary b in Figure 15. A second order convergent approximation for the quantity uN at position $i = 0$ is used:

$$u_0 N_0 = 2u_1 N_1 - u_2 N_2$$

and gives rise to a first order convergent approximation for advective flux at the open boundary. If diffusive flux in the x direction is assumed to be zero at $i = 1$, the implied boundary condition is

$$N_0(D_0 + D_1) = N_1(D_0 + 2D_1 + D_2) - N_2(D_1 + D_2)\,.$$

Model elements are partitioned into regions (see Section 5.4) in which the movement parameters u, v, D are constant throughout a season. Because the width of regions bordering open boundaries is generally greater than two elements, the two expressions given above reduce to the linear approximation

$$N_0 = 2N_1 - N_2\,.$$

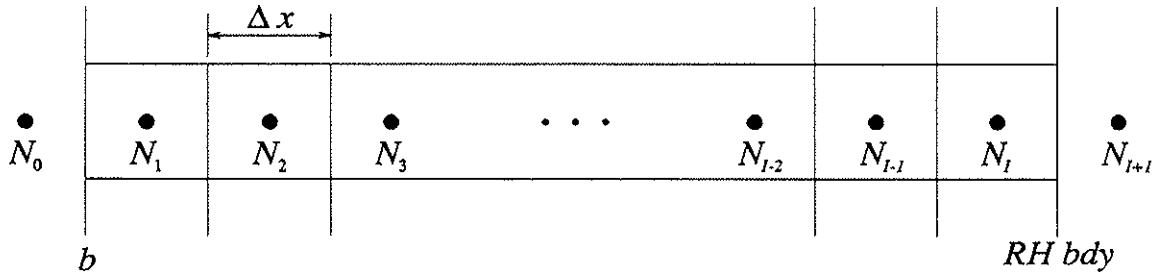

Figure 15: Grid setup showing grid point labels and open boundaries.

The initial conditions used are: $N^0_{i,j} = 0$ everywhere except where there is a release of tags, when N is set accordingly. For tag releases that occur after time 0, tag density at the corresponding positions is reassigned as the sum of the current and release values.

5.3 Conditions for non-negative values

When the time dependent advection-diffusion-mortality equation (2) has non-negative boundary and initial conditions, its solution must be non-negative for all time. This property should be reflected in the numerical solutions of Equation (2).

By considering the coefficients of the finite difference equations used in the ADI solver, sufficient conditions can be established to ensure that each field of non-negative tag values is replaced with another field of non-negative values (see Appendix 10.3).

Upwind form

Consider the first ADI equation in upwind form, represented in the appendix by the set of Equations (10).

The equations first have to be rearranged and expressed in standard form (12). If the movement parameters are taken to be global constants u, v, D, the requirement for strict diagonal dominance (13) becomes

$$\frac{2}{\Delta t} + (F_{i,j} + M) > 0$$

and is satisfied everywhere. The non-negativity condition (14) requires that,
for $u < 0$,

$$D \geq 0 \text{ and } Pe(x) \leq 1$$

$$\text{and} \quad \begin{cases} 0 \leq D \leq \frac{(\Delta y)^2}{\Delta t} + \frac{v\Delta y}{2}, & Pe(y) \leq 1, \quad v < 0 \\ 0 \leq D \leq \frac{(\Delta y)^2}{\Delta t}, & v = 0 \\ 0 \leq D \leq \frac{(\Delta y)^2}{\Delta t} - \frac{v\Delta y}{2}, & Pe(y) \geq -1, \quad v > 0\,; \end{cases}$$

for $u = 0$,

$$D \geq 0$$

$$\text{and} \quad \begin{cases} 0 \leq D \leq \frac{(\Delta y)^2}{\Delta t} + \frac{v\Delta y}{2}, & Pe(y) \leq 1, \quad v < 0 \\ 0 \leq D \leq \frac{(\Delta y)^2}{\Delta t}, & v = 0 \\ 0 \leq D \leq \frac{(\Delta y)^2}{\Delta t} - \frac{v\Delta y}{2}, & Pe(y) \geq -1, \quad v > 0\,; \end{cases}$$

for $u > 0$,

$$D \geq 0 \text{ and } Pe(x) \geq -1$$

$$\text{and} \quad \begin{cases} 0 \leq D \leq \frac{(\Delta y)^2}{\Delta t} + \frac{v\Delta y}{2}, & Pe(y) \leq 1, \quad v < 0 \\ 0 \leq D \leq \frac{(\Delta y)^2}{\Delta t}, & v = 0 \\ 0 \leq D \leq \frac{(\Delta y)^2}{\Delta t} - \frac{v\Delta y}{2}, & Pe(y) \geq -1, \quad v > 0\,. \end{cases}$$

A similar set of conditions arises for the set of ADI equations used for the second half time step. (If the recommendation of Section 8.1 were implemented, the generic variable D in the above conditions would be replaced by D_x in association with u and by D_y in association with v.)

If these conditions are satisfied in the case of globally constant parameters u, v, D, successive predictions for N based on initially non-negative values remain non-negative.

Centered-space form

Consider the first ADI equation in centered-space form, Equation (11).

The equation is first rewritten in the form (12) and again, if the movement parameters are taken to be global constants u, v, D, the requirement for strict diagonal dominance (13) gives

$$\frac{2}{\Delta t} + (F_{i,j} + M) > 0$$

and is met everywhere. Requirement (14) then gives rise to the conditions

$$|Pe\{x\}| \leq 2, \quad |Pe\{y\}| \leq 2 \quad \text{and} \quad D \leq \frac{\Delta y^2}{\Delta t}.$$

The same set of conditions arises by studying the coefficients of the set of ADI equations for the second half time step. (Again, if the recommendation of Section 8.1 were implemented, D in these conditions would be replaced by D_y, and D in the conditions for the second centered-space equation would be replaced by D_x.)

Thus if the Peclet constraints for non-oscillatory solutions are satisfied and the random movement parameter is bounded as shown, successive non-negative solutions result if the parameters u, v, D are global constants. These non-negativity constraints are more restrictive than those for the upwind scheme.

Caution

For the Hawaiian Islands tag-recapture model, the movement parameters are not global constants; they vary regionally and seasonally. Thus the conditions derived for the upwind and centered-space schemes cannot be applied literally except within specific regions and seasons; deviations from non-negative behavior may still occur across region boundaries and from season to season in a model where u, v and D are spatially and temporally variable.

5.4 Regionalization and re-parameterization

The numerical solution of (2) requires the specification of each model parameter at each grid point. In the present case this implies specifying $25 \times 30 = 750$ values of u, v, D and Z in Equation (2) at each time step for simulations of at least 2 years duration. Even if a large number of tag recaptures are available, direct estimation of so many parameters is impractical. Thus a means of reducing the number of parameters is required.

Tuna movement patterns are frequently represented by arrows on maps, often with months or seasons specified, to suggest general population movement at specific times and places (see Hunter *et al.*, 1986, for examples). Such presentations suggest subregional averaged movement over the given period of time. We borrow from this description by defining *regions* within the model as subdivisions of grid elements within which the movement parameters u, v

and D are constant; a *season* is defined as the period of time during which these parameters are constant.

Let $[R_{i,j}]$ be a matrix containing the region number for each model element indexed by (i,j) and let $[S^n]$ be a vector containing the season for each time step indexed by n; $[R_{i,j}]$ maps the model domain into specific regions and $[S^n]$ maps calendar time to seasons. The model parameters are specified at each grid point by

$$[u^n_{i,j}] = \mathcal{U}_{[R_{i,j}][S^n]}, \quad [v^n_{i,j}] = \mathcal{V}_{[R_{i,j}][S^n]} \quad \text{and} \quad [D^n_{i,j}] = \mathcal{D}_{[R_{i,j}][S^n]}\,.$$

$\mathcal{U}, \mathcal{V}$ and $\mathcal{D}$ are the matrices of parameters to be estimated. The Hawaiian model is regionalized using 6 regions and 4 seasons (see Figure 16); this reduces the number of movement parameters in the parameter estimation phase to at most $6 \times 3 \times 4 = 72$.

5.5 Parameter estimation

The predicted number of tags returned during 1 month is given by

$$\widehat{C}^n_{i,j;f} = \beta_f F^n_{i,j;f} N^n_{i,j} \tag{5}$$

where β_f is the reporting rate, i.e. the proportion of tags returned by fleet f with usable recapture information, $F^n_{i,j;f}$ is computed from Equation (4) and N satisfies Equation (2) at time level n (for a derivation, see Appendix 10.4).

Observed numbers of tag returns $C^n_{i,j;f}$ are related to predicted numbers of returns $\widehat{C}^n_{i,j;f}$ by the Poisson likelihood function

$$L(\mathcal{U}, \mathcal{V}, \mathcal{D}, q, M, C^n_{i,j;f}) = \prod_{i,j,n;f} \left[\frac{\widehat{C}^n_{i,j;f}{}^{C^n_{i,j;f}}\, e^{-\widehat{C}^n_{i,j;f}}}{C^n_{i,j;f}!} \right]. \tag{6}$$

This function assumes that the predicted number of tag returns in each grid cell during one month is the expected value of a Poisson random variable. The Poisson distribution is selected as it is appropriate for the observation of a rare event such as the radioactive decay of an atom (Feller, 1968) or the recapture and return of a tagged tuna.

Maximum likelihood parameter estimates are obtained by finding the values of the parameters that maximize Equation (6). The maximization is accomplished by minimizing the negative logarithm of (6) using a quasi-Newton numerical function minimiser which in turn depends on the gradient of partial derivative computed using adjoint functions (Griewank and Corliss, 1991):

$$\min_{\mathcal{U},\mathcal{V},\mathcal{D},q,M} \quad -log\, L(\mathcal{U}, \mathcal{V}, \mathcal{D}, q, M, C^n_{i,j;f})\,.$$

To assist the minimizer, bounds are placed on the values of the parameters $\mathcal{U}, \mathcal{V}, \mathcal{D}, q$ and M. Typical bounds used in the simulations are $|\mathcal{U}, \mathcal{V}| < 100$, $0 < \mathcal{D} < 100000$, $0 < q < 0.1$ and $0 < M < 0.5$; parameters $\mathcal{D}, q$ and M are positive and upper bounds are set high to prevent the parameter estimates from being functions of the bounds.

Alternative tag release strategies were explored by conducting Monte Carlo experiments. The predicted number of tag returns, $\widehat{C}^n_{i,j;f}$, is interpreted as the expected value of a Poisson random variable. Simulated tag recapture observations were generated by sampling from a Poisson distribution with expected value $\widehat{C}^n_{i,j;f}$. In this way, observed distributions of fishing effort were used to generate *replicate* tag recapture results. These results were analysed by the estimation procedure to generate sets of parameter estimates for each simulated recapture data set. The accuracy and variability of the parameter estimates were then compared statistically with the known parameter values used in the simulation. For each numerical experiment carried out, sets of 50 or 200 simulations were run.

6 Hypotheses

A regional and seasonal movement hypothesis, and several release and mortality hypotheses have been developed for Hawaiian yellowfin tuna populations.

6.1 Release sites

Three model "release sites" were selected: **Kauai**, the 1° square immediately south of Kauai; **Hawaii**, the 1° square immediately northwest of Hawaii and **Cross**, the 1° square in which Cross Seamount is located. These bins are respectively marked K, H, and C in Figure 16. The three sites are readily accessible to the nearshore fishermen and each recorded significant catches during 1991-92. The **Kauai** and **Hawaii** bins are on the island chain; the **Hawaii** bin is not fished by longliners. The **Cross** bin is off the island chain and we assume it is frequented only by the offshore handline fleet (see Section 3.5).

While in this work we assume that tags from **Cross** and the other sites are immediately available to all fleets, it should be noted that Cross Seamount may have restricted usefulness as a tag release site. Yellowfin caught there are typically small and therefore not likely to be caught by the remaining fleets which generally target large yellowfin. (Juveniles tagged at Cross could be accommodated in a practical sense if age structure were built into the model software—see Section 8.3.)

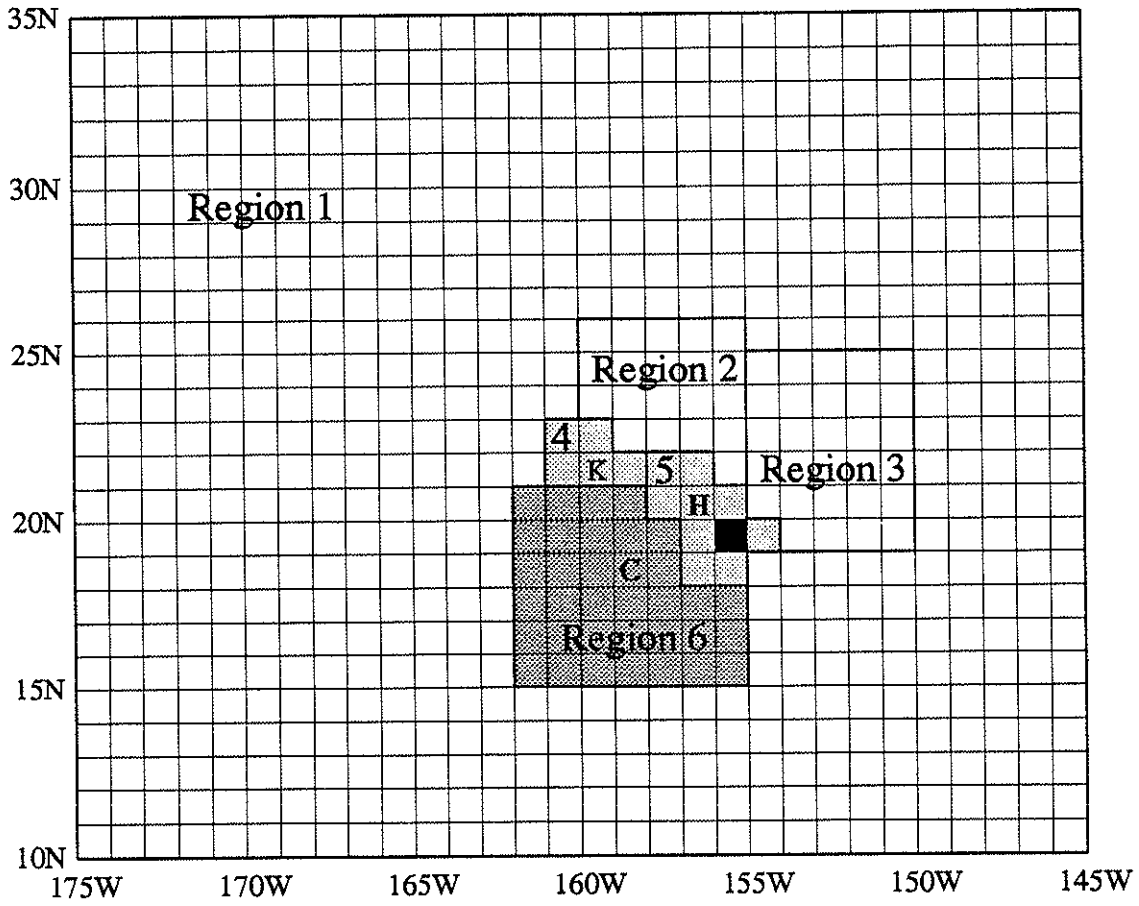

Figure 16: Regionalization of the Hawaiian model using 6 regions. K denotes the **Kauai** release site, H and C the **Hawaii** and **Cross** release sites. The three levels of shading used convey the convention that Regions 1, 2 and 3 share a common random movement parameter, as do Regions 4 and 5; Region 6 generally has a unique value (see Section 6.5).

6.2 Regionalization

The physical domain of Figure 1 is divided into 6 regions (Figure 16). Two regions are established along the island chain based on the **Kauai** and **Hawaii** release sites, immediate proximity to the major islands and bathymetric similarity. Region 4 consists of the **Kauai** release site and Region 5 the **Hawaii** release site; region 6 encompasses the **Cross** release site. The remaining regions are constructed in accordance with the predicted distribution of tagged tuna produced by the movement model. For example, very few tags are caught in the outer area of the model, so it is made into one region (Region 1). Regions 4 and 5 are approximately of the same size on the north-eastern side of the island chain.

6.3 Catch, effort, and "redistributed catch" at the release sites

Before considering a release strategy, the catch and effort records for 1991-92 at the chosen release sites will be examined.

A release strategy ought to be backed by the knowledge that the proposed number of releases is achievable. It is preferable to catch, tag and release fish at release sites than to transport them from elsewhere. Transporting fish takes time and induces stress, resulting in higher costs and tagging mortalities. No account is taken of tagging mortality here, though it should be included where transportation is necessary (see Section 8.4).

The catch (pounds) of yellowfin taken in the **Kauai**, **Hawaii** and **Cross** bins by troll and handline fleets is given in Figure 17. Catch by longliners at these sites is excluded because it is expressed as numbers of fish. Tonnages taken in the **Kauai** and **Hawaii** bins peak during the spring and summer months; peak tonnages in the **Cross** bin are taken during fall.

The modeling programs operate in *numbers* of fish, so for Figure 18 the unit of catch has been converted to numbers using Table 10. Total longline catch is now included and is seen to be generally small compared to total troll and handline catch.

The catch information used by the computer program is not, however, that of Figure 18. The program sees a catch distribution based on effort distribution which, for these three sites, is given in Figure 19. Effort peaks during spring and summer months in the **Kauai** and **Cross** bins and is fairly consistent throughout the year in the **Hawaii** bin. Effort in the **Cross** bin dips during summer because the offshore handliners move inshore seeking larger (more lucrative) yellowfin.

Catch (numbers) seen by the computer is shown in Figure 20 and will be referred to as the "redistributed catch". The trends shown in the effort plots of Figure 19 are generally reproduced in the redistributed catch plots and are quite different from those of actual catch in Figure 18. This is because redistributed catch is based on a catchability fixed for the year for each fleet.

6.4 Release strategy

For modeling purposes it is simplest to imagine quarterly releases of, say, 500 tags at each site in the first month of each quarter. This implies a quarterly release of 1500 yellowfin and a yearly total of 6000 releases.

On a practical note, it is likely that every fish caught will be tagged and released. Since bigeye are routinely caught in high percentages at Cross Seamount in particular, the yellowfin experiment will inevitably spawn a bigeye tag-recapture experiment, and many more than 6000 fish will have to be caught and tagged to meet the experiment's operational parameters.

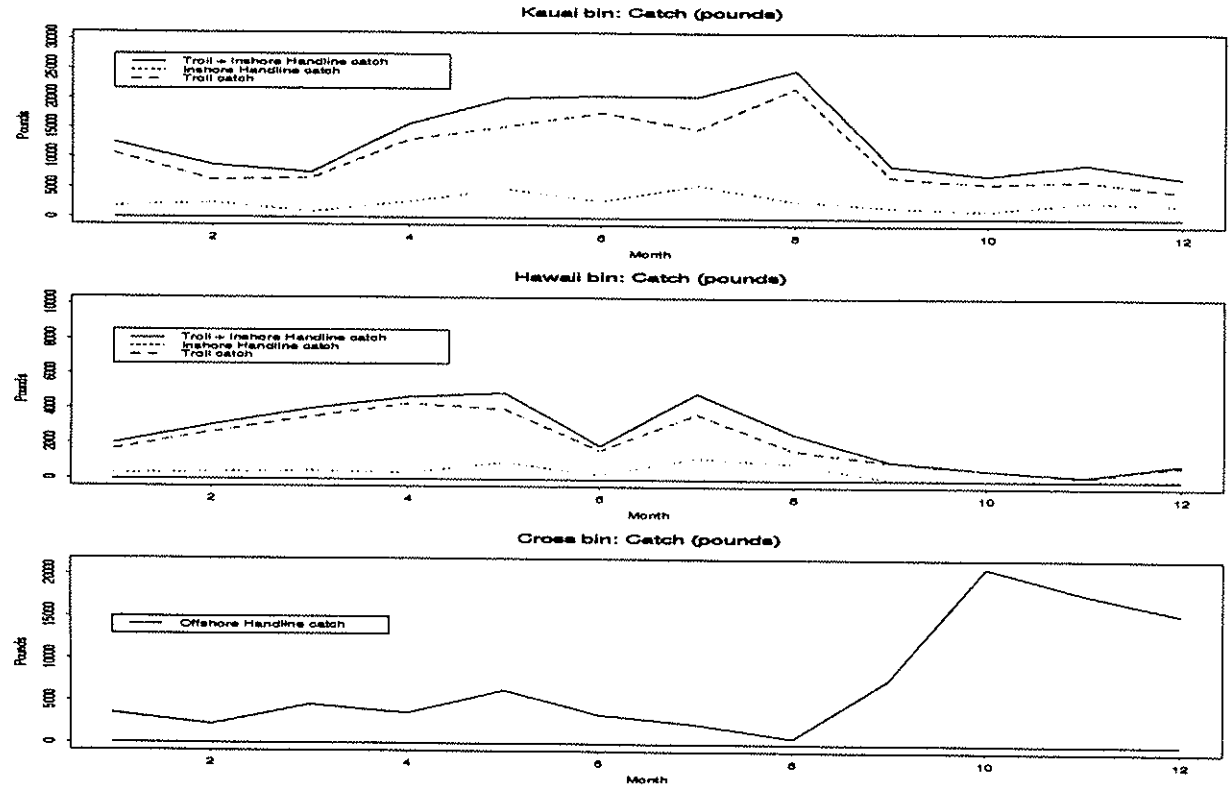

Figure 17: Catch (pounds) by troll and handliners in the **Kauai**, **Hawaii** and **Cross** bins.

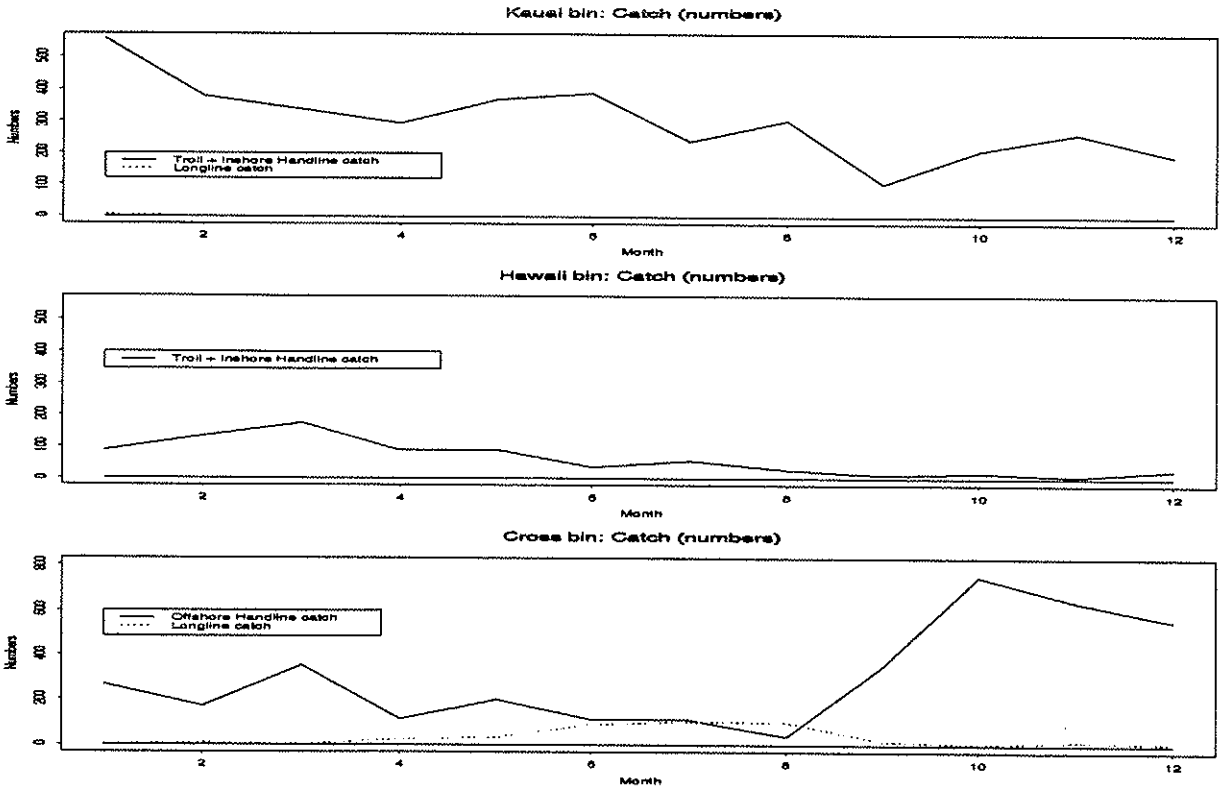

Figure 18: Catch (numbers) due to all fleets at **Kauai**, **Hawaii** and **Cross**.

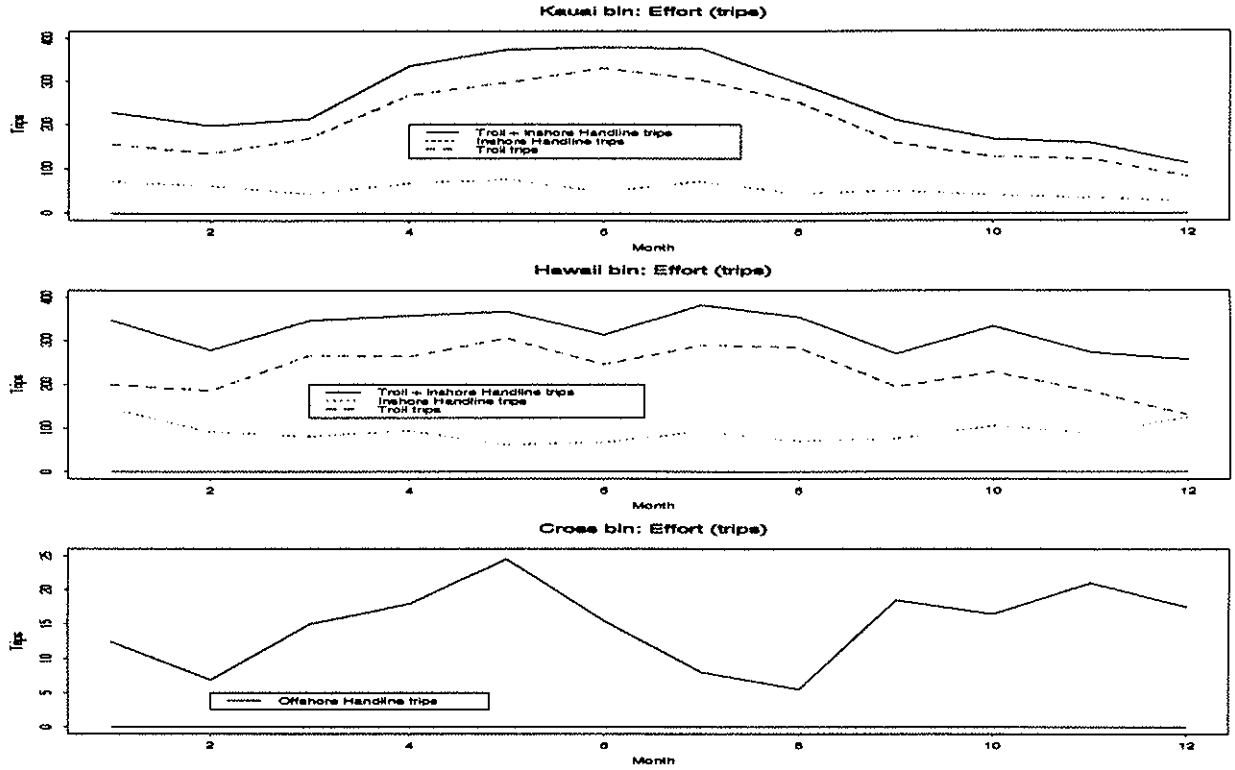

Figure 19: Effort (trips) expended in the **Kauai**, **Hawaii** and **Cross** bins.

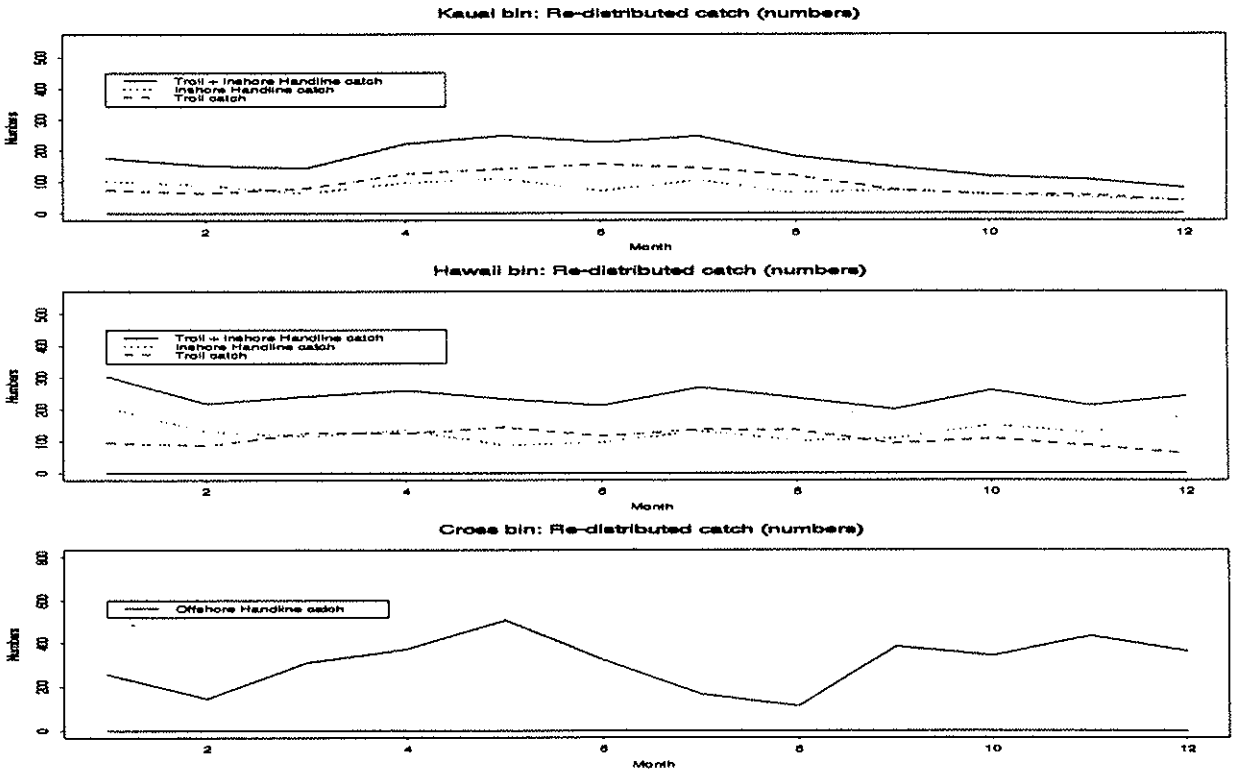

Figure 20: Redistributed catch (numbers) in the **Kauai**, **Hawaii** and **Cross** bins. "Redistributed catch" at each site is the fleetwise inner product of observed effort and CPUE.

Numerical tests reported in Section 7.1.4 show that the higher the number of tag releases, the greater the accuracy of the mean of parameter estimates and the tighter the corresponding confidence limits on the mean. Thus it is important to release as many tags as possible to optimize the success of the experiment.

6.5 Movement hypothesis

The movement hypothesis employed is summarized in Table 14.

Table 14: Seasonal movement hypothesis for yellowfin in the central Pacific; west-to-east (x) and south-to-north (y) directed movement and random movement values are listed for each season by region.

	Season 1 (Jul/Aug/Sep)			Season 3 (Jan/Feb/Mar)		
	Directed		Random	Directed		Random
Region	x (nm/dy)	y (nm/dy)	(nm^2/mo)	x (nm/mo)	y (nm/mo)	(nm^2/mo)
1	0	0	1000	0	0	4500
2	0	0	1000	0	0	4500
3	0	0	1000	0	0	4500
4	0	0	100	0	0	4500
5	0	0	100	0	0	4500
6	0	0	100	0	0	4500
	Season 2 (Oct/Nov/Dec)			Season 4 (Apr/May/Jun)		
	Directed		Random	Directed		Random
Region	x (nm/dy)	y (nm/dy)	(nm^2/mo)	x (nm/mo)	y (nm/mo)	(nm^2/mo)
1	0	-5	4500	0	5	4500
2	0	-5	4500	0	5	4500
3	0	-5	4500	0	5	4500
4	0	-0.5	450	0	0.5	450
5	0	-0.5	450	0	0.5	450
6	0	-2.5	2250	0	2.5	2250

During summer (Season 1, Jul/Aug/Sep) it is supposed that yellowfin feed and/or spawn in the Hawaiian Islands with no particular tendency to move away. During fall (Season 2, Oct/Nov/Dec) we suppose they move towards the equator, lingering along the island chain itself and in the Cross region. During winter (Season 3, Jan/Feb/Mar) we suppose they wander randomly. During spring (Season 4, Apr/May/Jun) we suppose they move northward again. This movement pattern reflects the annual north-south excursion of the North Equatorial Current (NEC) to Hawaiian latitudes. Seasonal mean surface currents showing the migration of the NEC are reproduced in Appendix 10.5 as Figures 42–45 (Qiu *et al.*, 1996).

The values used for directed and random movement were chosen as follows:

1. They are loosely based on the parameter estimates of Sibert *et al.* (1996) for skipjack in the western Pacific. Sibert *et al.* used tag-recapture data from the Skipjack Survey and Assessment Programme (SSAP) of 1977-82 and obtained regionally averaged directed motions of about 4 nm/day and random movement values of about 20000 nm^2/mo. For yellowfin we use a larger maximum directed movement component of 5 nm/dy and a smaller maximum random movement of 4500 nm^2/mo (corresponding to halving the radius of random movement). Adopting a higher directed component and lower random component of movement is consistent with the commonly expressed view that yellowfin are more directed and less random in their movement than skipjack. The influence of the Hawaiian Island chain within the surrounding expanse of the central Pacific may also be such as to reduce the random component of movement of yellowfin.
2. The values used also conform with the numerical requirement that $|Pe(x,y)| \leq 2$ if the centered-space scheme is used; the centered-space scheme should give more accurate parameter estimates from real data than the upwind scheme if the Peclet condition is adhered to. It may be true that yellowfin generally occupy a Peclet space $|Pe(x,y)| \leq 2$. If the random component of yellowfin movement is actually higher than 4500 nm^2/mo in Hawaiian waters and the directed component remains at 5 nm/dy, the Peclet criterion will certainly be satisfied. We arbitrarily scale the parameter values so that the Peclet number is the same in all regions.

Flament *et al.* (1996) analyzed drifter data and found that mean oceanic flows are generally of the order of 5 nm/dy in the Hawaiian Islands region; eddy-diffusivities in the NEC south of 18° N and windward of the Hawaiian islands are 3000–3750 nm^2/mo and increase to 6000–9000 nm^2/mo west of the island chain and west of 161° W. Thus if yellowfin were to exhibit no behavioral movement they would be transported by ocean waters at least the distance that is hypothesized as a typical directed movement and with a similar degree of random movement. Section 8.5 contains a recommendation that mean oceanic movements be included in the parameter estimation process as a background movement field.

6.6 Natural mortality hypotheses

Three natural mortality values were considered: a low value of 0.05 mo^{-1} (i.e. a 5% death rate by natural causes each month), a moderate value of 0.10 mo^{-1} and a high value of 0.30 mo^{-1}. These values are based on estimated natural mortality rates for size-classed yellowfin published by the South Pacific Commission (Figure 9, p.30, 1995). The 30% value approximately corresponds to a 6 month old fish and the 5% value to fish 12-18 months old. The 10% value can be taken as an average of the natural mortality values applicable to yellowfin.

7 Results

7.1 Multiple release site strategy

Within the same time-frame it is preferable to release tags at many sites than at a single site (Bertignac, 1995), the reason being that this strategy generally leads to increased recapture percentages in the vicinity of the release sites. Increased recapture percentages in turn lead to higher precision in parameter estimates.

This can be demonstrated using a single season random movement hypothesis with regional values as for Seasons 2 or 4 (fall or spring) of Table 14. The centered-space scheme was selected, and closed rather than open boundary conditions were used because firstly, in the absence of directed movement, most of the tags move within the central part of the model and few reach the external ocean boundary, and secondly, a large number of simulations were planned and experience with the parameter estimation program indicated that simulations using closed boundary conditions achieved convergence significantly faster than using open boundary conditions. Natural mortality was set to $0.10mo^{-1}$.

Four tests were conducted and in each a total of 6000 tags were released. The first test was a release of 1500 tags per quarter at the **Kauai** release site, the second a similar release at **Hawaii** and the third at **Cross**; the fourth test involved releases at each site of 500 tags per quarter. Figure 21 summarizes the results of 50 simulations conducted for each test. The estimate for random movement (Nm^2/mo) is plotted on the vertical axis; on the horizontal axis is plotted the natural logarithm of the average number of tag recaptures. The legend in the bottom right hand graph gives the "true" random movement value corresponding to the six regions of the model. The labeled horizontal lines on the graphs mark the positions of the true values. The mean of the estimates is plotted as a black diamond. Error bars extending two standard deviations are plotted as vectors; the lower error bar is truncated at the x axis if calculated to extend below it—the parameter estimation is constrained to positive values. Note that, for a particular "true" value, confidence in the estimates generally improves with a greater number of recaptures.

It can be verified from Figure 21 that the true values are accurately estimated for the regions in which the single-site tests were initiated; for **Cross** releases the error bars are noticeably broader than those for **Kauai** and **Hawaii** releases. In the case of **Kauai** releases, the true value for region 5 is not as accurately estimated and the reliability of the estimate is poor; in the case of **Hawaii** releases the true value for region 4 is poorly estimated and in the case of **Cross** releases the true values for each of regions 4, 5, and 6 are well estimated but the confidence on regions 4 and 5 estimates is poorer than for the single-site **Kauai** and **Hawaii** releases. Comparing these single-site releases with the results of the combined release strategy shows that combined releases do consistently well for estimating the true values for regions 4, 5, and 6 and the set of corresponding error bars shows high confidence

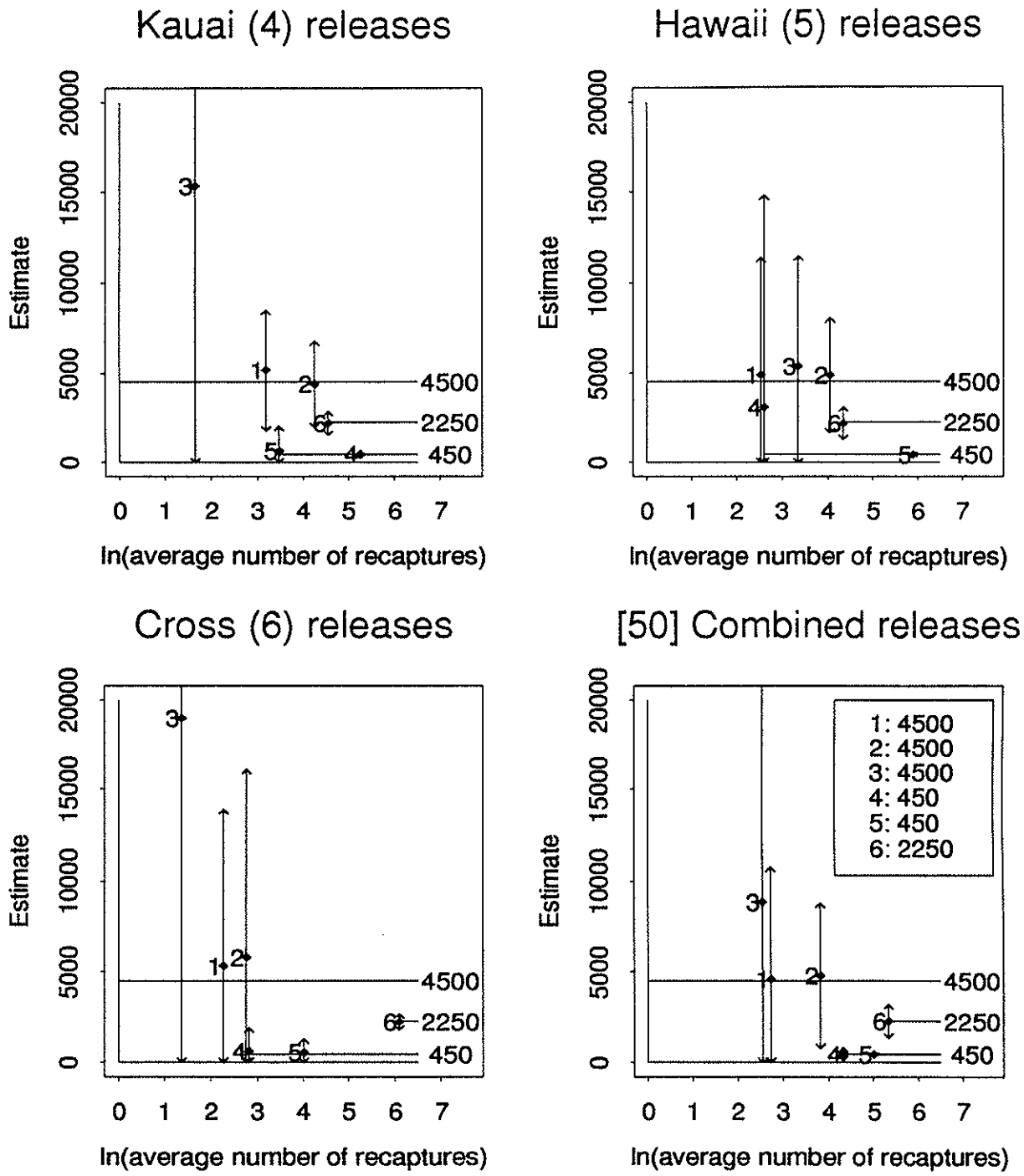

Figure 21: Random movement estimates from four tests (see text) each of 50 simulations. The legend in the bottom right plot lists "true" values of random movement for each region; the labeled horizontal lines correspond to these values. The mean of the estimates is plotted as a black diamond; error bars extending two standard deviations appear as vectors. The **Kauai** release site is in region 4, **Hawaii** in region 5, and **Cross** in region 6.

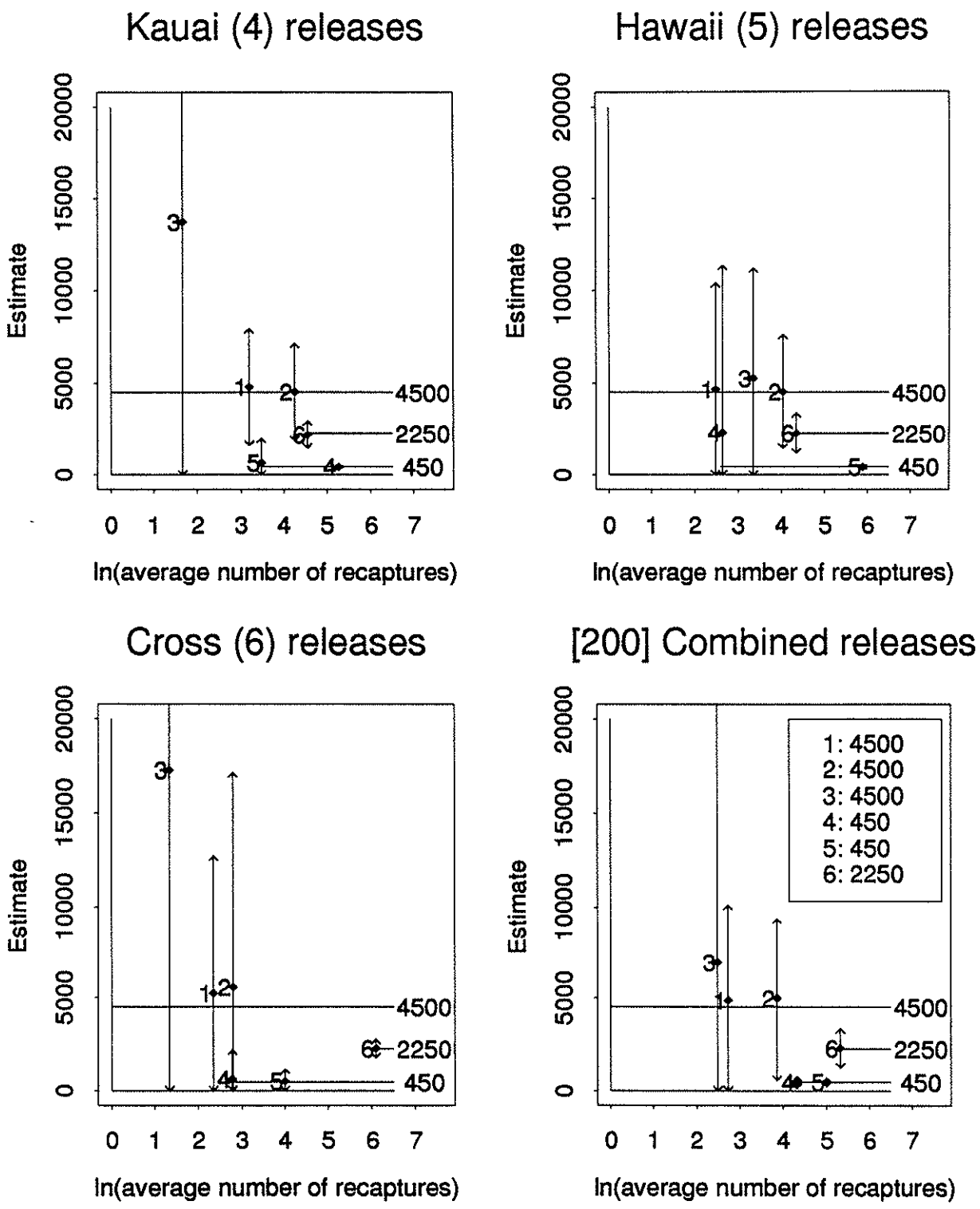

Figure 22: Random movement estimates from four tests each comprising 200 simulations. See caption to Figure 21 for further details.

except in the case of region 6. That is, based on these results, the random movement parameters are best estimated in the overall sense using a multiple-site release strategy.

The reliability of the results in Figure 21 could be challenged on the grounds that they summarize estimates from only 50 simulations. To answer this possible criticism, a further 150 simulations of each test were carried out and the results presented in Figure 22.

Comparison of Figures 21 and 22 suggests 200 simulations produces a similar set of results to 50, particularly for regions 4, 5 and 6, and reinforces the finding that a multiple-site release strategy gives better overall parameter estimates. The spread in the parameter estimates, however, is slightly greater for 200 simulations, probably because of the inclusion of more outliers.

A further presentation, this time comparing likelihood function value (see Section 5.5) with number of recaptures for each of 200 simulations made of the four release strategies, is given in Figure 23. This figure suggests that function value increases with number of recaptures and that this relationship is most direct, i.e., shows less scatter, for the multiple release-site strategy.

We now define the *standardized bias* as

$$\text{Standardized bias} \quad = \quad \frac{\text{Estimate} - \text{True value}}{\text{Standard deviation of the estimate}}. \tag{7}$$

The standardized bias statistic has unit standard deviation enabling comparison of estimates of different parameters. A value greater than 2 (or less than -2) implies a statistically significant bias; for example, if the distribution of the bias estimates is normal, approximately 95% lie within two standard deviations of zero. If the mean of the estimates is used in place of the true value, the standardised variable so defined has zero mean.

Figures 24 and 25 are **Splus** *boxplots* corresponding to the sets of 50 and 200 simulations. The height of each black rectangle is the difference between the first and third quartiles of data—the *interquartile distance* (IQD)—and indicates the spread of the data; thus the middle 50% of data values lies within the black rectangles. The median value is indicated by the white horizontal bar within the rectangle and estimates the center of the distribution. Dotted lines leaving the top and bottom of each box extend to the extreme values of the data (indicated by square brackets) or a distance 1.5×IQD from the center, whichever is less. If the data are Gaussian, 99.3% of the values fall inside these brackets; data outside the brackets may be outliers and are indicated by horizontal bars. The boxplots for 200 simulations show less volatility than those for 50 simulations but greater spread, as seen above when comparing Figures 21 and 22. For both sets of results, there are fewer outliers and the biases seem generally closer to zero for the multiple-site strategy.

The extreme and outlier catchability bias estimates of Figures 24 and 25 correspond to both low and high numbers of recaptures. This is illustrated by the scatter diagrams of Figure 26

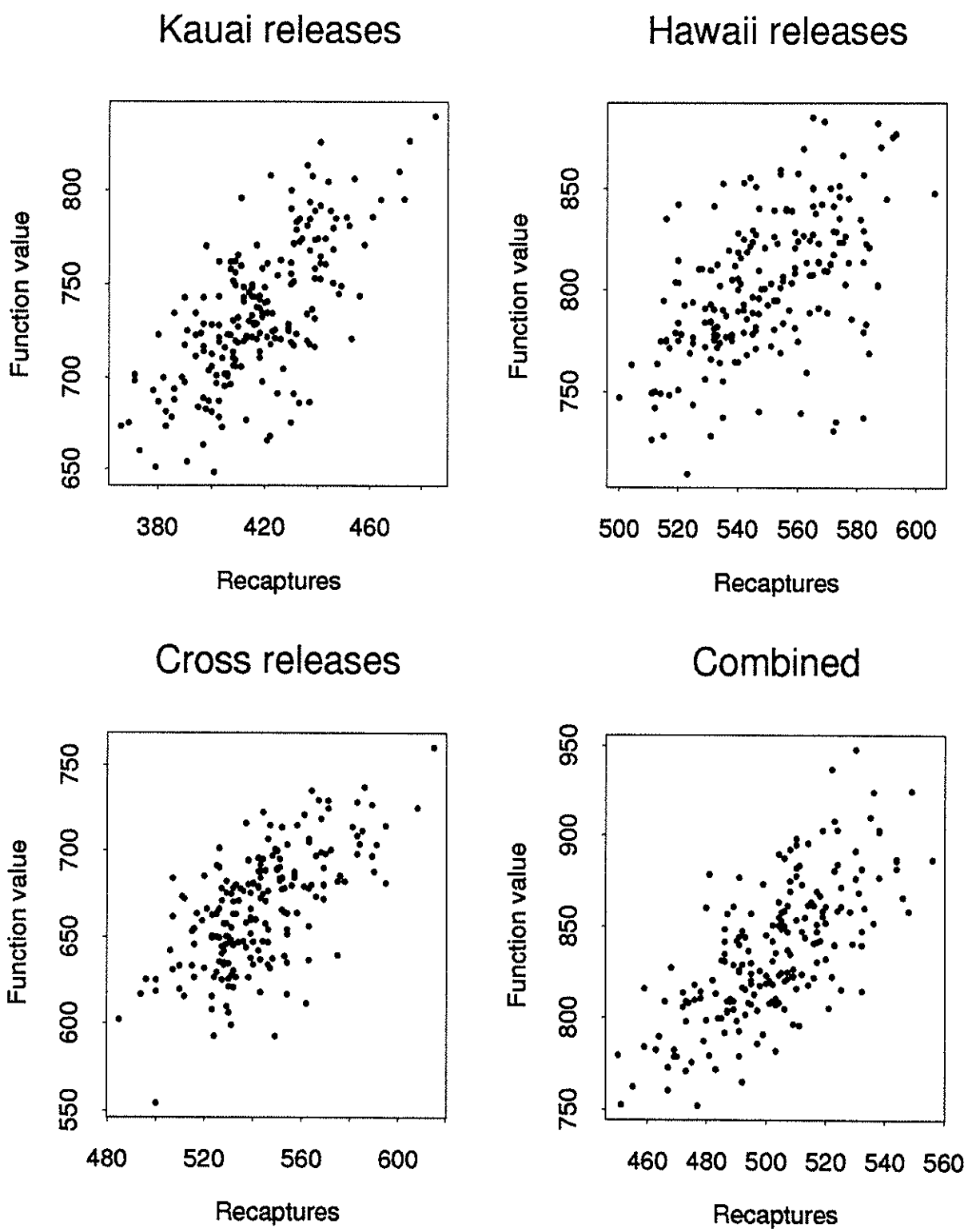

Figure 23: Scatter plots of function value versus recaptures for 200 simulations of four different release strategies.

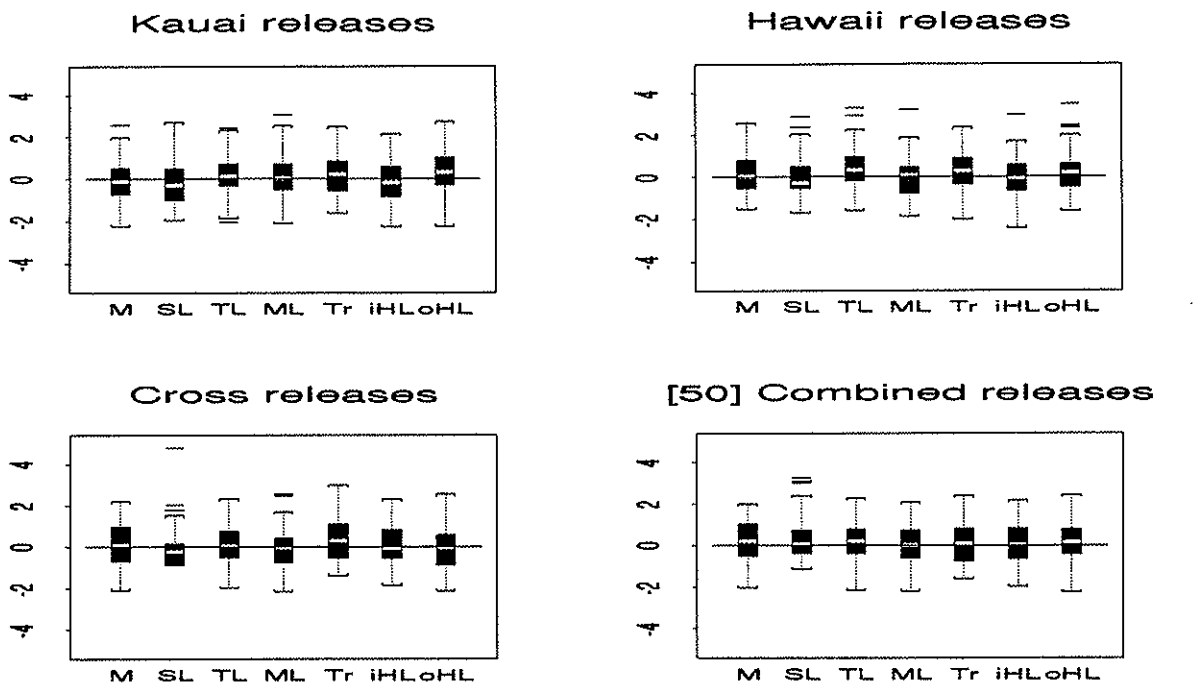

Figure 24: Distribution of standardized bias for natural mortality (M) and six catchabilities (SL=swordfish LL, ..., oHL=offshore handline) based on 50 simulations.

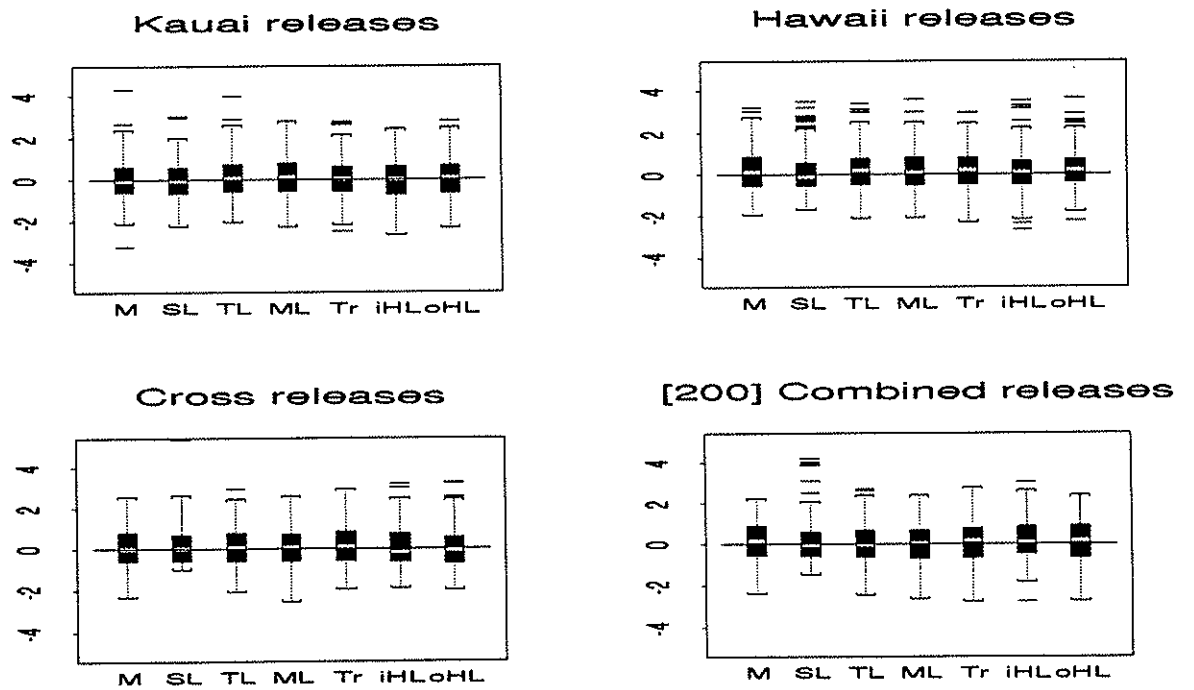

Figure 25: Distribution of standardized bias for natural mortality (M) and six catchabilities (SL=Swordfish LL, ..., oHL=offshore Handline) based on 200 simulations.

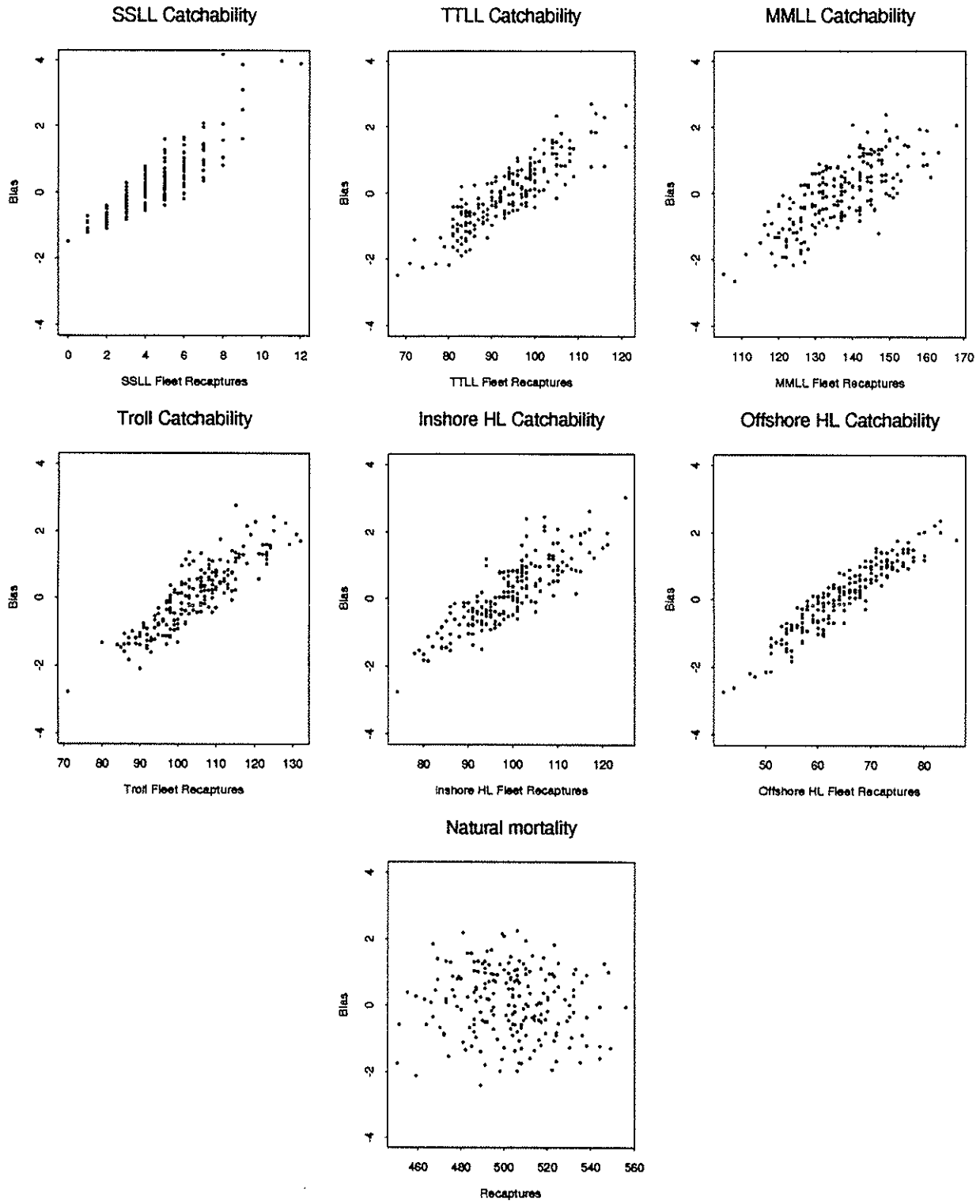

Figure 26: Scatter plots for catchability and natural mortality bias versus recaptures for the 200 simulations made for the multiple-site release strategy.

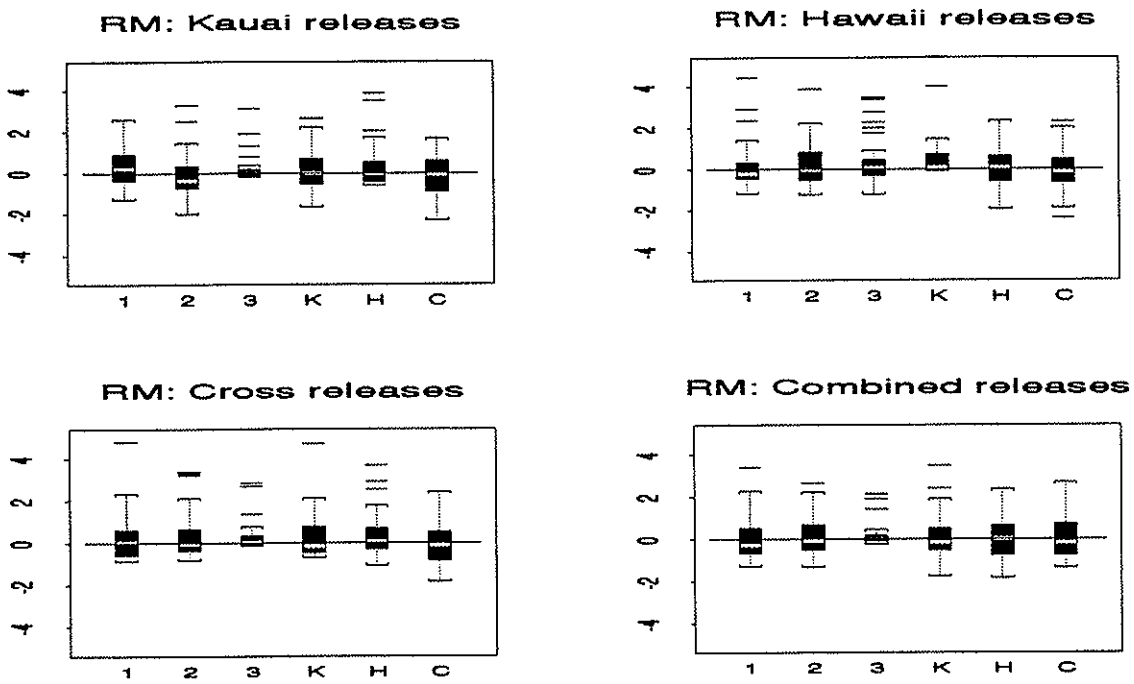

Figure 27: Standardized bias distributions for random movement estimates based on 50 simulations of four release strategies (K=Region 4, H=Region 5, C=Region 6).

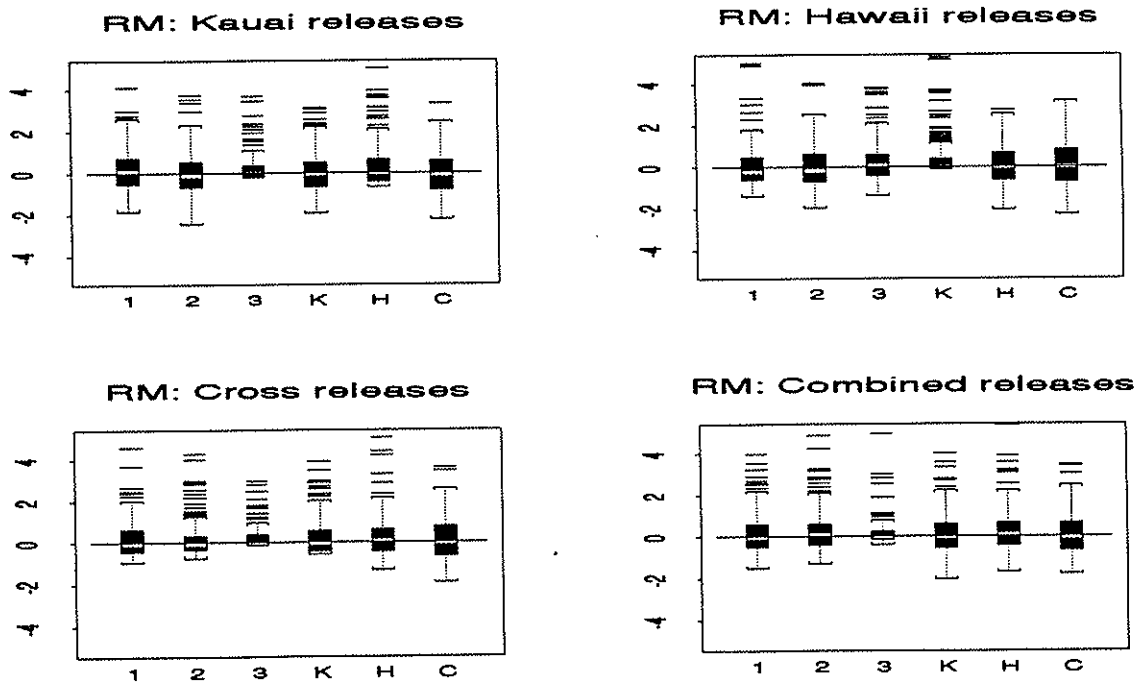

Figure 28: Standardized bias distributions for random movement estimates based on 200 simulations of four release strategies (K=Region 4, H=Region 5, C=Region 6).

for the set of 200 simulations made for the multiple-site release strategy. These diagrams suggest that the distribution of points is elliptical; the mortality bias-recapture distribution is nearly circular in comparison with that of the catchability bias estimates (the vertical scales in each case are the same but the horizontal scales for the catchability estimates are only half as expansive (for SSLL catchability it is one tenth)). The SSLL catchability plot shows very low recapture numbers. Each elliptical distribution is centered approximately on zero bias and the average recapture number for the fleet (in the case of the catchabilities) or for a simulation (in the case of natural mortality); to the nearest integer, the average number of recaptures for each fleet is 4 (SSLL), 94 (TTLL), 136 (MMLL), 105 (HIRT), 99 (HIIH) and 65 (HIOH), and the average number of recaptures per simulation is 502. If the total number of releases is increased, one might expect the minor axis of the ellipses to increase (see Section 7.1.4).

Figures 27 and 28 are boxplots for random movement for 50 and 200 simulations, respectively. In all cases the median bias is close to zero and the interquartile group is also clustered close to zero, suggesting that the parameters are being well estimated.

7.1.1 Simulated recaptures using $M = 0.05, 0.10$ and 0.30.

For reasons outlined in the previous section, all subsequent simulations use multiple-site releases. Also, for reasons of computational economy, only 50 simulations will be carried out for each test.

Three natural mortality values ($M = 0.05$, 0.10 and 0.30) were tested, two finite difference schemes (upwind and centered-space) and two methods for defining boundary conditions (open and closed). Simulations of these 12 combinations were conducted but only the results of the four $M = 0.10$ cases will be discussed in detail (next section).

Summary results for all 12 experiments, showing the distribution of standardised bias, are given in Appendix 10.6. Table 15 lists fleet recapture information for each experiment; the fleet recapture percentages may not sum to the total given because of round-off errors. For lower values of natural mortality a smaller time step is required to obtain similar accuracy from the simulations. The meaning of the function value is explained in Section 5.5; function value is higher for a greater proportion of recaptures.

The tabulated results show that lower natural mortality rates lead to higher recapture percentages and for a given scheme, recapture percentages are less sensitive to boundary conditions as natural mortality increases. This is expected because higher natural mortality values permit fewer tags to survive the journey to the outer boundaries of the model. Consequently, the differences in program code in the boundary region have less influence.

Okamoto and Nishimoto (1989) report the results of a tag-recapture experiment involving 1879 small yellowfin (0.5 to 8 pounds) released at 14 FADs (fish aggregation devices) and four

Table 15: Recapture percentages predicted by 12 numerical experiments. UP=Upwind scheme, CS=Centered-space scheme; natural mortality (M), time step (Δt, in days) and average function value (F) at minimum are also given.

Scheme	BC's	M	SL	TL	ML	TR	iHL	oHL	$\sum$%	Δt	F
UP	Open	0.05	0.11	1.90	2.79	2.06	1.88	1.28	10.03	3.00	1014.2
		0.10	0.07	1.38	2.11	1.67	1.52	1.15	7.89	3.75	755.4
		0.30	0.03	0.70	1.14	1.08	1.02	0.91	4.86	5.00	377.6
	Closed	0.05	0.14	1.97	2.93	2.10	1.89	1.30	10.34	3.00	1058.8
		0.10	0.08	1.42	2.16	1.69	1.53	1.15	8.04	3.75	781.5
		0.30	0.03	0.70	1.14	1.08	1.02	0.91	4.88	5.00	381.1
CS	Open	0.05	0.11	1.94	2.79	2.02	1.90	1.34	10.10	3.00	1087.1
		0.10	0.08	1.37	2.08	1.64	1.52	1.18	7.87	3.75	772.3
		0.30	0.03	0.68	1.11	1.06	1.00	0.91	4.80	5.00	364.9
	Closed	0.05	0.14	2.02	2.89	2.03	1.90	1.36	10.33	3.00	1043.9
		0.10	0.08	1.43	2.11	1.65	1.52	1.19	7.97	3.75	763.1
		0.30	0.03	0.68	1.11	1.06	1.00	0.91	4.80	5.00	365.8

open ocean sites from Kauai to Hawaii between March 1985 and July 1987. By December 1988, 233 (12.4%) had been recaptured and of these 76% (178) were recovered at their release sites.

It is interesting to note that by February 27, 1997, 2438 bigeye and yellowfin tags had been released through the Hawaii Tuna Tagging Project at Cross Seamount and NOAA Weather Buoy 2; 265 had been recaptured (10.9%). Of the tags released, 827 were yellowfin and 112 had been recaptured (13.5%); 1611 were bigeye and 153 had been recaptured (9.5%). Tag releases commenced in early 1996.

For comparison, of 33523 yellowfin tags released during the Regional Tuna Tagging Program of 1989–92, 10.3% were recovered by June 30 1995 (South Pacific Commission, 1995, p.12).

7.1.2 Results using $M = 0.10$

The recapture percentage predicted by the four $M = 0.10$ experiments is about 8%, which seems realistic. Adjustments to this figure could be made by altering the catchability coefficients—their true values can only be established by conducting a tag release-recapture experiment.

Figure 29 shows the estimates of mortality bias for the four sets of simulations. The upwind scheme with closed boundary conditions (CBC) and the centered-space scheme with open

boundary conditions (OBC) give the least skewed estimates for natural mortality (M) based on 50 simulations; skewness in the catchability bias estimates is also generally less for these schemes.

Figures 30–33 show biases in the random movement estimates obtained for Seasons 1–4 in each region. The outliers in these plots lie above the zero bias line because zero is the lower bound on random movement estimates. Figures 34–35 show biases in the directed movement estimates for Seasons 2 and 4.

For the tests using the upwind scheme with CBC and the centered-space scheme with OBC, an alternative presentations of results is given. Figures 36 and 37 are composed of four plots showing the mean of the estimates for random movement and associated error bars of length two standard deviations, and two plots showing the estimate mean and error bars for directed movement. The plots contain a legend giving the true values of directed or random movement for each region, taken from Table 14. Results for random movement in Season 3 are not as accurate as for the other seasons and the error bars show they are less certain; the reason for this is not known but our experience is that random movement estimates are easier to predict correctly if both directed and random movement are included. The movement parameters for Regions 4, 5 and 6 are generally reproduced with good accuracy.

7.1.3 Effect of altering reporting rate

A reporting rate R of 100% has thus far been used for the simulations. Realistically, however, reporting rate is less than perfect. To gauge the effect of altering R, the upwind CBC and centered-space OBC experiments were rerun with $R = 0.50$ and $R = 0.75$. As one would expect, the estimates obtained are generally less accurate and less reliable (i.e. the error bars broader) for lower reporting rates. Partial results for movement estimates in Season 4 and Regions 4, 5, and 6 are given in Figure 38.

The effect on recapture percentages is essentially linear, as can be seen in Table 16. Both schemes predict similar recapture percentages for the nearshore fleets. For the TTLL and MMLL fleets, the centered-space scheme predicts fewer recaptures than does the upwind scheme at higher values of reporting rate; for the handline fleets, centered-space predicts generally more recaptures.

7.1.4 Effect of altering tag release numbers

Now consider the effect on parameter estimates and recapture percentages as the tag release rate at each site is increased from 250/qtr (3000 total) to 500/qtr (6000 total) and to 1000/qtr (12000 total). Once again, only partial results for movement parameter estimates in Season 4 and Regions 4, 5, and 6 will be given (see Figure 39). The results again illustrate the

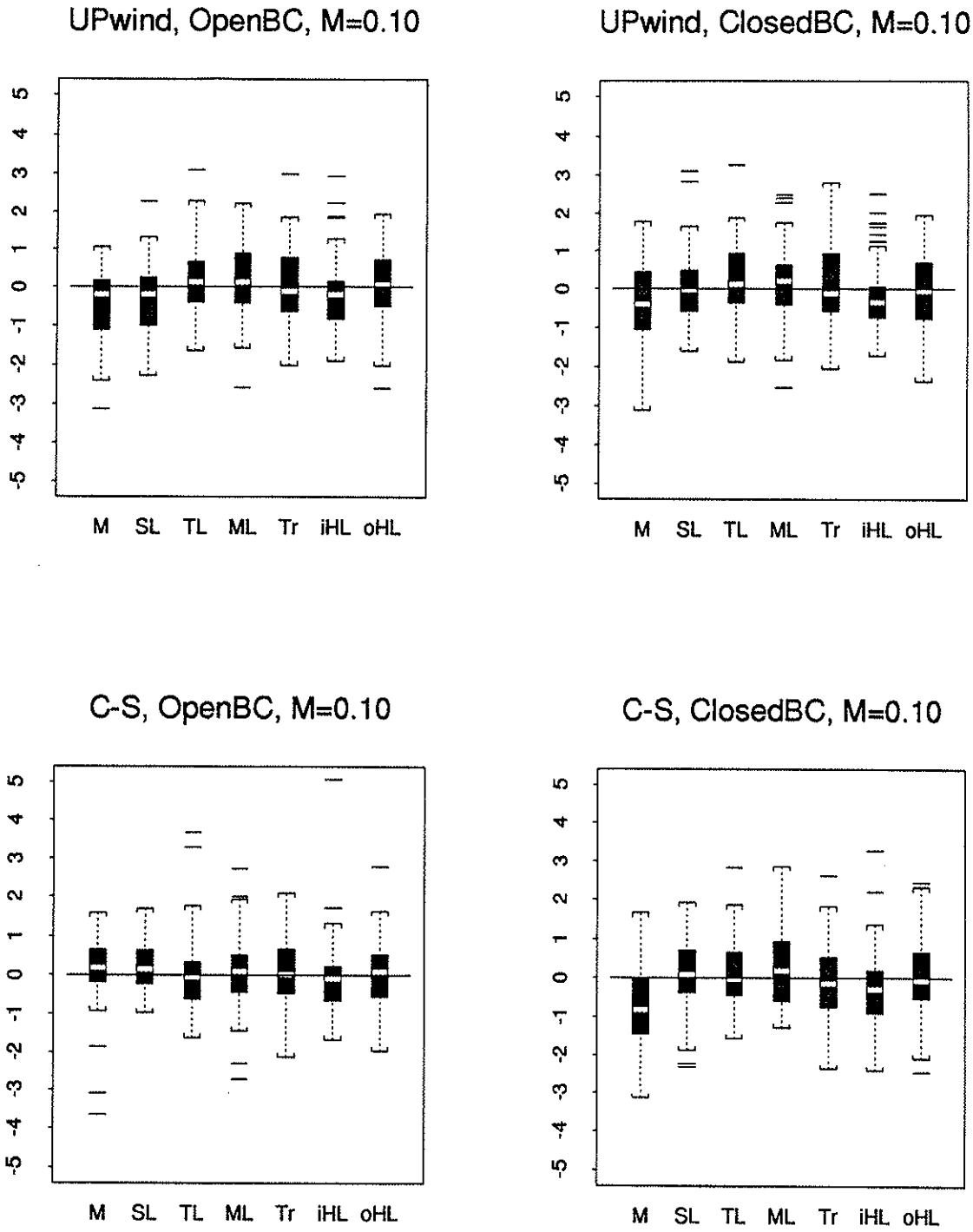

Figure 29: Distribution of standardized bias for natural mortality M and catchability based on 50 simulations of 4 numerical experiments (SL=swordfish LL, ..., oHL=offshore handline).

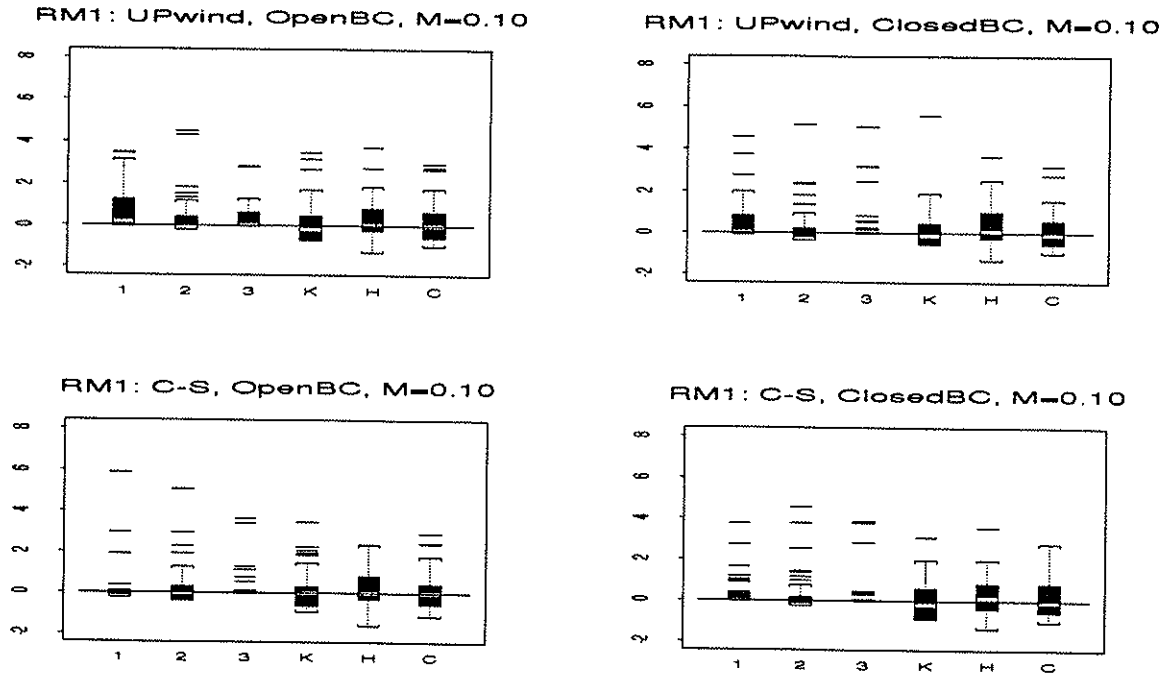

Figure 30: Distribution of standardized bias for random movement in Season 1 based on 50 simulations of four numerical experiments (K=Region 4, H=Region 5, C=Region 6).

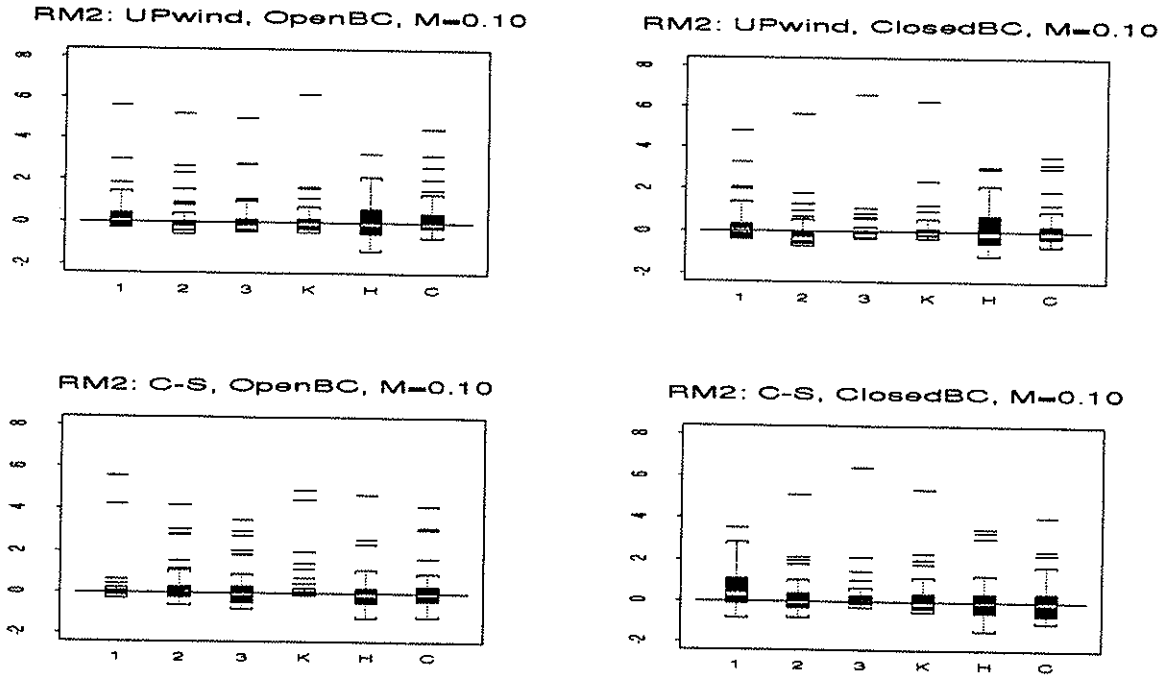

Figure 31: Distribution of standardized bias for random movement in Season 2 based on 50 simulations of four numerical experiments (K=Region 4, H=Region 5, C=Region 6).

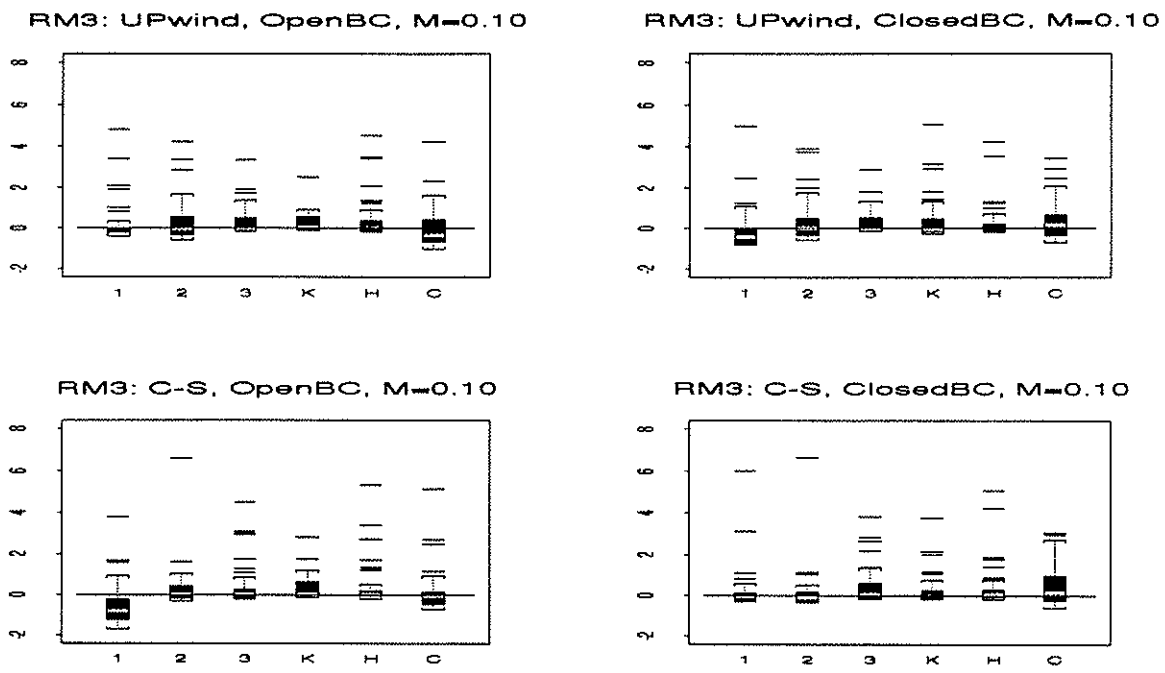

Figure 32: Distribution of standardized bias for random movement in Season 3 based on 50 simulations of four release strategies (K=Region 4, H=Region 5, C=Region 6).

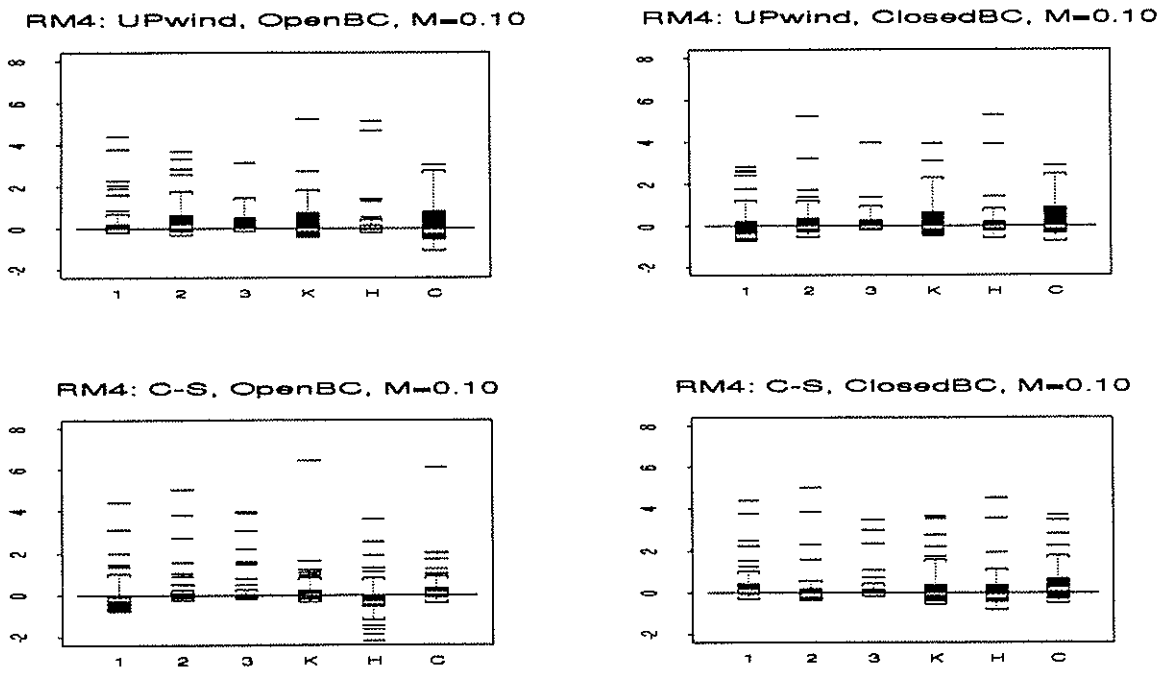

Figure 33: Distribution of standardized bias for random movement in Season 4 based on 50 simulations of four release strategies (K=Region 4, H=Region 5, C=Region 6).

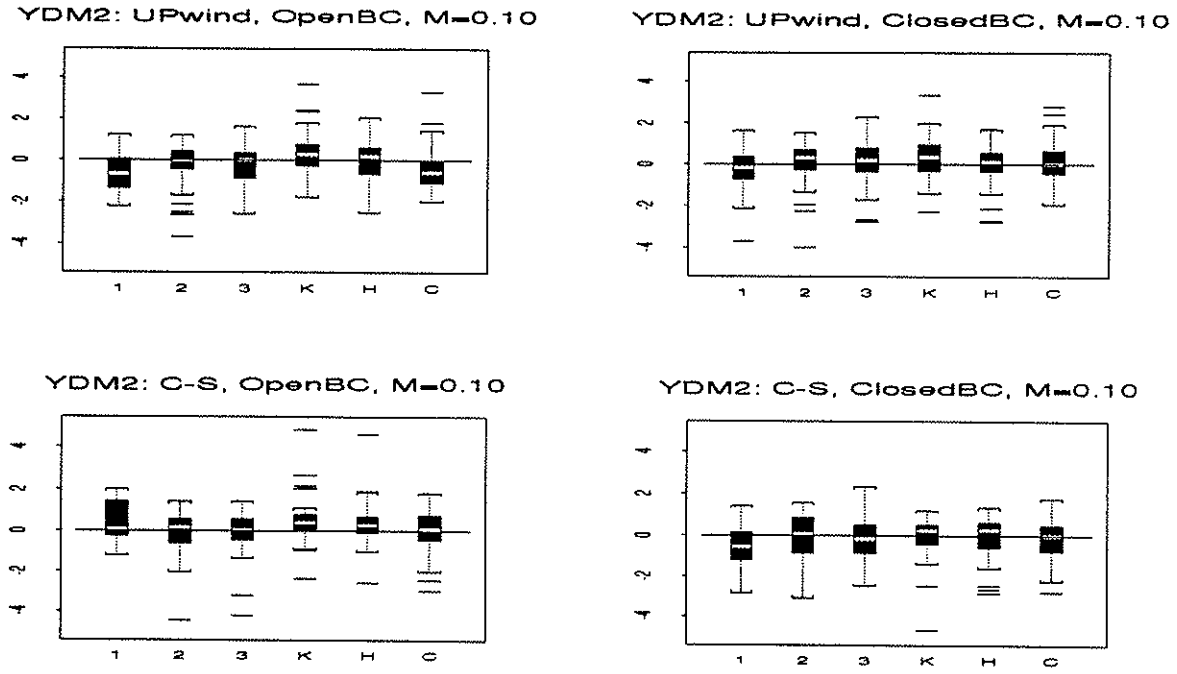

Figure 34: Distribution of standardized bias for directed movement in Season 2 based on 50 simulations of four release strategies (K=Region 4, H=Region 5, C=Region 6).

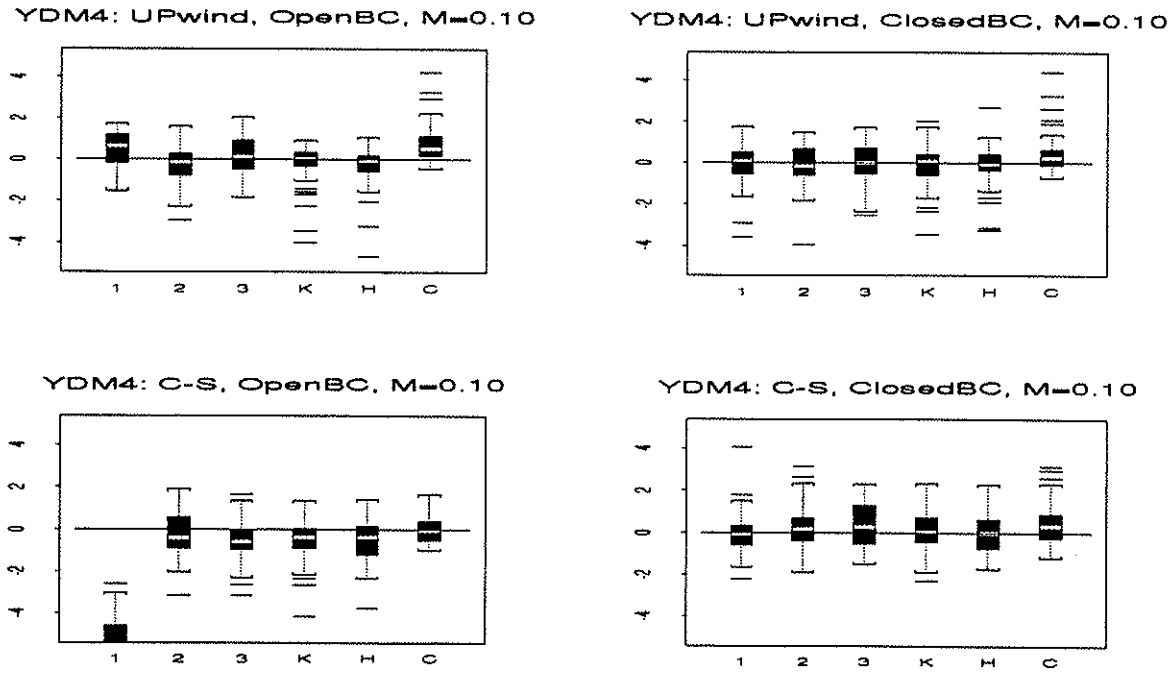

Figure 35: Distribution of standardized bias for directed movement in Season 4 based on 50 simulations of four release strategies (K=Region 4, H=Region 5, C=Region 6).

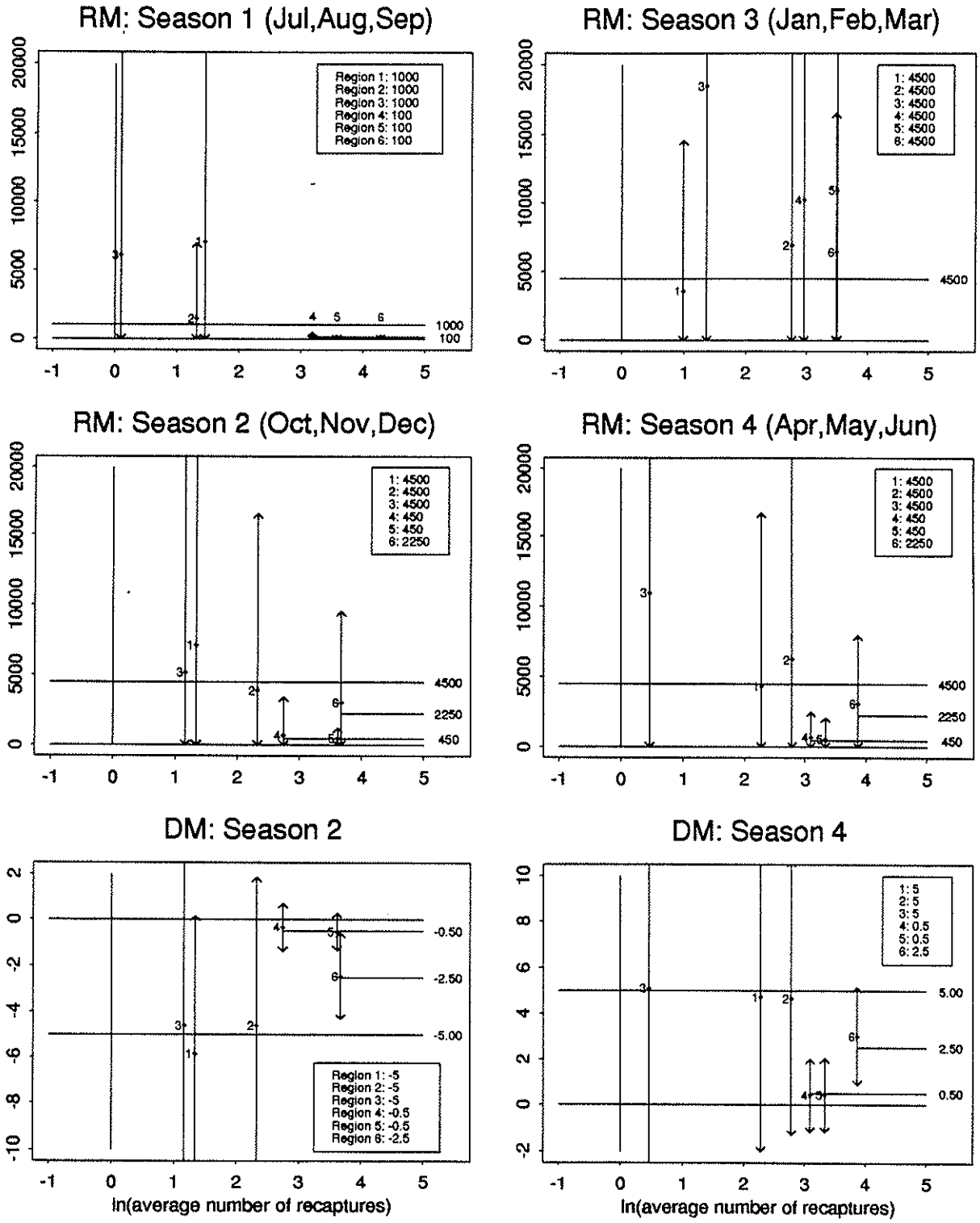

Figure 36: Mean estimates and error bars for random movement (RM) and directed movement (DM) using closed boundary conditions and the upwind scheme. Legends give seasonal "true" values for each region.

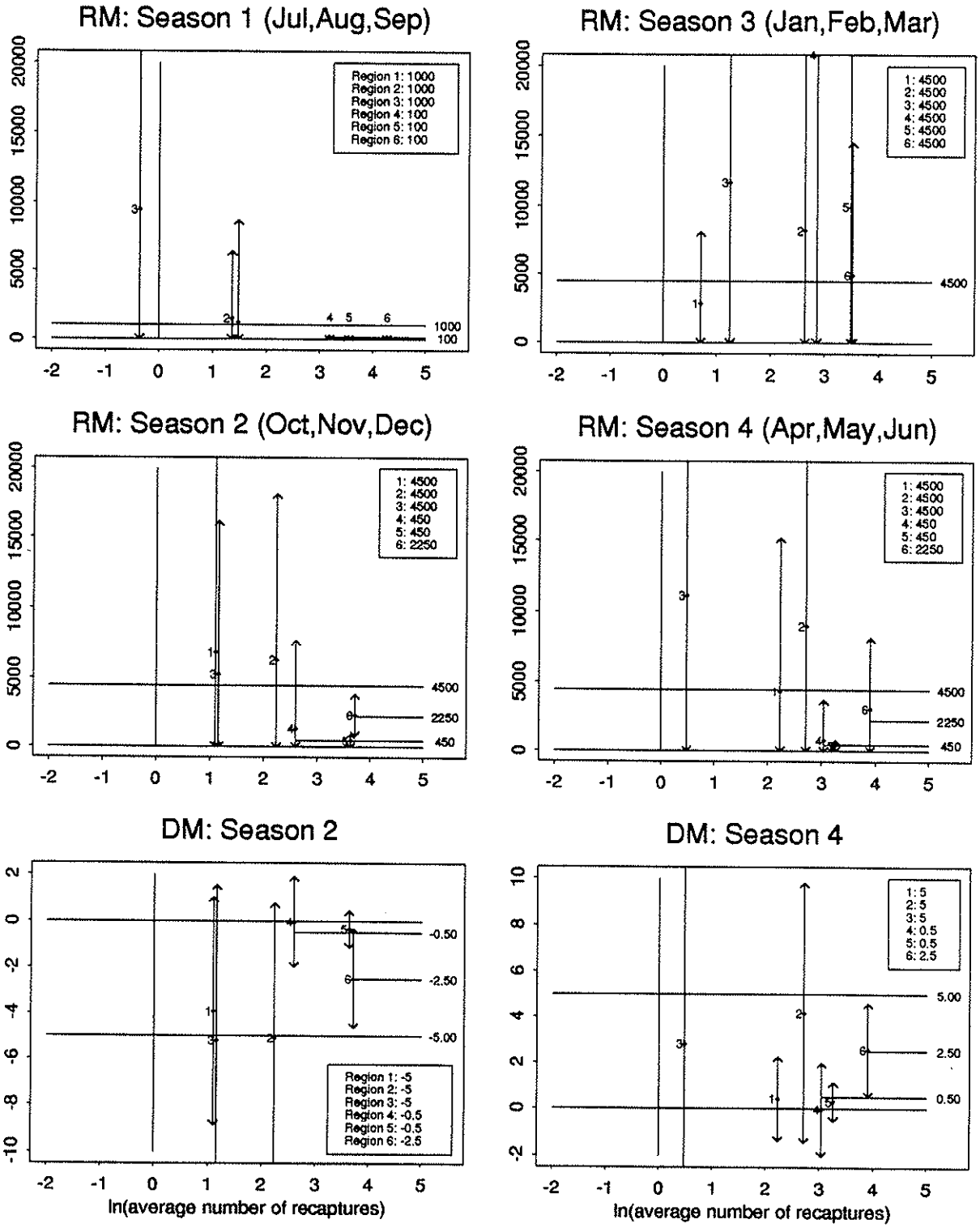

Figure 37: Mean estimates and error bars for random movement (RM) and directed movement (DM) using open boundary conditions and the centered-space scheme. Legends give seasonal "true" values for each region.

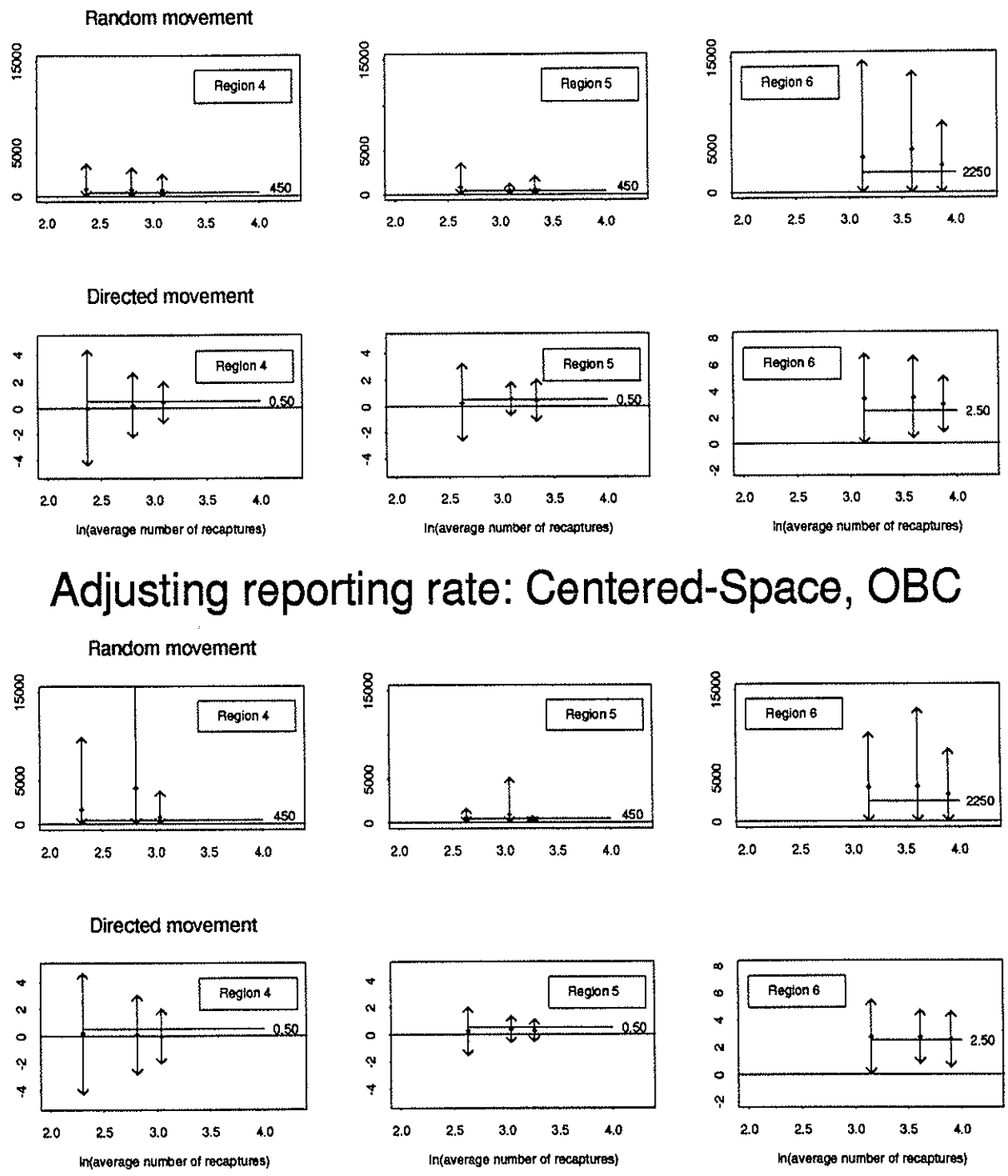

Figure 38: Mean estimates and error bars for random and directed movement using (top) upwind CBC and (bottom) centered-space OBC schemes with different reporting rates. Results are given for Season 4, Regions 4, 5, and 6, using reporting rates of (L to R in each plot) 50%, 75% and 100%. True values are marked.

Table 16: Recapture percentages predicted using reporting rates R of 100%, 75% and 50%. Subtotals may not sum to the total percentage given because of rounding errors.

Scheme	BC's	R	SL	TL	ML	TR	iHL	oHL	$\sum$%	F
UP	Closed	1.00	0.08	1.42	2.16	1.69	1.53	1.15	8.04	781.5
		0.75	0.06	1.09	1.59	1.28	1.17	0.90	6.08	660.6
		0.50	0.04	0.71	1.01	0.82	0.76	0.56	3.89	488.4
CS	Open	1.00	0.08	1.37	2.05	1.65	1.55	1.16	7.86	788.4
		0.75	0.05	1.04	1.52	1.27	1.17	0.91	5.97	643.0
		0.50	0.03	0.69	1.01	0.82	0.78	0.58	3.91	481.6

general finding that the true value is predicted with progressively greater accuracy and greater certainty as release numbers are increased.

The effect on recapture percentages is again approximately linear, as seen in Table 17 and again the centered-space scheme predicts generally fewer longline recaptures.

Table 17: Recapture percentages predicted as release numbers are increased. Subtotals may not sum to the total percentage given because of rounding errors.

Scheme	BC's	Releases	SL	TL	ML	TR	iHL	oHL	$\sum$%	F
UP	Closed	12000	0.17	2.88	4.22	3.35	3.14	2.34	16.10	1203.6
		6000	0.08	1.42	2.16	1.69	1.53	1.15	8.04	781.5
		3000	0.04	0.71	1.01	0.82	0.76	0.56	3.89	488.4
CS	Open	12000	0.15	2.81	4.14	3.30	3.05	2.35	15.80	1219.4
		6000	0.08	1.37	2.05	1.65	1.55	1.16	7.86	788.4
		3000	0.03	0.69	1.01	0.82	0.78	0.58	3.91	488.2

In Section 7.1 it was suggested regarding the scatter diagrams of standardized bias estimates of fleet catchability versus corresponding fleet recaptures that one might expect the minor axis of the ellipse distributions to increase as the total number of releases is increased. Figure 40 shows that this seems to be so. The effect is more evident with the centered-space simulations, suggesting that this scheme is more likely to produce estimates closer to zero than the upwind scheme, with the same number of releases.

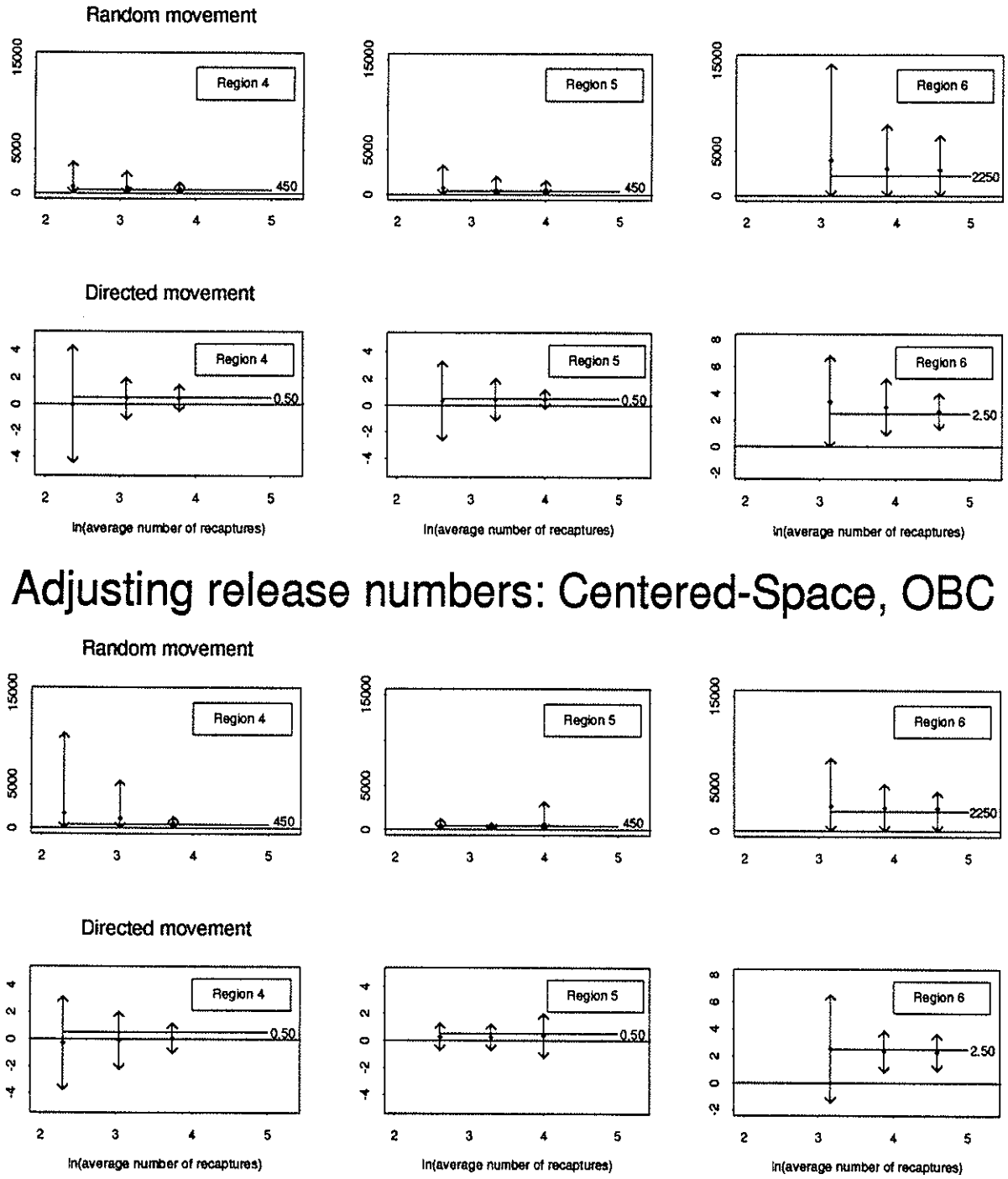

Figure 39: Mean estimates and error bars for random and directed movement using (top) upwind CBC and (bottom) centered-space OBC schemes with different release strategies. Results are given for Season 4, Regions 4, 5 and 6, using release rates increasing (L to R in each plot) from 250/qtr to 500/qtr to 1000/qtr. True values are marked.

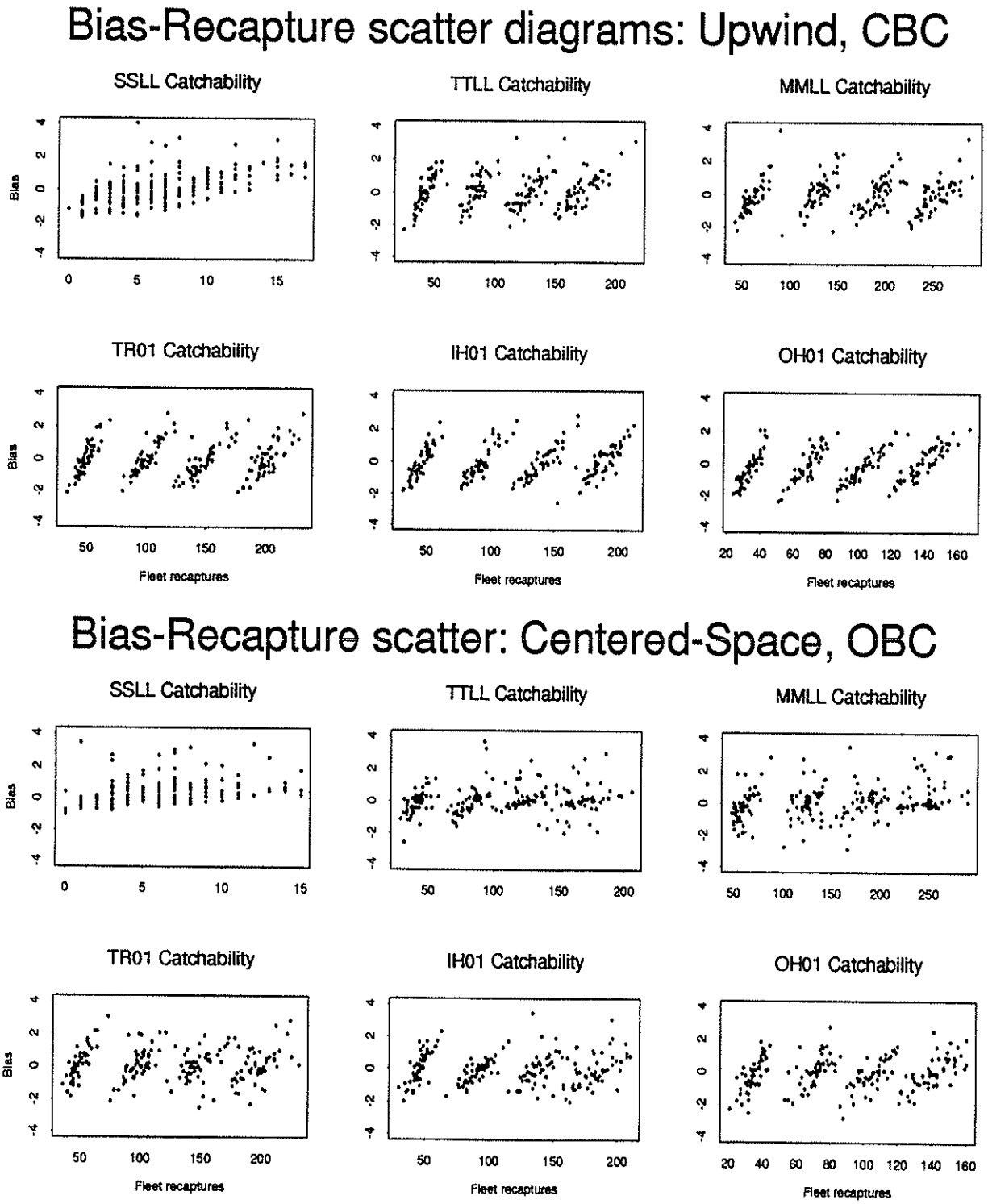

Figure 40: Standardized bias estimates for fleet catchability versus corresponding fleet recapture number using (top) upwind CBC and (bottom) centered-space OBC schemes with release strategies (L to R in each plot) increasing in increments of 250/qtr from 250/qtr (3000 total) to 1000/qtr (12000 total).

7.1.5 Modeling fleet interactions

Finally, if it is assumed that fleet-wise tag recapture percentages can be interpreted as yellowfin catch percentages, then fleet interactions can be tested by selectively removing fleets from the simulations.

The predicted effect of manipulating fleet composition on recapture percentages is shown in Table 18. If the offshore handline fleet is removed, the predicted catches of the remaining fleets vary according to the scheme used. One might expect the catches of the remaining nearshore fleets (TR and iHL) to increase but there is very little change; instead, both schemes predict an increase in catch by the TTLL fleet (TL) and a decrease in MMLL catch (ML). The reason for this is that both the TTLL and MMLL fleets are active at and near Cross seamount (for example, see Table 4) with the MMLL fleet having three times the CPUE (Table 12); with the offshore handliners excluded, the MMLL fleet picks up proportionally more of the available tuna.

Table 18: Recapture percentages predicted by experiments in which fleets are selectively removed. Subtotals may not sum to the total percentage given because of rounding errors.

Scheme	BC's	SL	TL	ML	TR	iHL	oHL	$\sum$%	F
UP	Closed	0.08	1.42	2.16	1.69	1.53	1.15	8.04	781.5
		0.07	1.45	2.13	1.67	1.52	–	6.84	733.1
		–	–	–	1.68	1.57	1.20	4.44	314.1
		–	–	–	1.69	1.58	–	3.27	274.5
		–	–	–	1.73	–	–	1.73	137.9
		–	–	–	–	1.62	–	1.62	134.0
		–	–	–	–	–	1.22	1.22	46.6
		0.09	1.43	2.18	–	–	–	3.71	470.9
CS	Open	0.08	1.37	2.05	1.65	1.55	1.16	7.86	788.4
		0.07	1.41	2.02	1.65	1.56	–	6.71	730.1
		–	–	–	1.64	1.55	1.22	4.41	351.8
		–	–	–	1.64	1.59	–	3.23	373.9
		–	–	–	1.67	–	–	1.67	215.0
		–	–	–	–	1.61	–	1.61	243.4
		–	–	–	–	–	1.24	1.24	61.7
		0.07	1.41	2.13	–	–	–	3.62	460.5

If the longline fleets are removed, both schemes predict that offshore handline catch increases while that of the trollers remains about the same; the upwind scheme predicts a higher inshore handline catch. Using the upwind scheme, offshore handline catch increases 4.3%

while the centered-space scheme predicts a 5.2% comparative increase. Thus the loss of catch to the offshore handliners due to longline operations is predicted to be 4-5%. If, in addition, the offshore handliners cease operations, both schemes predict about a 3% increase in inshore handline catch with little or no change to troll catch.

If just one of the nearshore fleets (troll, inshore handline or offshore handline) is in operation, that fleet understandably achieves a greater catch than when all fleets participate.

Finally, the effect of troll and handline operations on longline operations can be estimated by removing the former. Disregarding SSLL catches, since these are small, both schemes understandably predict an increase in MMLL and TTLL catch.

In percentage terms, the effects of fleet interaction are not high using the current movement hypothesis, certainly not as high as 10%. This may suggest that the yellowfin population is so large that it is easily able to withstand present rates of exploitation or that our movement hypothesis is inaccurate; our predictions may also be strongly tied to our estimates for catchability. These and other possibilities can be resolved by carrying out an actual tagging experiment.

In terms of numerical modeling, the selection of numerical scheme may be important. Perhaps a higher order scheme should be used, as suggested in Section 8.6, to obtain more definitive predictions.

8 Recommendations

8.1 Spatially variable random movement parameter

The original approach of Sibert and Fournier (1994) was to use a global constant D as the random movement parameter; Sibert *et al.* (1996) improved this model by allowing D to vary spatially but they did not consider it to consist of components D_x and D_y as Equation (2) allows. Such an extension of the programs would be straight-forward and may extract more information from the available data about behavioral movement at the expense of only one additional parameter evaluation per model region.

8.2 Catchabilities

The fleet specific catchabilities q_f were developed from global values of fleet CPUE but are applied to monthly varying effort fields to obtain estimated catch. Estimates of catch reflecting the seasonality of actual catch could be obtained by developing monthly values of q_f from monthly CPUE values. The monthly variability in CPUE for each fleet is illustrated

in Figure 41 using the monthly indexed data sets; while these plots are somewhat distorted due to the inclusion of data values from outside the model region in the case of the longline fleets, they illustrate the point that CPUE and therefore fleet specific catchability are more accurately taken as monthly variables. Thus in some future version of the programs, catchabilities should be incorporated as monthly variables; an interim step might be to incorporate them as varying quarterly.

8.3 Age structure

The problem with treating tags released at **Cross** in the same manner as those released at **Kauai** and **Hawaii** is that they have different mortality characteristics. Age structure could be built into the model by assigning the younger tags from **Cross** a higher natural mortality than the older tags at **Kauai** and **Hawaii** (and elsewhere). On the other hand, they should suffer a lower fishing mortality from the longline fleets that operate in the Cross region; as time progressed, surviving juveniles would grow and become more available to the longline, troll and inshore handline fleets.

8.4 Tagging mortality

Modeling work on tag release-recapture experiments that involve the transportation of fish to a release site should include a "tagging mortality" parameter to quantify the probability that a transported tag is likely to die sooner than a fish caught, tagged and released on-site. In the present work we assume there is no effect on the behaviour or mortality of fish that are caught, tagged and released.

8.5 Oceanic movement included as a background movement field

The drifter analyses of Flament *et al.* (1996) for Hawaiian waters show that typical mean oceanic surface currents are generally at least of the order of 5 nm/dy and typical eddy diffusivities are of the order of 4500 nm^2/mo. Since these values are numerically the same as those chosen to represent the behavioral movement of yellowfin in Hawaiian waters, it may be necessary to try to determine if there is a correlation between oceanic and behavioral movements of "Hawaiian" yellowfin. Work of this nature conducted at the SPC for both skipjack and yellowfin in the western Pacific suggests there is no significant correlation, i.e. that these tuna ignore the oceanic currents.

It is possible to incorporate oceanic components of directed and random movement as a background movement field. This background field would vary in space and time but can be assumed to be the same from year to year, and would therefore not participate in the parameter estimation process.

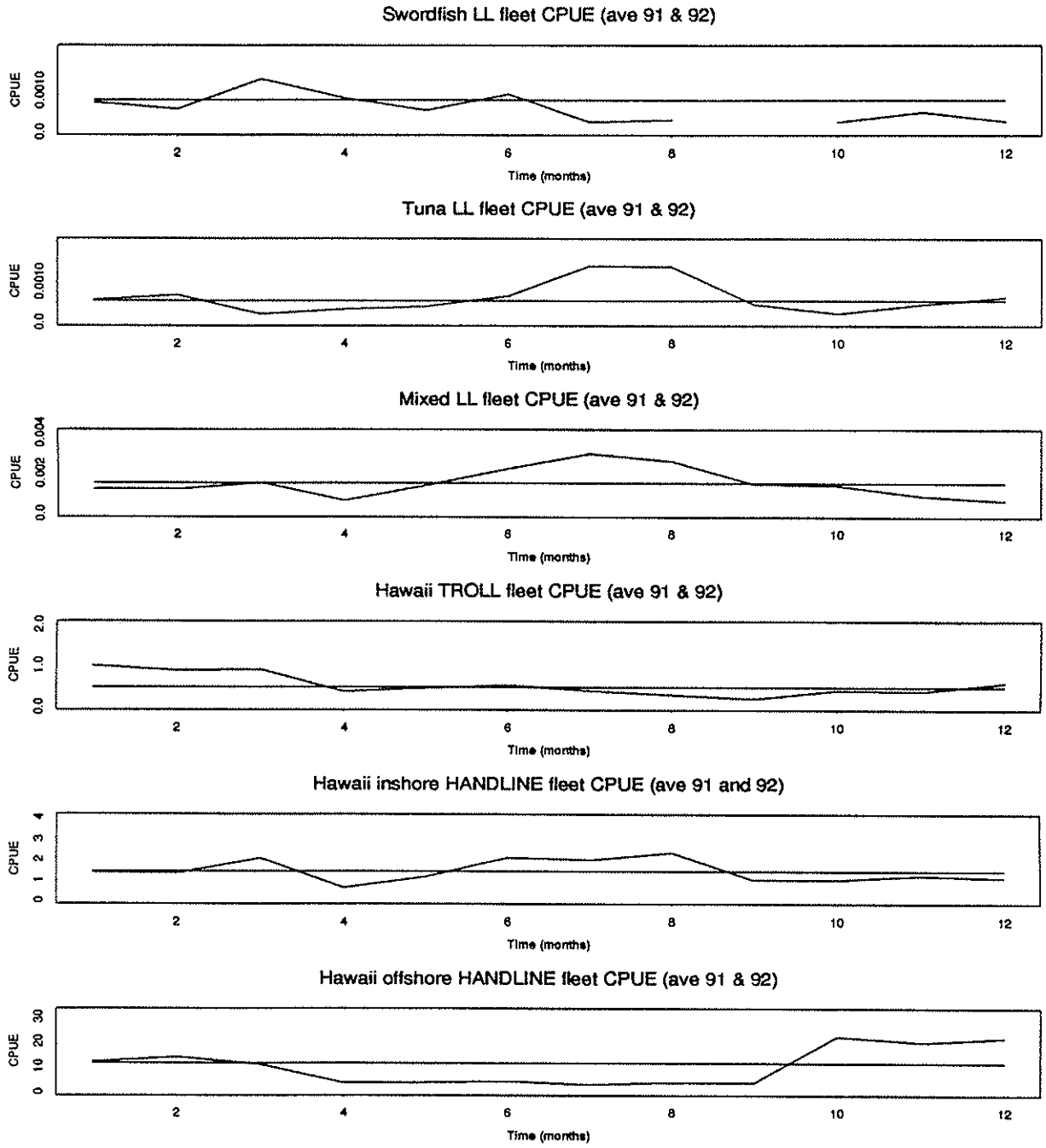

Figure 41: CPUE by month for each fleet considered. These plots are based on data from the monthly indexed data files—catch is in numbers for the troll and handliners—and so are slightly in error due to the inclusion of data values external to the model domain in the case of the longliners. However, they illustrate the point that catch would be more accurately estimated if the catchability coefficients were treated as monthly varying parameters.

8.6 Adopting a higher order numerical scheme

In overall terms, the centered-space scheme seems to give more accurate parameter estimates with generally narrower error bars than the upwind scheme. This improvement is obtained at typically double the computational cost compared to using the upwind scheme. If computational expense is not a restrictive factor, the Peclet criterion is certainly so and we recommend that a higher order scheme such as QUICKEST (Leonard, 1979; Abbott and Basco, 1989) be investigated. QUICKEST is third order and so does not suffer from the Peclet restriction.

8.7 Improving the prediction of tag return numbers

The main problem with estimating the number of predicted tag returns with Equation (18) is that it uses N values from the start of month. This leads to over-estimation of the number of recaptures in the vicinity of the release point because tags would be expected to rapidly diffuse upon release.

A more accurate discretization of Equation (15) than (18) is

$$\frac{Y_N|_{i,j}^{n+1} - Y_N|_{i,j}^{n}}{\Delta t} = \frac{1}{2}\left(F_{i,j;f}^{n+1} + F_{i,j;f}^{n}\right)\frac{1}{2}\left(N_{i,j}^{n+1} + N_{i,j}^{n}\right) .$$

That is, predicted tag numbers would be more accurately obtained using

$$\widehat{C}_{i,j}(t, t+\Delta t) = \Delta t \frac{1}{4}\left(F_{i,j;f}^{n+1} + F_{i,j;f}^{n}\right)\left(N_{i,j}^{n+1} + N_{i,j}^{n}\right) . \tag{8}$$

9 Conclusions

The technique of comparing observed catch with an estimated catch based on fleet CPUE (Section 3.5) is useful in identifying data anomalies. With it we discerned very high ratios of estimated to observed catch in the original handline fleet data, verifying information conveyed by NMFS about an "offshore handline" grouping and clarifying its target domain.

Examining Figures 17 and 18, compiled using 1991-92 data, suggests that a tagging program of 500 releases per quarter at **Kauai**, **Hawaii** and **Cross** could not have been mounted by the fishing industry of the day—not enough fish were caught! A sensible alternative is to use a dedicated scientific vessel to catch and tag the fish, simultaneously providing quality control on the tagging operation.

The exponential equation (17) should not be used in movement studies. Equation (19) is both more accurate and computationally cheaper.

A multiple-site release strategy is preferable to a single-site release on the grounds that the parameter estimates obtained are generally more accurate and more reliable.

Results from simulations using $M = 0.10$ suggest that both upwind and centered-space schemes, with open or closed boundary conditions, produce good estimates under the chosen movement hypothesis. Figures 36 and 37 show that the centered-space scheme generally produces more accurate estimates with a narrower spread; this is in spite of the fact that at Peclet number 2, the centered-space scheme is on the edge of its stable performance range.

When reporting rate is reduced, both the accuracy and reliability of parameter estimates are reduced (Figure 38). This is expected since the parameter estimator needs recapture information to do its job. Recapture percentages decrease in a linear fashion (see Table 16).

Similarly, as tag release numbers are increased, the accuracy and reliability of parameter estimates is increased (Figure 39). The effect on recapture percentages is again approximately linear (see Table 17).

Using fleet-wise tag recapture percentages as surrogate catch percentages, fleet interactions can be tested by selectively removing fleets in the simulations (see Table 18). If the longline fleets are removed, both numerical schemes predict an increase in offshore handline catch but only by 4-5% using the current movement hypothesis; troll catch stays about the same and the schemes differ in their prediction of changes to inshore handline catch. On the other hand, in the absence of the offshore handliners, longline catch is most affected with the TTLL fleet benefiting by 2-3% and the MMLL fleet losing at least 1% of their catch.

In percentage terms, the effects of fleet interaction are not high using the current movement hypothesis, certainly not as high as 10%. This may suggest that either the yellowfin population is so large that it is easily able to withstand present rates of exploitation or that our movement hypothesis is inaccurate. These and other possibilities can be resolved by carrying through with the tagging experiment. Also, to resolve some of the aspects of fleet interaction, it is clear that it matters which scheme is used. To get reliable predictions, it may be necessary to go to a higher order scheme than the centered-space scheme, such as the third order scheme QUICKEST (Leonard, 1979).

Acknowledgments

The first author wishes to acknowledge the guidance of collaborator John Sibert throughout this work and to thank him for the use of his programs upon which the work is based. Frequent discussions on the progress and direction of the work have certainly enriched the final product.

Several thoughtful discussions with Chris Boggs (NMFS, Honolulu) proved very important to the progress of the work. We wish to thank NMFS for allowing us to use the 1991-92

yellowfin logbook data—Xi He in particular worked toward presenting it to us in usable form. In addition, the authors would like to thank David Itano (JIMAR, HIMB) and Dr John Hampton (South Pacific Commission) for their helpful suggestions.

This work was funded by Cooperative Agreement Number NA37RJ0199 (Grant 2042-01) from the National Oceanic and Atmospheric Administration. The views expressed herein are those of the authors and do not necessarily reflect the views of NOAA or any of its subagencies.

The authors would like to thank Richard Bailey for his programming assistance.

Bibliography

Abbott, M. B., and Basco, D. R. (1989), *Computational Fluid Dynamics: An Introduction for Engineers*, Longman Scientific and Technical, xiv + 425 pp.

Bertignac, M. (1995), A simulation model of tagging experiments of yellowfin in the Western Indian Ocean, Paper No: 5-2 submitted to the Second FAO Expert Consultation on Interactions of Pacific Tuna Fisheries in Shimizu, Japan, January 1995, 14 pp.

Beverton, R. J. H., and Holt, S. J. (1957), On the dynamics of exploited fish populations, U.K. Ministry of Agriculture, Fisheries and Food: Fishery Investigations, Series II, Volume XIX, 533 pp.

Curran, D. S., Boggs, Christofer H., and He, Xi (1996), Catch and Effort from Hawaii's Longline fishery summarized by quarters and five degree squares, U.S. Dept. Comm., NOAA Technical Memorandum NMFS-SWFSC-225, iii + 68 pp.

Feller, W. (1968), An Introduction to Probability Theory and its Applications, John Wiley & Sons, N.Y. 509 pp.

Flament, P., Lumpkin, C., and Firing, J. (1996), Pacific Pelagic Fisheries: Current Projects and Related Research, ed. J. Sibert and M. Nunn, Abstracts of Workshop papers presented in November 28-30, 1995 at Honolulu, Hawaii.

Griewank, A., and Corliss, G. F. (1991), Automatic Differentiation of Algorithms: Theory, Practice and Application. SIAM, Philadelphia, 353 pp.

He, X,. K. A. Bigelow, and C. H. Boggs, Cluster-analysis of longline sets and fishing strategies within the Hawaii-based fishery, *Fish. Res.*, in press.

Hunter, J. R., Argue, A. W., Bayliff, W. H., Dizon, A. E., Fonteneau, A., Goodman, D., and Seckel, G. (1986), The dynamics of tuna movements: an evaluation of past and future research, FAO Fish. Tech. Pap. 227, 78 pp.

Huyakorn, P. S., and Pinder, G. F. (1983), *Computational Methods in Subsurface Flow*, Academic Press, 473 pp.

Lantz, R. B. (1971), Quantitative evaluation of numerical diffusion (truncation error), *Society of Petroleum Engineers Journal 11, American Institute of Mining, Metallurgical and Petroleum Engineers, Transactions*, 315–320.

Leonard, B. P. (1979), A stable and accurate convective modelling procedure based on quadratic upstream interpolatio', in *Computer Methods in Applied Mechanics and Engineering, 19*, North-Holland Publishing Company, pp. 59–98.

Neuman, S. P. (1981), A Eulerian-Lagrangian numerical scheme for the dispersion-convection equation using conjugate space-time grids, *J. Computational Physics, 41*, pp. 270–294.

Noye, J. (1987), Numerical methods for solving the transport equation, in *Numerical Modelling: Applications to Marine Systems*, ed. J. Noye, Elsevier Science Publishers B. V. (North-Holland Mathematics Studies: 145), pp. 195–229.

Noye, J. (1988), Finite-difference methods for the one-dimensional transport equation in *Computational Techniques & Applications: CTAC-87*, Ed. J. Noye and C. Fletcher, Elsevier Science Publishers B. V. (North-Holland), pp. 539–562.

Okamoto, H. and Nishimoto, R. (1989), Movement study of small yellowfin tuna (*Thunnus albacares* in Hawaiian waters, unpublished report, Department of Land and Natural Resources, Division of Aquatic Resources, 11 pp. + figures and tables.

O'Brien, J. J. (1986), The hyperbolic problem, in *Advanced Physical Oceanographic Numerical Modelling*, ed. James J. O'Brien, NATO ASI Series, Series C: Mathematical and Physical Sciences, Vol. 186, D. Reidel Publishing Company, pp. 165–186.

Price, H. S., Varga, R, S., and Warren, J. E. (1966), Application of oscillation matrices to diffusion-convection equations, *J. Math. Physics, XLV*, Number 3, pp. 301–311.

Press, W. H., Teukolsky, S. A., Vetterling, W. T. and Flannery, B. P. (1992), *Numerical Recipes in C: the Art of Scientific Computing*, 2nd ed., Cambridge Univ. Press, 994 pp.

Qiu, B., Koh, D., Lumpkin, C., and Flament, P. (1997), On the existence and formation mechanism of the North Hawaiian Ridge Current, *J. Phys. Oceanogr.*, 27(3),432-444.

Roache, P. J. (1972), *Computational Fluid Dynamics*, Hermosa Publishers, Albuquerque, N.M., vii + 434 pp.

Sibert, J. R. and Fournier, D. A. (1994), Evaluation of advection-diffusion equations for estimation of movement patterns from tag recapture data, in Interactions of Pacific tuna fisheries, Volume 1—Summary report and papers on interaction, FAO (Food and Agriculture Organisation of the United Nations) Fisheries Technical Paper 336/1, pp. 108–121.

Sibert, J. R., Hampton, J., and Fournier, D. A. (1996), Skipjack movement and fishery interaction, in Proceedings of the Second FAO Expert Consultation on Interactions of Pacific Ocean Tuna Fisheries, January 1995, Shimizu, Japan; ed. R. S. Shomura, J. Majkowski and R. F. Harman. In press.

Skillman, R. A., Boggs, C. H. and Pooley, S. G. (1993), Fishery interaction between the tuna longline and other pelagic fisheries in Hawaii, NOAA Technical Memorandum NMFS, NOAA-TM-NMFS-SWFSC-189, iii + 45 pp.

South Pacific Commission (1995), Oceanic Fisheries Programme: Work Programme Review 1994-95 and Work Plan 1995-96, viz. Working Paper 5 presented at the Eighth Standing Committee on Tuna and Billfish, Oceanic Fisheries Programme, SPC, Noumea, New Caledonia, July 1995, ii + 44 pp.

10 Appendix

10.1 Non-physical diffusion from upwind differencing

It is well known that upwind differencing of the advection terms introduces numerical or "non-physical" diffusion, also referred to as "computational" or "artificial viscosity" (O'Brien, p. 168, 1986). In fact, O'Brien states: "It is very popular in meteorology and oceanography because of the ease of implementation. However, this author strongly opposes the use of upstream differencing because it is a very dissipative finite difference scheme." To examine the cause of this effect, we omit the physical diffusion terms of Equation (2) and consider only pure advection:

$$\frac{\partial N}{\partial t} + \frac{\partial uN}{\partial x} + \frac{\partial vN}{\partial y} = 0.$$

For the case $u > 0$ and $v > 0$, we construct the ADI scheme for this equation. During the first half time step, updating in the x direction,

$$\frac{N_{i,j}^{n+\frac{1}{2}} - N_{i,j}^{n}}{(\Delta t/2)} + \frac{u_{i,j}N_{i,j}^{n+\frac{1}{2}} - u_{i-1,j}N_{i-1,j}^{n+\frac{1}{2}}}{\Delta x} = -\frac{v_{i,j}N_{i,j}^{n} - v_{i,j-1}N_{i,j-1}^{n}}{\Delta y},$$

where superscripts indicate time level and subscripts indicate horizontal position using the Cartesian framework. During the second half time step, updating in the y direction,

$$\frac{N_{i,j}^{n+1} - N_{i,j}^{n+\frac{1}{2}}}{(\Delta t/2)} + \frac{v_{i,j}N_{i,j}^{n+1} - v_{i,j-1}N_{i,j-1}^{n+1}}{\Delta y} = -\frac{u_{i,j}N_{i,j}^{n+\frac{1}{2}} - u_{i-1,j}N_{i-1,j}^{n+\frac{1}{2}}}{\Delta x}.$$

Adding these equations gives the finite difference approximation for time levels n to $(n+1)$.

$$\frac{N_{i,j}^{n+1} - N_{i,j}^{n}}{\Delta t} + \frac{u_{i,j}N_{i,j}^{n+\frac{1}{2}} - u_{i-1,j}N_{i-1,j}^{n+\frac{1}{2}}}{\Delta x} + \frac{v_{i,j}\,\frac{1}{2}(N_{i,j}^{n+1} + N_{i,j}^{n}) - v_{i,j-1}\,\frac{1}{2}(N_{i,j-1}^{n+1} + N_{i,j-1}^{n})}{\Delta y} = 0 \quad (9)$$

Clearly the overall scheme is time centered. (Because of the use of upwind differencing it is not, however, space centered. In addition, although the scheme is time centered, the time centering is asymmetric with respect to x and y in the advection terms: in the differencing for the v advection term the approximation $\frac{1}{2}(N_{i,j}^{n+1} + N_{i,j}^{n})$ for $N_{i,j}^{n+1/2}$ has truncation error $O(\Delta t^2)$ whereas the term $N_{i,j}^{n+1/2}$ in the differencing for the u advection term is accessed directly; in order to make the scheme time-symmetric for the advection terms it is necessary to reverse the direction of computations and compute the first half time step in the y direction and the second half time step in the x direction.)

Expanding in a Taylor series about $N = N_{i,j}^{n+\frac{1}{2}}$ (and $u = u_{i,j}$, $v = v_{i,j}$) we find that Equation (9) is consistent with the following partial differential equation:

$$\frac{\partial N}{\partial t} + \frac{\partial uN}{\partial x} + \frac{\partial vN}{\partial y} =$$

$$
\begin{aligned}
& & & -\frac{(\Delta t)^2}{24}\frac{\partial^3 N}{\partial t^3} + \frac{(\Delta t)^2}{8} v \frac{\partial^3 N}{\partial y \partial t^2} + \frac{(\Delta t)^2}{8}\frac{\partial v}{\partial y}\frac{\partial^2 N}{\partial t^2} + \cdots \\
+ & \frac{\Delta x}{2}\left[u\frac{\partial^2 N}{\partial x^2} + 2\frac{\partial u}{\partial x}\frac{\partial N}{\partial x} + N\frac{\partial^2 u}{\partial x^2}\right] + \frac{(\Delta x)^2}{6}\left(u\frac{\partial^3 N}{\partial x^3} + 3\frac{\partial u}{\partial x}\frac{\partial^2 N}{\partial x^2} + 3\frac{\partial u^2}{\partial x^2}\frac{\partial N}{\partial x} + N\frac{\partial^3 u}{\partial x^3}\right) + \cdots \\
+ & \frac{\Delta y}{2}\left[v\frac{\partial^2 N}{\partial y^2} + 2\frac{\partial v}{\partial y}\frac{\partial N}{\partial y} + N\frac{\partial^2 v}{\partial y^2}\right] + \frac{(\Delta y)^2}{6}\left(v\frac{\partial^3 N}{\partial y^3} + 3\frac{\partial v}{\partial y}\frac{\partial^2 N}{\partial y^2} + 3\frac{\partial v^2}{\partial y^2}\frac{\partial N}{\partial y} + N\frac{\partial^3 v}{\partial y^3}\right) + \cdots
\end{aligned}
$$

The numerical diffusion terms are those in square brackets; numerical diffusion increases with grid element size. These are first order terms which also constitute the leading term of the truncation error for the upwind scheme. The reason for the appearance of v and $\partial v/\partial y$ among the time derivative terms is the temporal asymmetry mentioned above in the differencing of the advection terms.
Neuman (1981, p. 271) and Noye (1988, p. 201) report that the masking effect of physical diffusion by numerical diffusion can be reduced by taking a grid sufficiently fine, and they cite Lantz (1971) in this regard.

10.2 Half time step discretizations

In the case of upwind differencing, the first ADI equations can be expressed as

$$
\begin{aligned}
& N_{i-1,j}^{n+\frac{1}{2}}\left[\begin{Bmatrix} -\frac{u_{i-1,j}}{\Delta x} \\ - \end{Bmatrix} - \frac{D_{i-1,j}+D_{i,j}}{2(\Delta x)^2}\right] \\
+ \; & N_{i,j}^{n+\frac{1}{2}}\left[\begin{Bmatrix} \frac{u_{i,j}}{\Delta x} \\ -\frac{u_{i,j}}{\Delta x} \end{Bmatrix} + \frac{D_{i-1,j}+2D_{i,j}+D_{i+1,j}}{2(\Delta x)^2} + \frac{2}{\Delta t} + (F_{i,j}+M)\right] \\
+ \; & N_{i+1,j}^{n+\frac{1}{2}}\left[\begin{Bmatrix} - \\ \frac{u_{i+1,j}}{\Delta x} \end{Bmatrix} - \frac{D_{i,j}+D_{i+1,j}}{2(\Delta x)^2}\right] \\
= \; & -\Bigg[N_{i,j-1}^{n}\left(\begin{Bmatrix} -\frac{v_{i,j-1}}{\Delta y} \\ - \end{Bmatrix} - \frac{D_{i,j-1}+D_{i,j}}{2(\Delta y)^2}\right) \\
& \quad + N_{i,j}^{n}\left(\begin{Bmatrix} \frac{v_{i,j}}{\Delta y} \\ -\frac{v_{i,j}}{\Delta y} \end{Bmatrix} + \frac{D_{i,j-1}+2D_{i,j}+D_{i,j+1}}{2(\Delta y)^2} - \frac{2}{\Delta t}\right) \\
& \quad + N_{i,j+1}^{n}\left(\begin{Bmatrix} - \\ \frac{v_{i,j+1}}{\Delta y} \end{Bmatrix} - \frac{D_{i,j}+D_{i,j+1}}{2(\Delta y)^2}\right) \Bigg]
\end{aligned}
\tag{10}
$$

The first ADI equation in centered-space form is

$$
\begin{aligned}
& N_{i-1,j}^{n+\frac{1}{2}}\left[-\frac{D_{i-1,j}+D_{i,j}}{2(\Delta x)^2}-\frac{u_{i-1,j}}{2\Delta x}\right] \\
+\; & N_{i,j}^{n+\frac{1}{2}}\left[\frac{D_{i-1,j}+2D_{i,j}+D_{i+1,j}}{2(\Delta x)^2}+\frac{2}{\Delta t}+(F_{i,j}+M)\right] \\
+\; & N_{i+1,j}^{n+\frac{1}{2}}\left[-\frac{D_{i,j}+D_{i+1,j}}{2(\Delta x)^2}+\frac{u_{i+1,j}}{2\Delta x}\right] \\
=\; & -\Bigg[\quad N_{i,j-1}^{n}\left(-\frac{D_{i,j-1}+D_{i,j}}{2(\Delta y)^2}-\frac{v_{i,j-1}}{2\Delta y}\right) \\
& \qquad + N_{i,j}^{n}\quad\left(\frac{D_{i,j-1}+2D_{i,j}+D_{i,j+1}}{2(\Delta y)^2}-\frac{2}{\Delta t}\right) \\
& \qquad + N_{i,j+1}^{n}\left(-\frac{D_{i,j}+D_{i,j+1}}{2(\Delta y)^2}+\frac{v_{i,j+1}}{2\Delta y}\right)\quad\Bigg]
\end{aligned}
\tag{11}
$$

10.3 Mathematical requirements for non-negativity

Noye (1988) shows that any implicit 3-point 2-level finite difference formula in the form

$$\tau_i^{n+1}=d_{-1}\tau_{j-1}^{n+1}+d_1\tau_{j+1}^{n+1}+e_{-1}\tau_{j-1}^{n}+e_0\tau_j^{n}+e_1\tau_{j+1}^{n} \tag{12}$$

has non-negative solutions when it is *strictly diagonally dominant* and has *non-negative coefficients*, i.e. when

$$d_{-1}+d_1<1 \tag{13}$$

and

$$d_{-1}\geq 0,\quad d_1\geq 0,\quad e_{-1}\geq 0,\quad e_0\geq 0\quad\text{and}\quad e_1\geq 0\,. \tag{14}$$

These are not necessary conditions; in some cases the numerical solution can be non-negative even if some of the coefficients are not.
To write, for example, Equation (10) in the form (12), move the off-diagonal terms on the left hand side of (10) to the right hand side and divide through by the coefficient of the (remaining) diagonal term on the left.

10.4 Predicted number of tag returns

If the yield of tags in numbers is Y_N, the rate of yield is (Beverton and Holt, p. 36, 1957)

$$\frac{\partial Y_N}{\partial t}=FN, \tag{15}$$

where F is the fishing mortality coefficient and N is the number of tagged fish, given by the solution of Equation (2).
An approximate solution of (2) which is readily calculated but, unfortunately, ignores the movement of the tags, can be obtained as follows: "... if the mortality coefficients are much greater than the transport coefficients the abundance of fish in any area is largely determined by the former" (Beverton and Holt, p. 151, 1957). In such a case

$$\frac{\partial N}{\partial t} \simeq -ZN$$

and the corresponding approximate solution of (2) is

$$N(t) \simeq N_0 e^{-Zt}. \tag{16}$$

The form of this solution holds for each tag cohort released. The rate of yield is therefore approximately

$$\frac{\partial Y_N}{\partial t} \simeq F N_0 e^{-Zt},$$

where N_0 changes with each release. Assuming that the value for N_0 is up-to-date, integration over the period $(t, t+\Delta t)$ gives

$$Y_N(t+\Delta t) - Y_N(t) \simeq \frac{F}{F+M} N_0 e^{-Zt}\left[1 - e^{-Z\Delta t}\right].$$

The left hand side expression is the predicted number of tags caught, $\widehat{C}(t, t+\Delta t)$, so

$$\widehat{C}(t, t+\Delta t) \simeq \frac{F}{F+M} N(t)\left[1 - e^{-Z\Delta t}\right]. \tag{17}$$

Tag returns may be calculated in this manner if mortality effects dominate transport effects. If transport is significant, a formula inclusive of such effects should be used.
In principle, a solution of Equation (15) for tag yield that includes both mortality and transport effects can be obtained because Equation (2) can be solved numerically with arbitrary accuracy. Consider the following finite difference approximation for Equation (15):

$$\frac{Y_N|_{i,j}^{n+1} - Y_N|_{i,j}^{n}}{\Delta t} = F_{i,j;f}^{n} N_{i,j}^{n}, \tag{18}$$

which can be reformulated as

$$\widehat{C}_{i,j}(t, t+\Delta t) = \Delta t F_{i,j;f}^{n} N_{i,j}^{n}. \tag{19}$$

This formulation is used in the present work for determining the predicted number of tags caught; $N_{i,j}^{n}$ denotes the number of tags in cell (i,j) at the start of the month. A correction factor to account for fleet reporting rates β_f is further incorporated to give Equation (5). The estimate is calculated once per month so $\Delta t = 1$ is used. See Section 8.7 for a recommended formulation based on semi-monthly values of F and N.
Calculation (19) is not only more accurate than (17) but is quicker to compute since it eliminates a computationally expensive exponential computation for each bin for every month of a simulation.

10.5 Seasonal oceanographic flow patterns from a numerical model

Qiu *et al.* (1996) have provided a sequence of oceanographic surface flow patterns which confirm that the North Equatorial Current has a north-south migration over a period of a year (see Figures 42–45). These flow patterns have been taken from a numerical simulation and have been substantiated by the results of drifter data produced by Flament *et al.* (1996).

10.6 Complete results of 12 tests

The plots in Figures 46-52 summarize the analysis of estimates obtained from 50 simulations of 12 numerical experiments. The 12 experiments arise from considering three natural mortality values, two finite difference schemes and two ways of defining boundary conditions. In order to easily compare the results, a standardized bias statistic has been created for each variable. This statistic has unit standard deviation; its distribution is plotted and shows the bias of the estimates relative to zero, the unbiased value.

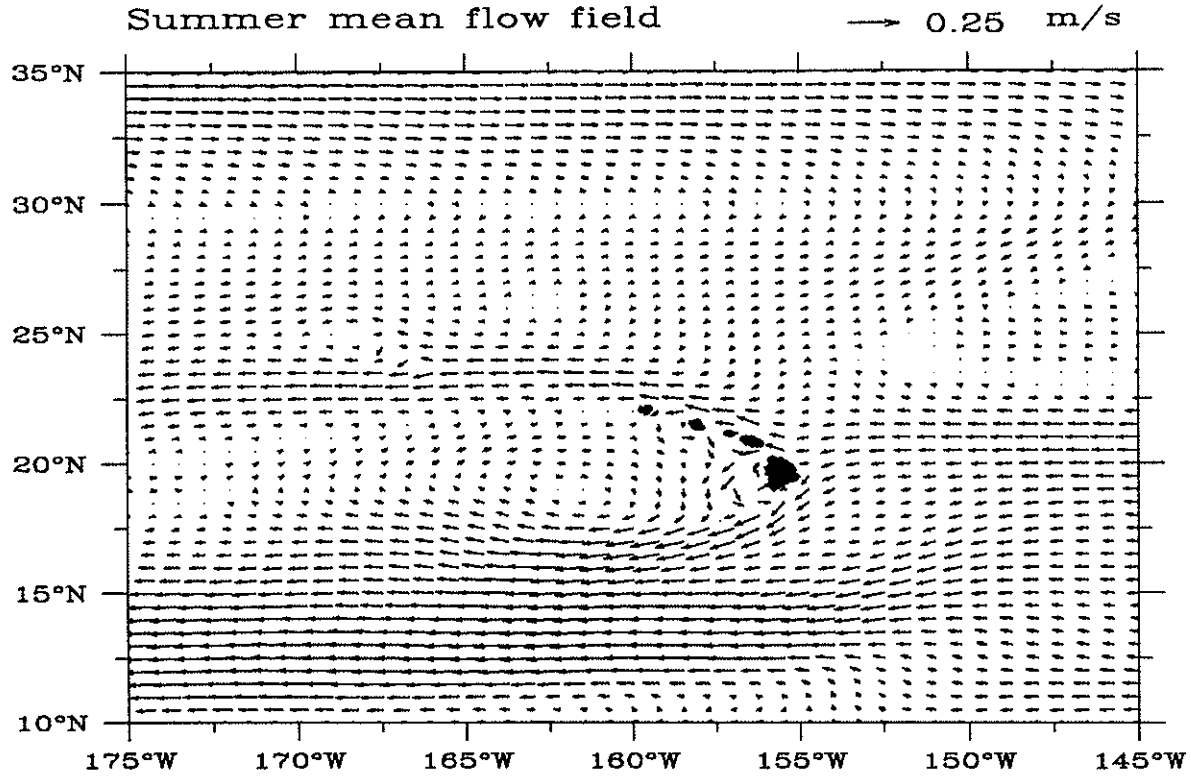

Figure 42: Mean oceanographic surface flow for summer (Season 1) from a numerical model of the north Pacific due to Qiu *et al.* (1996).

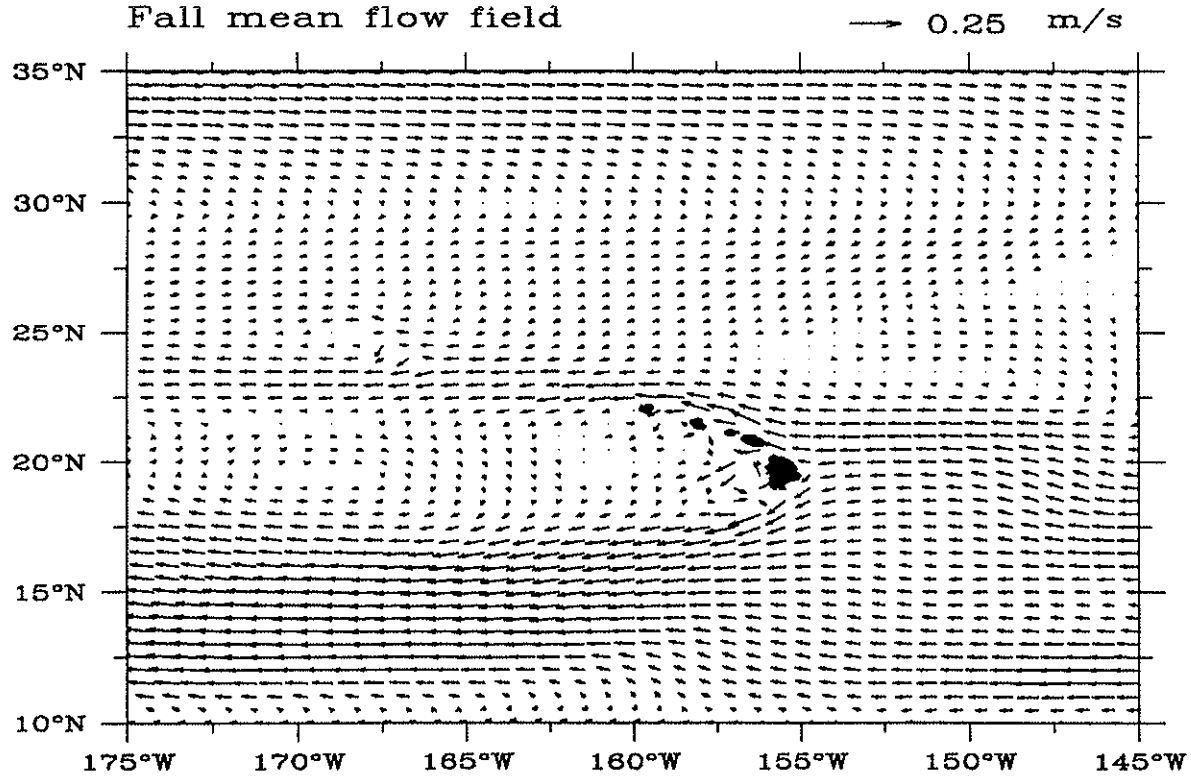

Figure 43: Mean oceanographic surface flow for fall (Season 2) from a numerical model of the north Pacific due to Qiu *et al.* (1996).

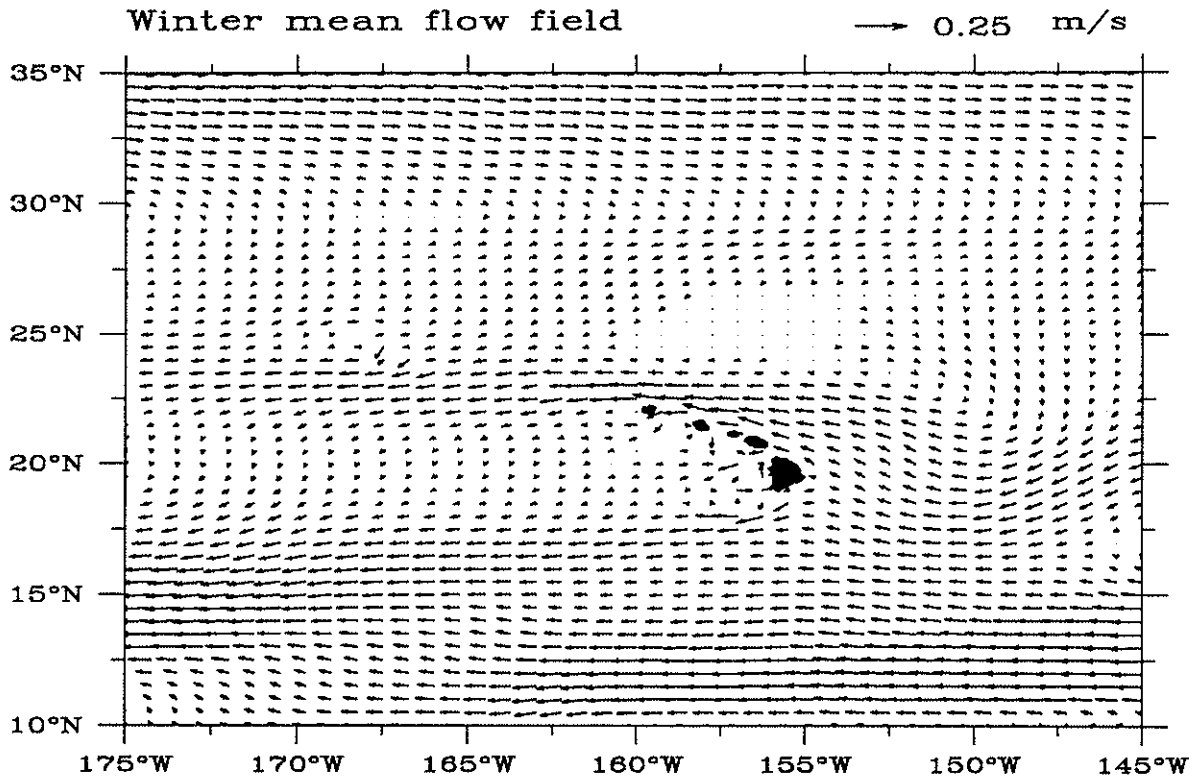

Figure 44: Mean oceanographic surface flow for winter (Season 3) from a numerical model of the north Pacific due to Qiu *et al.* (1996).

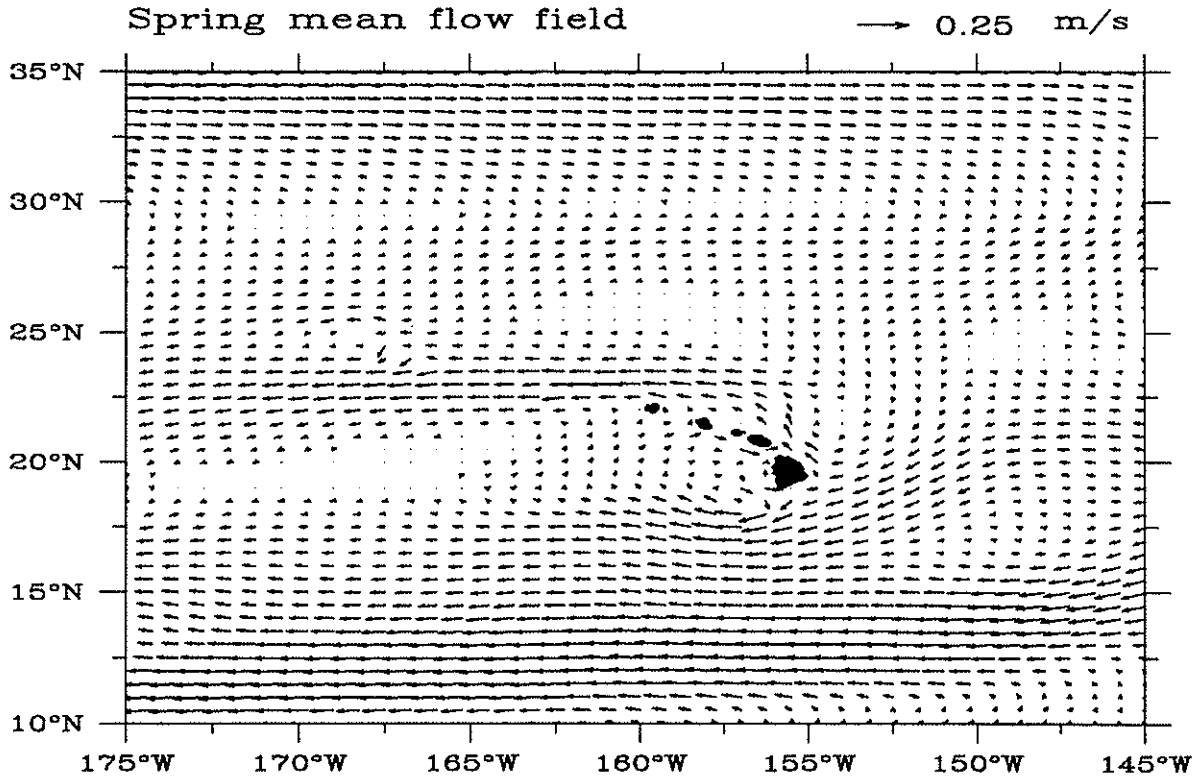

Figure 45: Mean oceanographic surface flow for spring (Season 4) from a numerical model of the north Pacific due to Qiu *et al.* (1996).

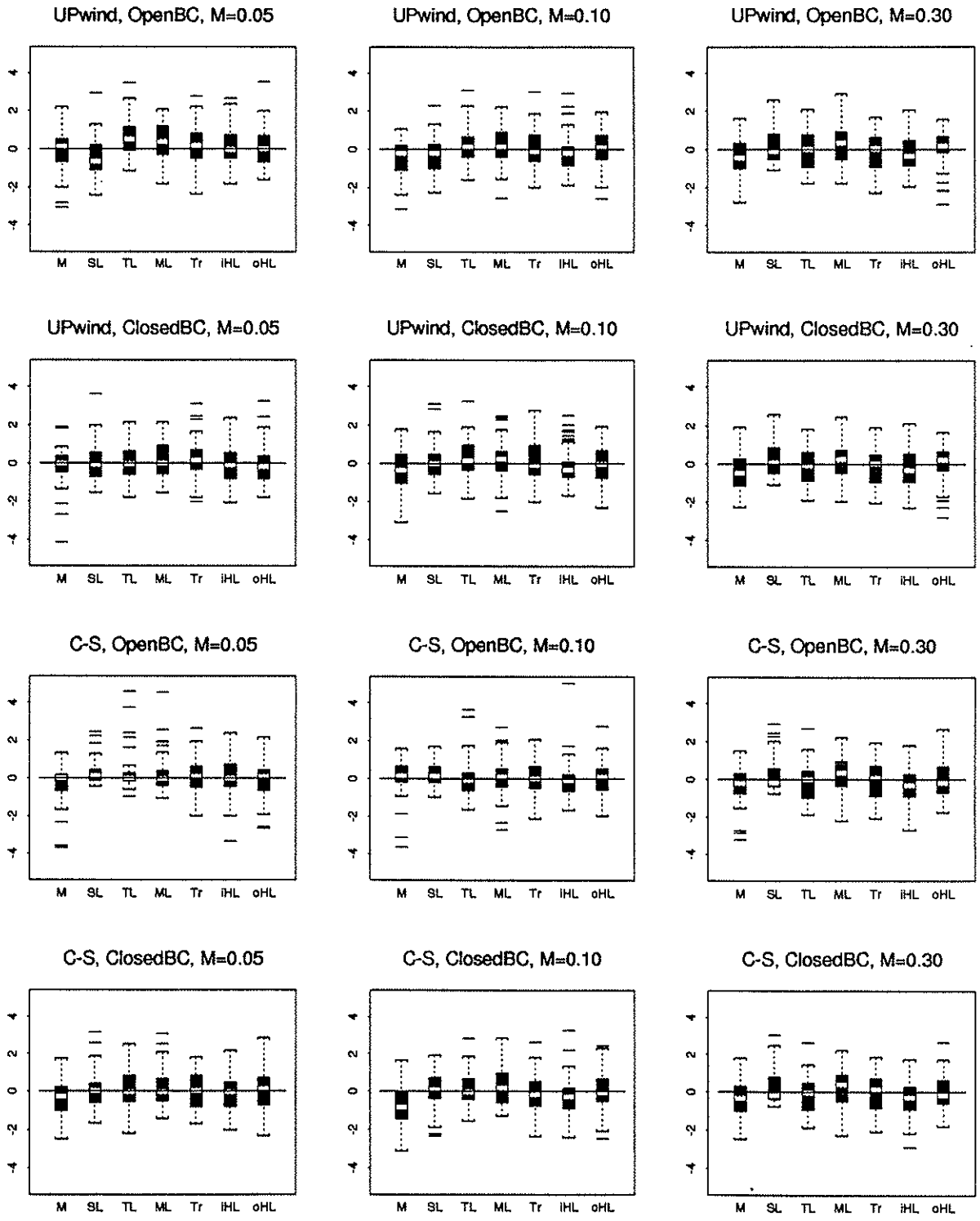

Figure 46: Distribution of standardized bias for mortality estimates based on 50 simulations of 12 numerical experiments (M=Natural mortality, SL=Swordfish LL catchability, ...).

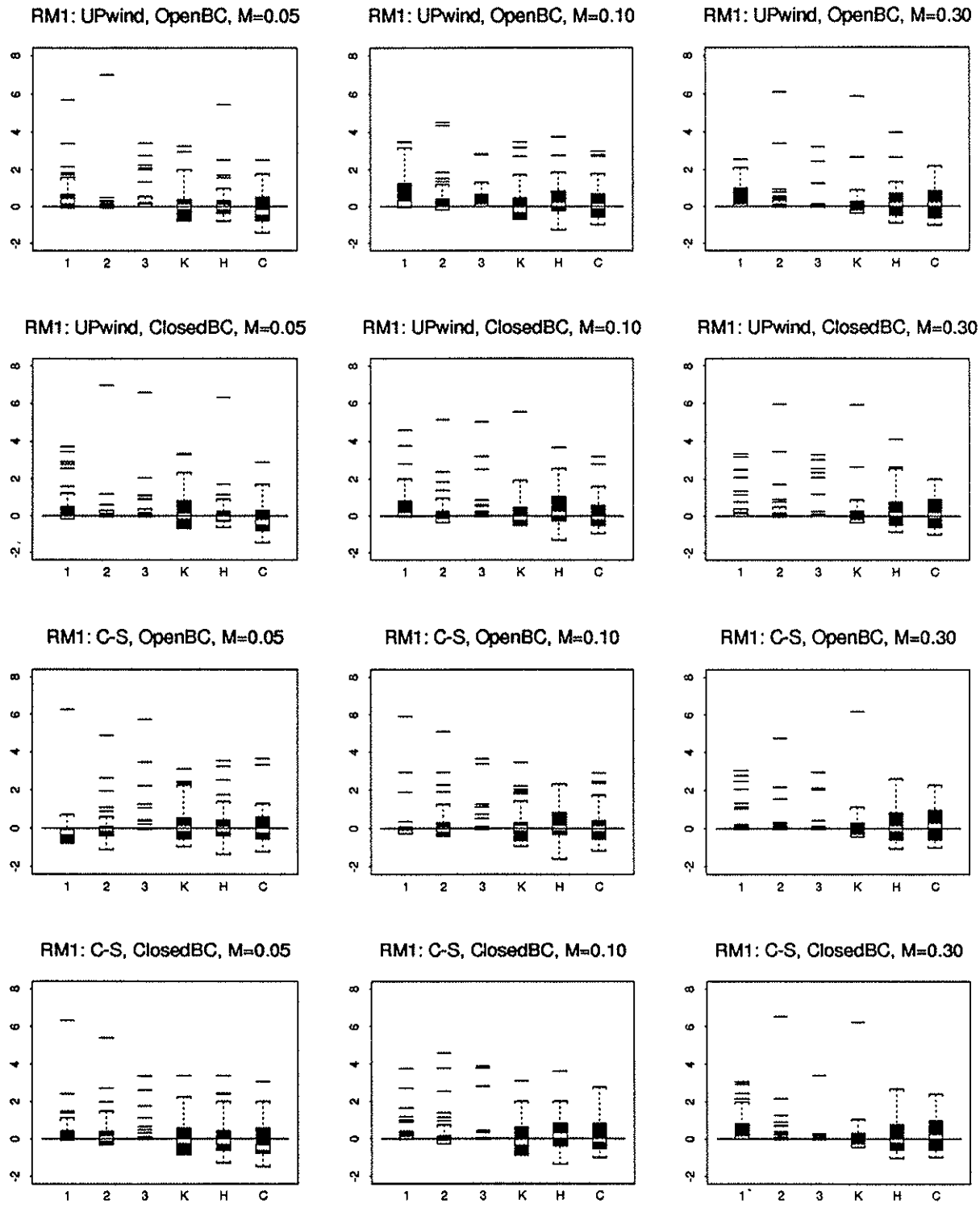

Figure 47: Distribution of standardized bias for random movement estimates in Season 1 based on 50 simulations of 12 numerical experiments. RM1=Random movement in Season 1; region identifiers are given on the x-axis.

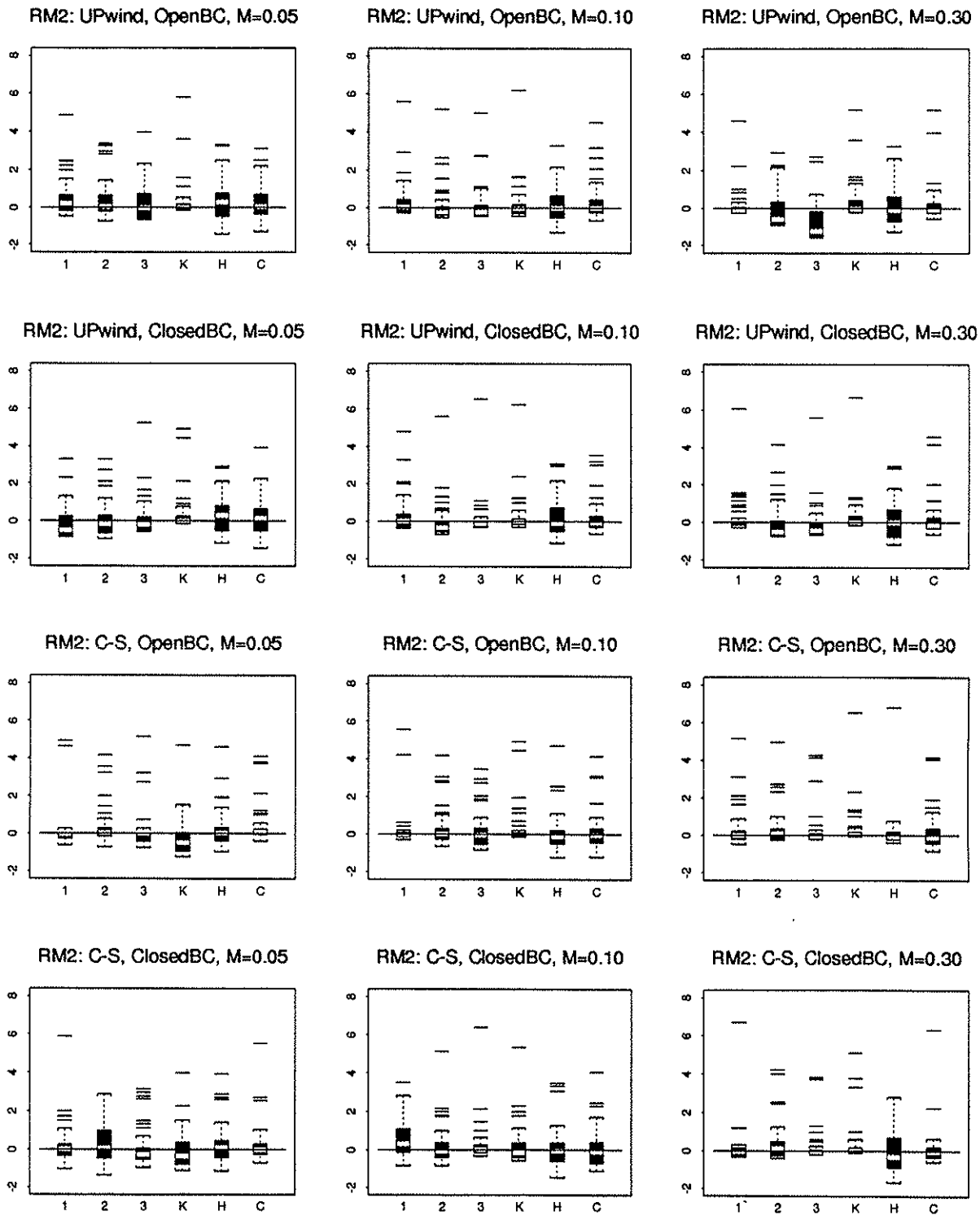

Figure 48: Distribution of standardized bias for random movement estimates in Season 2 based on 50 simulations of 12 numerical experiments. RM2=Random movement in Season 2; region identifiers are given on the x-axis.

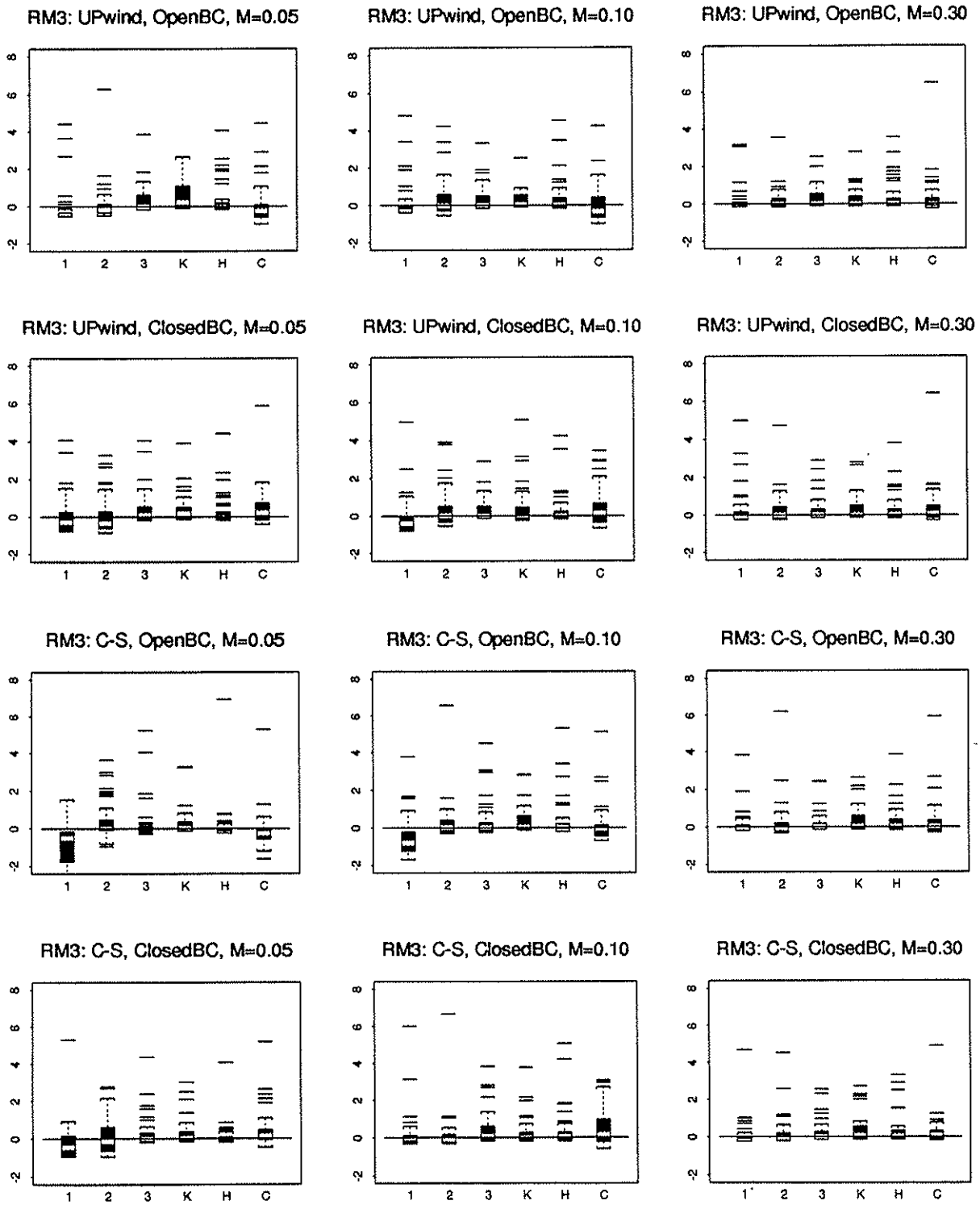

Figure 49: Distribution of standardized bias for random movement estimates in Season 3 based on 50 simulations of 12 numerical experiments. RM3=Random movement in Season 3; region identifiers are given on the x-axis.

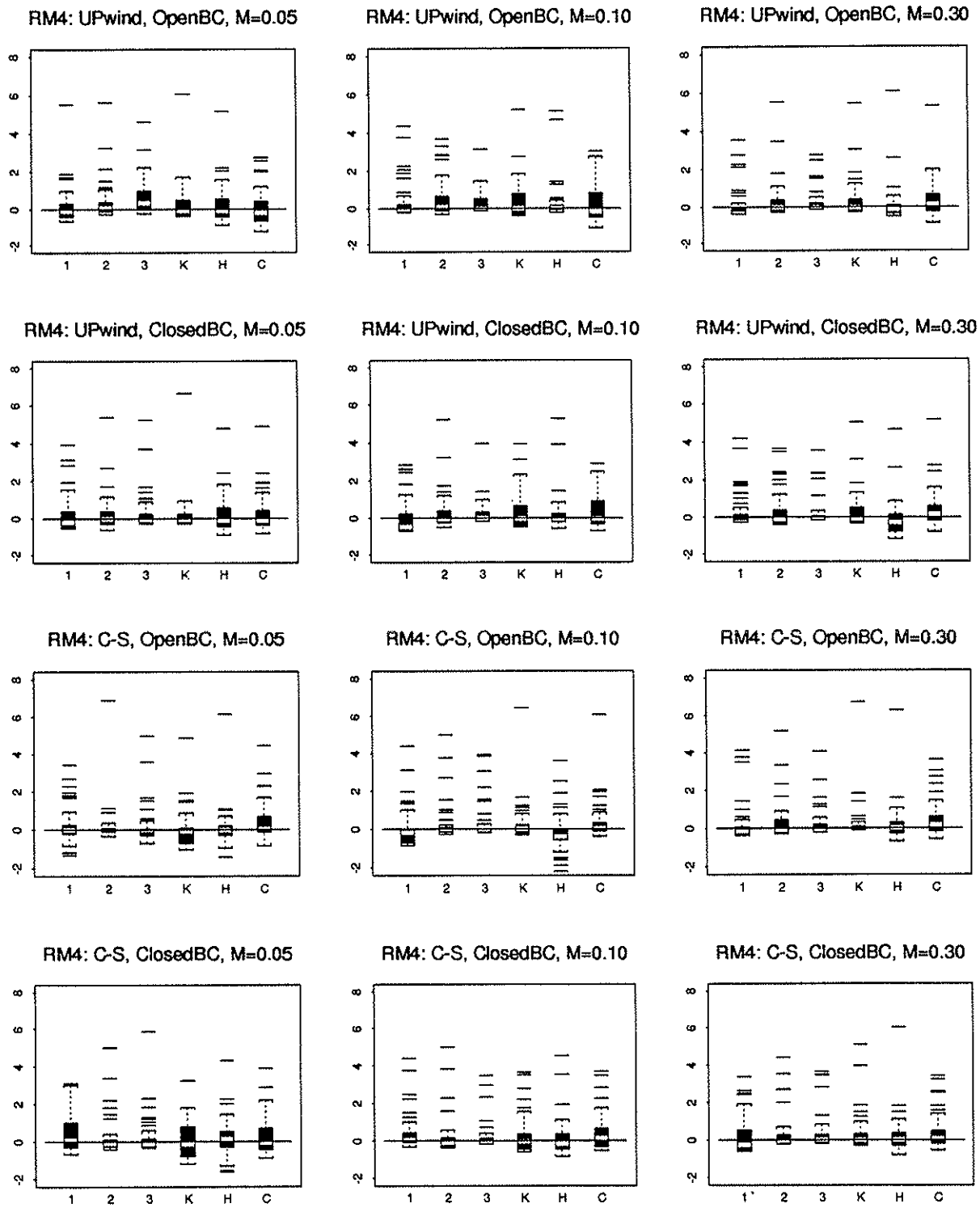

Figure 50: Distribution of standardized bias for random movement estimates in Season 4 based on 50 simulations of 12 numerical experiments. RM4=Random movement in Season 4; region identifiers are given on the x-axis.

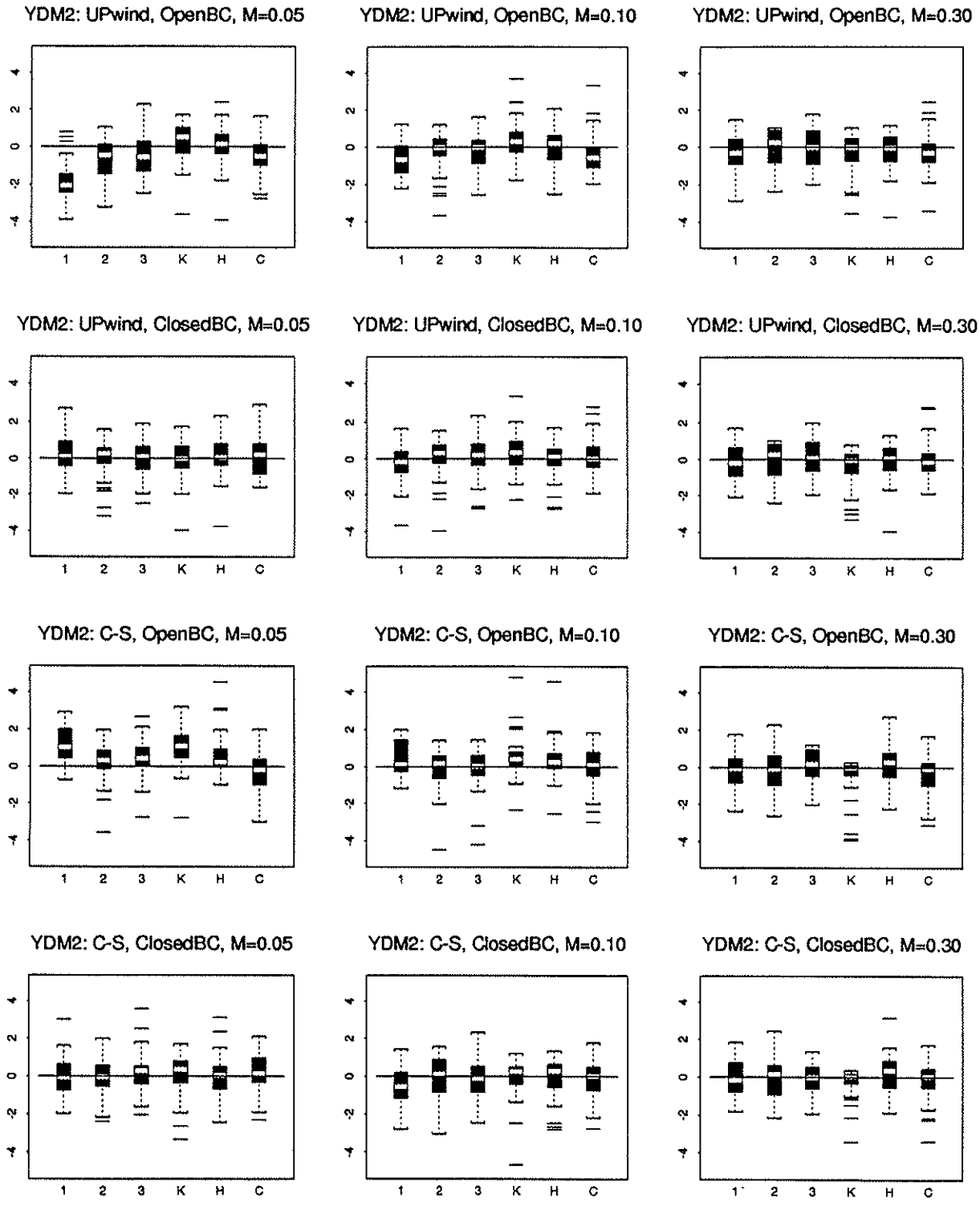

Figure 51: Distribution of standardized bias for directed movement estimates in Season 2 based on 50 simulations of 12 numerical experiments. YDM2=Directed movement for Season 2 in the y direction; region identifiers are given on the x-axis.

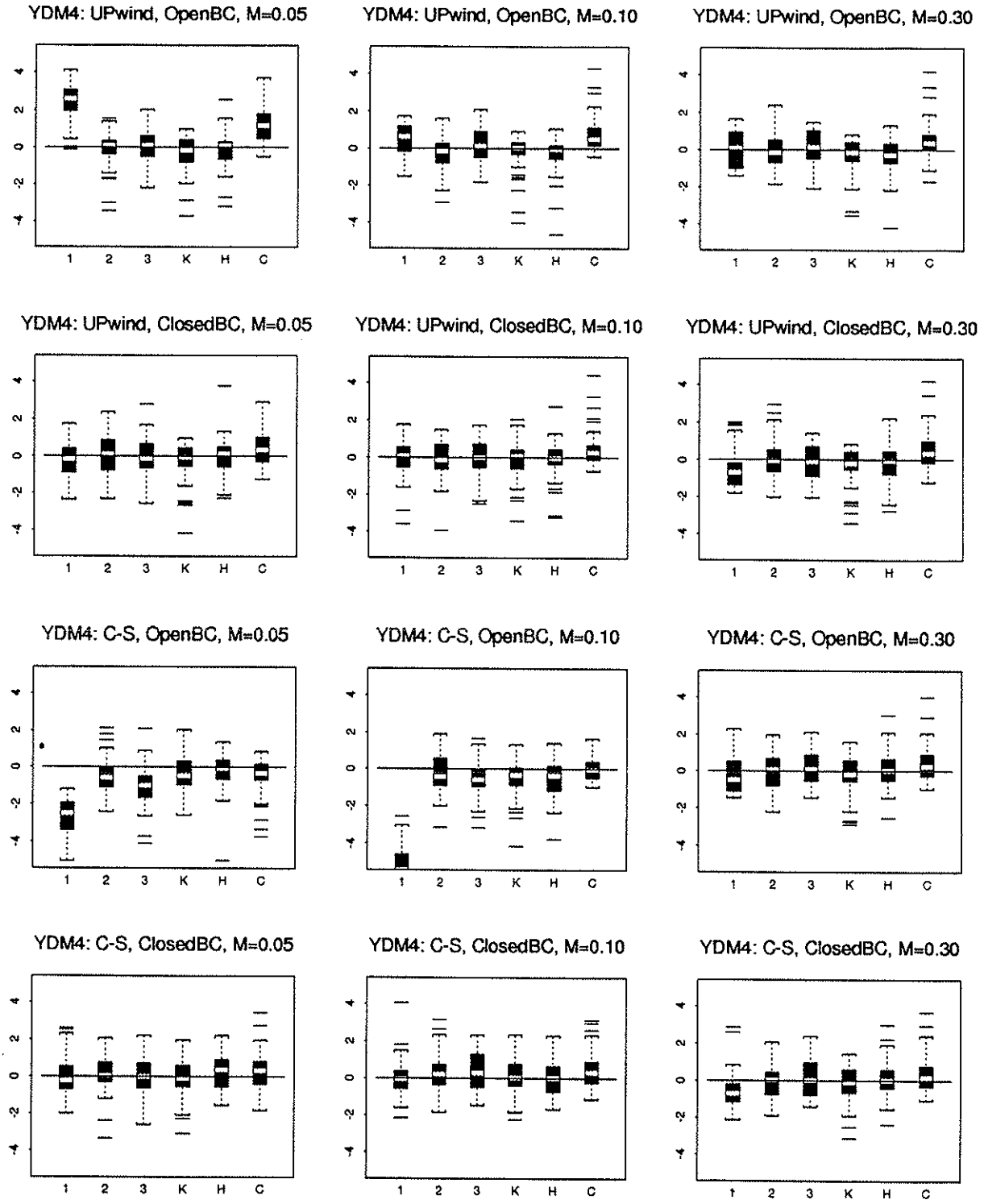

Figure 52: Distribution of standardized bias for directed movement estimates in Season 4 based on 50 simulations of 12 numerical experiments. YDM4=Directed movement for Season 4 in the y direction; region identifiers are given on the x-axis.